Weltdatenzentrum Abfluss
Bundesanstalt für Gewässerkunde
Koblenz, Deutschland

Global Runoff Data Centre (GRDC)
Federal Institute of Hydrology (BfG)
Koblenz, Germany

Report No. 26

Modelling raster-based monthly water balance components for Europe

Carmen Ulmen

November 2000

P.O.Box 20 02 53
D-56002 Koblenz

Am Mainzer Tor 1
D-56068 Koblenz

Phone: (49 261) 1306-5224; Fax: (49 261) 1306-5280; E-Mail: grdc@bafg.de; http://www.bafg.de/grdc.htm

Preface

The terrestrial runoff component is a comparatively small but sensitive and thus significant quantity in the global energy and water cycle at the interface between landmass and atmosphere. As opposed to soil moisture and evapotranspiration which critically determine water vapour fluxes and thus water and energy transport, it can be measured as an integrated quantity over a large area, i.e. the river basin. This peculiarity makes terrestrial runoff ideally suited for the calibration, verification and validation of general circulation models (GCMs).

Gauging stations are not homogeneously distributed in space. Moreover, time series are not necessarily continuously measured nor do they in general have overlapping time periods. To overcome this problems with regard to regular grid spacing used in GCMs, different methods can be applied to transform irregular data to regular so called gridded runoff fields.

Some are based on mere interpolation. More sophisticated approaches optionally take into account the drainage network and the discharge balance between gauging stations. The degree of freedom inherent to these approaches can be reasonably reduced by introducing some suitable spatial pattern function as an additional external constraint to the interpolation process, e.g. runoff patterns as computed from global water balance models. This has been impressively demonstrated in a GRDC co-operation with researchers from the University of New Hampshire, USA, the results of which were presented to the public in GRDC-Report 22.

The present work aims to directly compute the gridded components of the monthly water balance (including gridded runoff fields) for Europe by application of the well-established raster-based macro-scale water balance model WABIMON used at the Federal Institute of Hydrology, Germany. Model calibration and validation is performed by separate examination of 29 representative European catchments. Results indicate a general applicability of the model delivering reliable overall patterns and integrated quantities on a monthly basis. For time steps less then too weeks further research and structural improvements of the model are suggested.

The work presented here once again made apparent the need for large amounts of high quality hydrological information, being the prerequisite for successful research and eventually for more reliable climate change impact analyses. The Global Runoff Data Centre (GRDC) therefore repeats its call upon national hydrological services and the scientific community to not neglect to supply hydrological data and information to the GRDC.

This report was derived by Mrs. Carmen Ulmen from her diploma thesis, submitted to the Geographical Institute of the University of Bonn, Germany, where it was given highest marks and moreover honoured by a special prize of the faculty. The GRDC likes to thank Mrs. Ulmen for her excellent work. Thanks are also due to Dr. Wolfgang Grabs, former head of the GRDC, for initiating this research. We also owe many thanks to Mr. Peter Krahé, staff member of the Federal Institute of Hydrology for his share in supervising the work as the WABIMON expert.

As it has been stated repeatedly, the GRDC has a standing invitation to visiting scientists to assist the Centre in the scientific exploitation of its database. A couple of valuable co-operations and reports arose from these invitations in the past. Therefore, I would like to encourage others to follow this proved tradition.

Koblenz, October 2000

Thomas Maurer
Head, GRDC

CONTENTS

1 MOTIVATION AND SCIENTIFIC PROBLEM

The anthropogenic emission of greenhouse gases will amplify the natural greenhouse effect already in the course of this century with growing scientific consensus. Climatological and hydrological processes are interrelated via the hydrological cycle of evaporation, cloud formation, precipitation and runoff, and, hence, influence each other:

- General Circulation Models (GCM) require reliable hydrological input data to produce both reliable fields of current atmospheric water vapour and precipitation and to produce reliable climate change scenarios.
- Vice versa, climate change has severe implications on the water cycle and river runoff.

Verification and validation of coupled ocean-atmosphere GCMs has revealed that the component of terrestrial runoff is not yet captured with sufficient reliability. In their World Climate Programme - Water (WCP-Water) the World Meteorological Organization (WMO) in Geneva, therefore, brought the project B.3 "Development of Grid-related Estimates of Hydrological Variables" [GOTTSCHALK & KRASOVSKAIA 1998] into being.

The objective of this project is to make more reliable gridded runoff available as input for GCMs. Possible approaches are the transformation of measured, catchment-based runoff to grid cells, the estimation of grid cell runoff using empirical relationships or the use of raster-based macro-scale hydrological models to simulate gridded runoff, the latter of which is favoured here. In the current study the water balance model WABIMON, based on THORNTHWAITE & MATHER (1957), is improved and validated on the European scale and then employed to provide gridded runoff estimates for Europe.

For the long term, the GRDC intends this water balance model a) to be validated and applied on a global scale, b) to serve as a basis for a regular publication of global gridded runoff data and c) to be used for climate change sensitivity analyses and as a prognosis model for the generation of runoff predictions with climate change scenarios as input.

2 METHOD OF MODEL VALIDATION

2.1 Description of the method

Monthly runoff on a 0.5° x 0.5° raster is estimated with the help of the conceptual macro-scale hydrological model WABIMON that is based on the approach of THORNTHWAITE & MATHER (1957). WABIMON is applied for Greater Europe within the study area of 34°-73°N and 25°W-60°E (chapter 5).

For model validation 29 representative European test catchments with a catchment size of 10.000 – 60.000 km² differing in climate, elevation, runoff regime types, hydrogeology, dominant soil type and land use have been identified. Results of the raster-based modelled runoff are aggregated on the catchment level and compared with catchment-based measured runoff. Model parameters are calibrated in order to minimize residuals (differences between modelled and measured runoff). The overall model quality is evaluated by the **model efficiency (ME)** given in equation (2.1), also called **Sutton-Rathcliffe's Coefficient** [NASH & SUTCLIFFE 1970, SINGH 1995: 536, BERGSTRÖM & FORSMAN 1973: 155].

$$ME = 1 - \frac{\sum_{i=1}^{n}(P_i - O_i)^2}{\sum_{i=1}^{n}(O_i - \overline{O})^2} \quad \text{with } ME \in]-\infty;+1] \tag{2.1}$$

with P_i modelled or predicted runoff data [mm/month]
O_i measured or observed runoff data [mm/month]
$\overline{O}$ mean of observed runoff [mm/month]

The fraction contains the variance of the residuals in the numerator and the variance of all observed runoff values in the denominator. If the residual variance exceeds the variance of observed runoff, the model efficiency becomes negative. But ME ≤ 0.0 means that accepting the model predictions is no better than using the mean of observed data. The index i can either be interpreted temporally or spatially. So values of ME can either be calculated for each catchment with the index i running through the months from January to December, or ME values are determined for each month with the index i standing for all the test catchments (see chapter 5.1).

2.2 Principal methodical problems

1. A fundamental problem is the method itself: runoff is naturally referred to basins but meteorologists and climatologists often work on the basis of rasters. The sum of aggrega-

ted grid areas is always unequal to the real catchment size and shape. Decreasing the raster size can only reduce but never remove the error. The smaller the catchment which is tried to be approximated by an aggregation of grid cells, the higher the percentage error becomes. This is why the size of the test catchments should not fall below 10.000 km².

A grid that refers to latitudes and longitudes has the additional disadvantage that the grid sizes differ in latitudinal direction. Table 2-1 gives an overview of 0.5° x 0.5° grid sizes of the study area. As a consequence at least absolute errors grow in N-S direction.

Table 2-1: Grid lengths in W-E direction and areas of 0.5° x 0.5° grids.

	grid length in latitudinal direction [km]	*grid area [km²]*
north border of the study area (73.0° N)	16.255	916.64
grid cell containing the city of Bonn (centre point: 50.75° N)	35.177	1955.76
south border of the study area (34.0° N)	46.093	2555.08

2. No routing model is coupled with the model to calculate the transport time of the water from its origin to the outlet of the basin. WABIMON only computes the water balance of each grid cell without any knowledge of all neighbouring cells. The assumption is that the total amount of a month‘s runoff – surface runoff, snow melt and base flow – reaches the outlet by the end of the month. The error of this assumption grows with the size of the watershed. For this reason catchment sizes should not exceed 50.000 km². This condition could not be fulfilled for the river Oka in Russia, a tributary of the river Volga, and the river Western Dvina, rising in the Russian Valdai Hills and flowing into the Baltic Sea near the city of Riga. Otherwise no test catchment of the European part of Russia could have been taken into account, since data of gauging stations were not available for smaller basins. It has to be emphasized that coupling a routing model would be imperative if the water balance model was used with a daily instead of a monthly time resolution.

3. A third problem arises from the fact that on the European scale a validation on the grid level is impossible due to lack of data. The validation on the catchment level by aggregation of the raster-based modelled runoff can only be second choice because errors in the model results of each contributing grid might equal each other out when they are aggregated. Therefore the model validation on the catchment level should turn out better than on the grid level. This has to be kept in mind when testing whether the model efficiency exceeds zero significantly on the catchment level (see chapter 5.3.5). If it is significantly higher than zero on the catchment level, it cannot be concluded that this is true on the grid level as well.

4. There are problems in the validation on the catchment level as well. First observed run-off data at the gauging station cannot be distinguished in the three components surface run-off, snow melt and base flow as the model does. The differentiation of surface runoff and base flow is almost impossible if data are only available as long-term means in a monthly

time resolution. Methods for separating base flow only exist for hydrographs with a daily time step [DEMUTH 1993, SCHWARZE ET AL 1991, SCHWARZE ET AL 1989, INSTITUTE OF HYDROLOGY 1980, KILLE 1970, WUNDT 1958, NATERMANN 1951]. Thus, a direct comparison of *each* of the three modelled runoff *components* with observed data is impossible. Evaluation of the model is reduced to the analysis of the residuals between modelled and observed *total* runoff.

Statements on the quality of certain modules of the model can only be made *indirectly*. The snow melt component of the observed runoff may be separated visually by interpreting runoff peaks that cannot be the impact of extreme precipitation events as snow melt. A regression analysis of modelled and measured total runoff can additionally give hints about an over- or underestimation of base flow.

5. The second problem concerning model validation on the catchment level is that the observed runoff at gauging stations often is not the result of the natural runoff regime. Reasons are man-induced changes of the runoff regime by reservoir management, diversion of stream water through channels, supply of drinking water from riverbank filtrate, industrial water use and discharge of industrial effluents and by agricultural irrigation.

6. As a last problem it should be mentioned that residuals between observed and modelled total runoff may not only be attributed to the bad quality of the modules computing surface runoff, snow melt and base flow, but may be explained by other parts of the water balance. An overestimation / underestimation of total runoff can as well be caused

- by an underestimation / overestimation of potential and actual evapotranspiration or
- by an overestimation / underestimation of precipitation.

Over- or underestimation of evaporation can easily occur, as the underlying equations are empirical and very simple (see chapter 3.1.2). Precipitation, the most important input data, can be inexact or rough, due to measurement errors and because there are uncertainties in the algorithm transforming point information of meteorological gauging stations to grid information. This error decreases with the number of meteorological stations within a grid cell. Since in the former USSR fewest stations are installed, precipitation input data are probably most inaccurate there.

Table 2-2: Summary of principal methodical problems.

➢ sum of areas of aggregated grids is unequal to real catchment size and shape
➢ no coupled routing model
➢ no validation on the grid level for the application on the European scale
➢ observed catchment runoff not exactly distinguishable in the three components surface runoff, snow melt and base flow
➢ man-induced changes of the natural runoff regime (e. g. by reservoirs and channels)
➢ errors in the precipitation and evapotranspiration fields

3 THE WATER BALANCE MODEL

3.1 Description of the used water balance model

The water balance model WABIMON which is used in this investigation is based on the ideas of THORNTHWAITE & MATHER (1957, 1955). Changes have already been made by WILLMOT ET AL (1985), VÖRÖSMARTY ET AL (1989), VÖRÖSMARTY & III MOORE (1991) and by the German FEDERAL INSTITUTE OF HYDROLOGY (1997).

WABIMON is a *conceptual*, *macro-scale* hydrological model. The range of scales in hydrology is generally smaller by at least one order of magnitude than that used in atmospheric sciences. In a special research programme of the Deutsche Forschungsgemeinschaft (DFG) "*macro-scale*" is referred to scales with lengths greater than 10 km and areas greater than 100 km² [BECKER ET AL 1999]. In contrast, SCHULTZ ET AL (1995: 40) define a hydrological model as "*macro-scale*" if considered lengths exceed 100 km and areas cover at least 10.000 km² respectively. Unfortunately, it is not made absolutely clear, whether lengths and areas have to be referred to the grid cells or the whole study area. According to the first definition, WABIMON operating on 0.5° x 0.5° grid cells is macro-scale, according to the second definition, it is not (compare Table 2-1). Relating the definitions to the study area covering a whole continent, WABIMON can be called macro-scale in both cases.

"*Conceptual*" models are based upon the idea of representing all phenomena "using either empirical formulas or the impulse response of subsystems" [SCHULTZ ET AL 1995: 36]. In contrast, physically-based models represent the catchment or grid cell behaviour "in terms of all differential equations discretized in time and space, expressing mass and momentum balance" [SCHULTZ ET AL 1995: 37]. Conceptual models are generally characterized by a lower degree of prior knowledge than physically-based models [FRANCHINI & PACCIANI 1990: 162]. Model parameters of conceptual models are not a priori known, but have to be calibrated by adjusting model results to measured data. Physical parameters can a priori be measured in the field – at least theoretically.

3.1.1 Gaining a first insight into the model structure

Figure 3-1 shows the model as a black box with its input and output data. WABIMON provides estimates of surface runoff, snow melt runoff and base flow on a monthly time scale. The three mentioned runoff components can be summed to total monthly runoff. In order to give runoff estimates, the model requires two kinds of input data:

- climatological data like monthly mean temperature and monthly precipitation,
- a set of physical geographic information which are needed to derive model parameters.

The model is realized as a program in the programming language Fortran 90. It has been programmed by Peter Krahé from the German Institute of Hydrology in Koblenz and has been extended during this study.

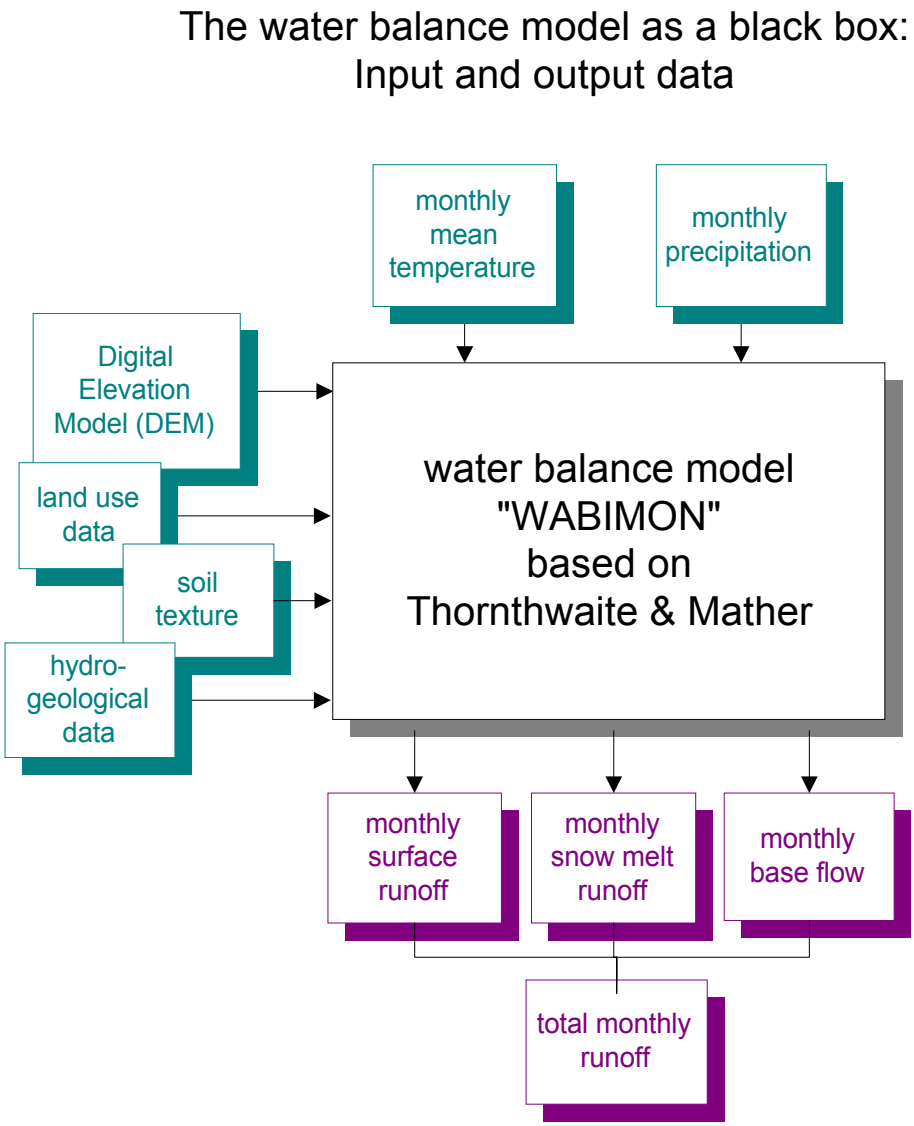

Figure 3-1: The water balance model as a black box – Input and output data.

The flowchart in Figure 3-2 can help to get an insight into the internal structure of the program. First, climatological and other GIS data as well as the configuration file with the calibration parameters are read into the memory. In the outer loop runoff values are computed for all land-surface cells. For each grid cell there is an inner loop for all months, in which the water balance is computed with the help of six modules. Appendix A provides graphical overviews of each of them.

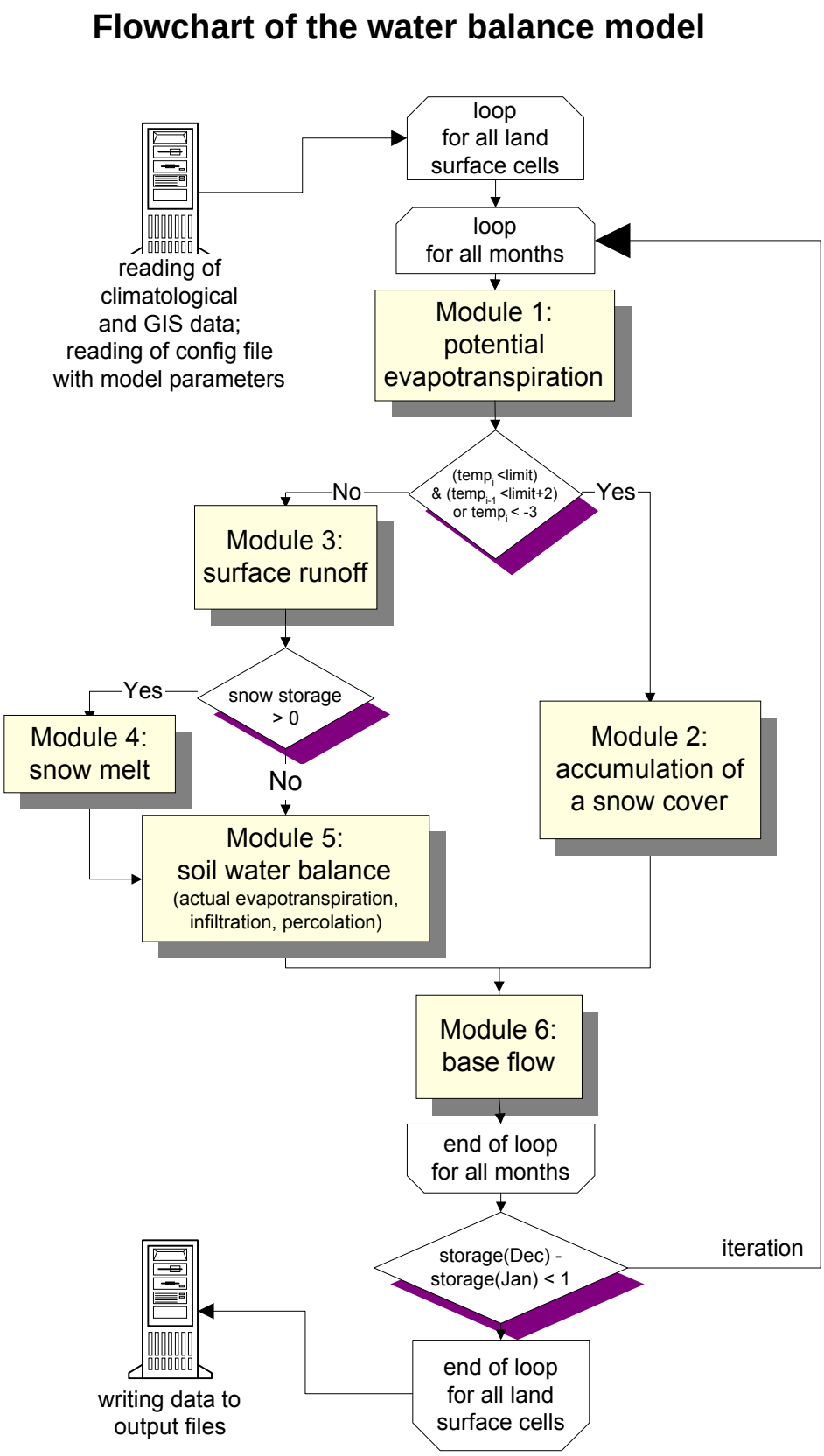

Figure 3-2: Flowchart of the water balance model. The iteration is only performed when working with long-term means, not when working with time-series.

3.1.2 Module 1: Potential evapotranspiration

Definitions

Evapotranspiration is the sum of evaporation, interception and transpiration. **Evaporation** means the direct evaporation from water bodies, the soil surface, the soil volume and the groundwater. **Transpiration** is defined as evaporation from the inner plants, and **interception** as the immediate evaporation from the plant surface [DIN 4049, ARBEITSGEMEINSCHAFT BODENKUNDE 1971: 74].

Definitions of potential evaporation are connected with the condition that the atmospheric transport capacity of water vapour must always be fully satisfied [BAUMGARTNER & LIEBSCHER 1990: 333]. Since this condition is clearly fulfilled on free water, **potential evaporation** is often defined as evaporation from free water.

The International Commission of Irrigation and Drainage (ICID) defines **potential evapotranspiration (ET_p)** for vegetated soils as the maximum amount of water vapour that is transferable per time unit from a totally or partly vegetated area with optimal and unhindered water and nutrient supply under the given meteorological, soil physical, vegetation specific and plant cultivational circumstances into the Atmosphere. [BAUMGARTNER & LIEBSCHER 1990: 334].

The fact that different ET_p-formulas result in different ET_p-estimates led to the definition of the **FAO grass reference evapotranspiration** [ALLEN ET AL 1994]. According to DVWK (1996), it substitutes the qualitative and therefore imprecise description of ET_p given by the ICID. The grass reference evapotranspiration is founded on the Penman-Monteith relation [MONTEITH 1973] and is defined as the evapotranspiration of grass of 12 cm height with a soil water content of at least 70 % of the available field capacity. The minimum surface resistance r_c is determined as 70 s/m. The aerodynamic resistance r_a results in 208 s/m for a wind speed of 1 m/s [WENDLING 1995: 602].

Thornthwaite formula of potential evapotranspiration

Several formulas – partly empirically, partly physically based – have been developed to estimate ET_p [VÖRÖSMARTY ET AL 1998, FEDERER ET AL 1996, DVWK 1996, DEYHLE 1995]. Unfortunately, almost all of them require meteorological input data like wind speed, vapour pressure and radiation (see Appendix B), which are not available on the European scale for this study. Therefore, these formulas could not be used on this macro-scale level.

Thornthwaite knew that ET_p mainly depends on the net radiational heating of the land surface and, to a lesser extent, on the wind speed, temperature and relative humidity. But since the net radiation flux at the surface was unavailable at the global scale, THORNTHWAITE (1948) decided to use the available surface air temperature as a substitute and developed an empirical formula that only needs temperature as input:

- the mean monthly temperatures and
- the long-term mean monthly temperatures.

$$ET_{p_i} = 16 \cdot d_i \left(\frac{10 T_i}{J} \right)^a \tag{3.2}$$

$$J = \sum_{k=1}^{12} \left(\frac{T_k^M}{5} \right)^{1.514} \tag{3.3}$$

$$a = 6.75 \cdot 10^{-7} J^3 - 7.71 \cdot 10^{-5} J^2 + 1.792 \cdot 10^{-2} J + 0.49239 \tag{3.4}$$

$$d_i = \frac{l_i}{12} \cdot \frac{n_i}{30} \tag{3.5}$$

with

	ET_p	monthly potential evapotranspiration in mm
	J	warmth index
	l_i	mean length of day in the i-th month [h]
	n_i	number of days in the i-th month
	T_i	monthly mean temperature [°C] of time series
	T_i^M	monthly mean temperature [°C], long-term means
	a	empirically derived exponent

If time series of mean monthly temperature are inserted in equation (3.2), time series of the sum of monthly ET_p will be computed. Optionally, these time series of temperature can be substituted by long-term means. If long-term monthly mean temperatures are inserted in equation (3.2) instead of time series, long-term means of the monthly ET_p are provided. For the model application on the European scale long-term means of monthly temperature are inserted because time series are not available.

This set of equations is only defined for positive temperatures T_i. Otherwise, the numerator of the fraction in equation (3.2) would be negative producing a senseless negative ET_p. In the program ET_p is generally set to zero in months with a temperature T_i lower than 0°C.

Furthermore, there are several restrictions due to the warmth index J. First the warmth index must not fall below zero, since in this case ET_p would be negative (d_i and T_i are positive) which again is senseless. Therefore, all long-term mean temperatures of equation (3.3) with $T_k^M < 0$ °C are set to zero. If the warmth index J itself becomes zero a second problem arises. Equation (3.2) is mathematically not defined if J in the denominator of the fraction equals zero. This second point is solved by setting ET_p to zero, if the warmth index is zero.

The purpose of the factor d_i in equation (3.2) is to take different day-lengths into consideration which influence the amount of ET_p. The day-length l_i of equation (3.5) is determined in a special subroutine as it depends on the latitude and the season.

Dependency on the vegetation cover

ET_p differs with stand heights and densities of vegetation [DVWK 1996: 39]. Evaporation determined by the Thornthwaite formula is the ET_p of "well-watered grass". Although Thornthwaite did not call it "grass reference evapotranspiration" in 1948, the estimates derived by his formula can approximately be understood as it.

In comparison to well-watered grass, ET_p is enlarged in forests and reduced in fallowed land and areas of dereliction. In fact, actual evapotranspiration from wet forest canopies during and after rainfall can even exceed ET_p of well-watered grass [LOCKWOOD 1995: 246]. The DVWK (1996: 49) provides month-depending coefficients for different crops varying between 0.65 in winter and 1.5 for completely developed stands. As neither these coefficients nor exact information on heights, densities or the leaf area index of the vegetation are available for all USGS land use classes on the European scale, ET_p estimates have not been corrected for the model applications performed here.

Restrictions concerned with the Thornthwaite formula

Thornthwaite developed his formula for a geographical region in the eastern and central USA that is generally dryer than Western Europe, especially in the second half of the year. Since relative humidity is not considered in his formula, this leads to an overestimation of potential evapotranspiration for Europe in the second half of the year [SCHRÖDTER 1985, SIEGERT & SCHRÖDTER 1975, UHLIG 1959] with the consequence of a systematic underestimation of total runoff.

MINTZ & SERAFINI (1992) justified the Thornthwaite approach on a global scale by comparing ET_p a) as calculated by Thornthwaite, b) as calculated by the physically based Penman formula [PENMAN 1948], c) as calculated by ZUBENOK (1965), who used the Budyko equivalent of the Penman equation, and d) as measured with lysimeters. They found out that the calculations of Zubenok and Penman and the lysimeter measurements are closer in phase to the declination of the sun than is the Thornthwaite calculation. This phase error was already noted by CHANG (1959) and by THORNTHWAITE & HARE (1965). It gives justice to the fact that in the extratropics the air temperature typically lags behind the sun declination by about a month.

Furthermore, Mintz & Serafini concluded – partly in contrast to Schrödter – that where the soil is moist the calculations of Thornthwaite and Budyko produce roughly the same results in the summer season in the extratropics. It is only in the winter extratropics, when both radiation and temperature are small, that the Thornthwaite calculation is larger than the Budyko calculation. But in regions of dry soil, the Thornthwaite calculation is always smaller than the one of Budyko [MINTZ & SERAFINI 1992: 19]. This underestimation of evapotranspiration will be a problem in the Mediterranean region.

In spite of these restrictions, the Thornthwaite formula is of great practical use: NOAA and the USDA use it to produce their weekly and monthly Palmer Drought Severity Index (PDSI) and Crop Moisture Index (CMI) maps [PALMER 1965, 1968]. The Canadian Climate Centre produces weekly maps of available soil moisture with it [LOUIE & PUGSLEY 1981].

3.1.3 Module 2: Accumulation of a snow cover

In the original model version of THORNTHWAITE & MATHER (1957), precipitation was assumed to fall as snow if the mean monthly temperature fell below -1°C. The snow was accumulated to a snow cover and was assumed not to melt till the next month with a mean temperature exceeding -1°C.

In the current version of the model this limit temperature is regarded as a calibration parameter. A snow cover is created either if the current mean monthly temperature is lower than -3°C or if both of the following conditions are fulfilled:

- the mean monthly temperature falls below the limit temperature and
- the mean temperature of the previous month was already less than 2°C higher than the limit temperature.

First applications of the model had revealed that the amount of snow melt was overestimated hinting that the accumulated snow cover was already overestimated. Obviously, precipitation of the in-between seasons with mean temperatures only slightly below the limit temperature falls partly as snow and partly as rain. The soil seems to be not yet cold enough for the snow to keep lying till the next month. Instead, the first snow in autumn already melts in the current month. With the introduction of the second condition two objectives are pursued. One the one hand, it is considered that snow will not keep lying if the previous month was still much warmer. On the other hand, the total amount of snow accumulation during winter months is reduced.

Hence, if the mentioned conditions are met, the snow storage STS is enlarged by the complete amount of precipitation P of that month (equation (3.6)). Actual evapotranspiration, surface runoff, snow melt runoff, infiltration into the soil and the percolation to the groundwater are all set to zero in this case.

$$STS_i = STS_{i-1} + P_i \tag{3.6}$$

with STS_i snow storage at the end of the actual month [mm]
STS_{i-1} snow storage at the end of the previous month [mm]
P_i precipitation = snowfall of the actual month [mm]

3.1.4 Module 3: Surface runoff

THORNTHWAITE & MATHER (1957) have neglected surface runoff at all. According to the theory of HORTON (1933), exceeding the infiltration capacity of the soil due to high precipitation intensities leads to surface runoff. For in humid climates this kind of runoff is very dominant, neglecting this process leads to an overestimation of actual evapotranspiration in evaporation-intensive summer months [KRAHÉ ET AL 1996].

FERGUSON (1996) published a model called changing-CN method to estimate monthly direct runoff in the Thornthwaite water balance. It consists of a further development of the SCS method of the U.S. Soil Conservation Service [SOIL CONSERVATION SERVICE 1972, 1986]. But this model cannot be embodied here for two reasons. Firstly, Ferguson's model, up to now, has only been calibrated for the climatic situation in the USA. In order to calibrate it for Europe, time series of daily precipitation would be necessary but are not available. Secondly, the changing-CN method does not apply to direct runoff during periods of significant snow melt [Ferguson 1996: 270], which are given in the study area.

The FEDERAL INSTITUTE OF HYDROLOGY (1997) introduced a module to estimate monthly surface runoff, that does not have to be calibrated with the help of daily precipitation data. Two different cases were regarded:

1. For each grid cell the portion of urbanized areas (variable *urban_p*) was determined with the help of a Geographic Information System. The urbanized areas were assumed to have a certain impervious area portion (variable *seal*), for example 60 %. So, the impervious area portion of the whole grid cell can be computed by equation (3.7). On these impervious areas 100 % of the monthly precipitation P_i becomes surface runoff which is expressed by equation (3.8).
2. For all non-urbanized areas a runoff factor (which is the relation of surface runoff to precipitation) is introduced which depends on the season. This differentiation is an attempt to simulate the dependence of infiltration on the actual soil water content. The higher the soil water content is, the less precipitation can infiltrate and the higher runoff factors have to be set. In summer soils are much dryer than in winter, thus, in summer the portion of surface runoff is lower than in winter. The FEDERAL INSTITUTE OF HYDROLOGY (1997) used a runoff factor of 15 % for January to April, 10 % for the summer months from May to September and 20 % for October to December. The surface runoff for non-urbanized areas is yielded by multiplying the monthly precipitation P_i by the portion of non-urbanized areas and by the actual runoff factor.

The sum of the two surface runoff components resulted in the total amount of surface runoff. The difference between monthly precipitation P_i and the total amount of surface runoff will be called effective precipitation $P_{eff,\,i}$.

The impervious area portion of urbanized regions (*seal*) and the runoff factors for each month (*runoff_factor*) can be used as calibration parameters. Since the variable *seal* is very insensitive on the macro-scale level of 0.5° x 0.5° grid size, it is held constant and set to 0.6 in all applications performed here.

For the current model applications this module has been expanded in two directions:

a) It is not only differentiated between urbanized and non-urbanized areas but between four classes of land use:
   - vegetation
   - water bodies (lakes and rivers)
   - snow and ice
   - urbanized areas

   100 % of the precipitation onto the water bodies and the snow and ice areas becomes surface runoff, see equations (3.9) and (3.10). Surface runoff for the urbanized areas is determined as described above (equations (3.7) and (3.8)). The runoff factors are only required for the vegetated areas (equation (3.11)).

b) Since runoff portions in reality do not only depend on the actual soil water content but on the slope steepness as well, runoff factors are additionally differentiated in a second dimension, that is concerning the relief. The steeper the slope, the higher the percentage of precipitation not infiltrating into the soil but flowing above-ground. Three relief classes are built from the mean slope of 2500 elevation pixels of the Digital Elevation Model within each 0.5° x 0.5° grid cell. In order to minimize the total number of calibration parameters, runoff factors for slopes lower than 2° are kept invariant and those for steeper slope classes are determined as a multiple of the originals. This approach manages with only two calibration parameters, *slope_fac1* and *slope_fac2* (see Table 3-1).

Table 3-1: Runoff factors in dependence of the season and the steepness of the mean slope of the grid cell (slope_fac1 and slope_fac2 are calibration parameters with slope_fac1 > 1.0 and slope_fac2 > slope_fac1).

	January - April	***May - September***	***October - December***
slope ≤ 2°	15 %	10 %	20 %
2° < slope ≤ 10°	15 % • slope_fac1	10 % • slope_fac1	20 % • slope_fac1
slope > 10°	15 % • slope_fac2	10 % • slope_fac2	20 % • slope_fac2

The sum of the four surface runoff components in equation (3.12) results in the total amount of surface runoff. As the percentage area portions of each land use class are considered, this sum represents an area-weighted mean. The second output value of this module, the effective precipitation, is calculated by subtracting the surface runoff from the monthly precipitation as done in equation (3.13).

$$imp = seal \cdot urban\_p \tag{3.7}$$

$$rsurf\_imp = P \cdot imp \tag{3.8}$$

$$rsurf\_ice = P \cdot ice\_p \tag{3.9}$$

$$rsurf\_water = P \cdot water\_p \tag{3.10}$$

$$rsurf\_veg = P \cdot veg\_p \cdot runoff\_factor[month, relief] \tag{3.11}$$

$$rsurf = rsurf\_water + rsurf\_veg + rsur\_ice + rsurf\_imp \tag{3.12}$$

$$P_{eff} = P - rsurf \tag{3.13}$$

with

P	precipitation [mm]
P_{eff}	effective precipitation [mm]
seal	degree of sealing (= 0.6)
imp	impervious area [%]
direct [month, relief]	proportion of direct runoff to precipitation
water_p	area fraction of water bodies [%]
veg_p	fraction of vegetated areas [%]
urban_p	fraction of urbanized areas [%]
ice_p	area fraction of snow & ice [%]
rsurf_water	surface runoff on water bodies [mm]
rsurf_veg	surface runoff in vegetated areas [mm]
rsurf_imp	surface runoff in impervious areas [mm]
rsurf_ice	surface runoff on snow & ice [mm]

3.1.5 Module 4: Snow melt

The energy that is required to melt snow is 335 Jg^{-1}. The amount and speed of snow melt is influenced by various parameters like radiation, sensible and latent heat fluxes which depend on air temperature and vapour pressure gradients, by the temperature and the amount of rain falling on the snow and by the temperature of the soil under the snow cover [BAUMGARTNER & LIEBSCHER 1990]. Radiation provides the greatest portion of energy especially in the mountains.

Due to lack of meteorological data THORNTHWAITE & MATHER (1957) tried to simulate snow melt runoff with the following two parameters:

- mean elevation of the grid cell,
- number of successive months with snow melt.

Elevation classes

THORNTHWAITE & MATHER (1957) differentiated two elevation classes: grid cells with a mean elevation of lower than 1600 meters and those with a higher mean elevation. After some model applications on the European level, it became clear that two elevation classes are insufficient to simulate snow melt because in the lowland snow melts much faster than in mountainous regions. On the basis of an analysis of the mean elevations within the test

catchments and their hydrographs of measured runoff, it was decided to build three elevation classes listed in Table 3-2.

Table 3-2: Elevation classes used for the model applications.

lowland	≤ 500 m
mountainous areas	> 500 – ≤ 1600 m
high mountains	> 1600 m

Number of successive months with snow melt

A simple counter calculates the number of successive months with snow melt. In the lowland nearly all of the accumulated snow melts in the first month of snow melt. In the high mountains, however, snow melt is delayed. Glaciers, typically, do not melt before summer. Thus, for all three elevation classes three subcases are differentiated (compare Table 3-3).

Table 3-3: Melting percentages for nine snow melt cases (smro = snow melt runoff, STS = snow storage, low1, low2, low3, mid1, mid2, mid3, high1, high2, high3 are the percentages by which the snow storage is reduced).

	number of successive months with snow melt		
	= 1	= 2	≥ 3
Lowland	$smro_i = STS_{i-1} \cdot low1$	$smro_i = STS_{i-1} \cdot low2$	$smro_i = STS_{i-1} \cdot low3$
Mountainous areas	$smro_i = STS_{i-1} \cdot mid1$	$smro_i = STS_{i-1} \cdot mid2$	$smro_i = STS_{i-1} \cdot mid3$
high mountains	$smro_i = STS_{i-1} \cdot high1$	$smro_i = STS_{i-1} \cdot high2$	$smro_i = STS_{i-1} \cdot high3$

Without a lower border the snow storage would never melt totally as the value 0.0 mm can only be approximated by these melting percentages. THORNTHWAITE & MATHER (1957), therefore, let the snow melt totally by setting the snow melt runoff equal to the snow storage if the snow cover at the end of the previous month was not deeper than 50 mm.

With this approach the model applications on the European scale led to a clear overestimation of snow melt runoff and an underestimation of base flow in cold climates. For this reason another solution of the above problem has been chosen here. In the current version of the model the snow storage is reduced down to a deepness of 30 mm. This rest is added to the effective precipitation (which was precipitation reduced by surface runoff). It infiltrates into the soil and percolates to the groundwater if the soil's water holding capacity is exceeded so that the amount of snow melt runoff is decreased and base flow is increased. This approach agrees with the perception that soils are very wet and their water content is near the water holding capacity after the snow cover has melted.

After the amount of snow melt is determined, the snow storage STS is reduced by it:

$$STS_i = STS_{i-1} - smro_i \tag{3.14}$$

with $smro_i$ snow melt runoff in the current month [mm]
STS_{i-1} snow storage at the end of the previous month [mm]
STS_i snow storage at the end of the current month [mm]

There is still one problem concerned with this solution. In elevation classes where calibration forbids to set the last of the three melting percentage to 1.0, there is no guarantee that the accumulated snow cover is melted completely during the summer months. In the High Mountains of the Alps and the Scandinavian Mountains the snow storage is that high in spring that the number of summer months with snow melt is insufficient to reduce the snow to an amount of 30 mm. Instead the snow storage at the end of the year can be higher than the one at the beginning. Modelled changes of the snow storage have to be considered when comparing measured and modelled total annual runoff.

3.1.6 Module 5: Soil water balance

As input data the module gets the potential evapotranspiration which has been calculated in module 1 (chapter 3.1.2), the effective precipitation that has been computed in module 3 (chapter 3.1.4) and the water holding capacity of the grid cell which is determined from soil texture and land use information (see chapter 4.2.2). The module provides predictions on a) the actual evapotranspiration, b) the changes in the soil storage due to infiltration, evapotranspiration and percolation processes and c) groundwater recharge.

3.1.6.1 Urbanized areas

Infiltration into the soil and percolation to the groundwater are set to zero for the impervious parts of urbanized areas. Even in areas which are not totally sealed by buildings, streets or paved places the soil is mostly so compressed that infiltration is very restricted.

In a first approximation actual evapotranspiration is set to zero as well for two reasons:

a) In sealed areas neither interception nor transpiration nor evaporation from the soil or the groundwater can occur.

b) Immediate evaporation from the sealed surface occurs but is restricted since precipitation is quickly drained through the canalization.

3.1.6.2 Snow & ice

Due to the snow or ice cover and the fact that the soil is frozen, infiltration of water into the soil is impossible. Therefore, infiltration and percolation are set to zero.

Evaporation from the snow surface occurs but only to a very limited amount. Evaporation from an ice cover is even lower. The reason is that the energy that must be provided for the evaporation of melted water or sublimation is a multiple of the one that is required to melt the snow (see Table 3-4).

Table 3-4: Energy expenditure for snow melting and snow evaporation (after BAUMGARTNER & LIEBSCHER 1990: 286-287*).*

	Energy expenditure in Jg^{-1}
melting of snow	335
evaporation of melted snow	2503
evaporation of snow (sublimation)	2838

RACHNER (1987) published results of snow evaporation measurements at the research station Harzgerode in the former German Democratic Republic. In addition, he gives an overview of field studies in other parts of Europe as they are reported in literature. According to his investigations in both parts of Germany and in Scandinavia, mean net evaporation from a snow cover varies between 0.00 – 0.36 mm/day, that is 0.0 – 10.8 mm/month. Extreme values of 0.4 – 1.3 mm/day have only been measured in the European part of the former USSR [ALPAT'V & PERCENOK 1963, cited from RACHNER 1987].

KONSTANTINOW (1966), cited from BENGTSSON (1980), summarizes Russian measurements and finds mean evaporation rates between 0.4 – 0.8 mm/day in spring. BENGTSSON (1980: 230) states:

"Evaporation from snow cover in sub-arctic areas is indeed moderate, since in the winter darkness very little solar energy is available and in spring air currents having the requisite combination of warmth and dryness are infrequent."

There are formulas to estimate snow evaporation [BENGTSSON 1980, RACHNER 1987] but they need meteorological input data like wind speed, vapour pressure or the dewpoint, which are not available on the macro-scale. Since snow evaporation is negligible for the water balance anyway, ET_a is also set to zero as a first approximation.

3.1.6.3 Water bodies

Infiltration and percolation again are regarded to be zero, since the model in general presupposes effluent[1] runoff conditions[2].

ET_a is set to ET_p only if precipitation is higher than or equal to ET_p. Otherwise it is set equal to the amount of precipitation. If precipitation exceeds ET_p, the surplus is simply regarded as surface runoff.

[1] In humide climates *effluent* runoff conditions are dominant. Under these conditions the stream's surface is part of the groundwater table so that it receives its water from the groundwater – in contrast to *influent* conditions where the water moves from the stream to the deeper groundwater which is typical for aride climates [HÖLTING 1996: 45, PRESS & SIEVER 1995: 258-259].

[2] This assumption does not always seem to be met as measured runoff of the river Rhône for example is sometimes lower downstream than upstream.

A brief comparison with real conditions reveals that this approach represents a quite profound simplification. In reality, in lakes and standing waters as well as in rivers ET_a and ET_p are always equal – independent of the amount of precipitation. If precipitation is lower than ET_p, water supply for evapotranspiration is guaranteed by the water storage of the lake or the current water contribution from the upstream part of a river (at least if the lake or river is not run dry). Continued evapotranspiration in lakes leads to a lower water-level and a reduced surface area of the lake. Rivers get low water and, depending on the shape of the valley, might diminish their surface area as well.

But since the model only receives the percentage area of water bodies within a grid cell, but is not provided with any vector information like stream lines or lake polygons, neither water-levels nor high or low flows of rivers nor variable surface areas of lakes nor the retention function of lakes can be modelled.

The latter point even evokes systematic errors on model results, because most water areas in the model are lakes[3] and floods are always weakened by lakes. Thus, in case of high-intensity rainfalls as well as snow melts the model systematically overestimates direct runoff.

3.1.6.4 Vegetated areas

This part of the module exactly follows the approach of THORNTHWAITE & MATHER (1957, 1955) and THORNTHWAITE (1948). General question for the soil water balance is whether the month is rather dry with the soil water moving upwards or rather moist with the soil water moving downwards.

→ ***Case A: Dry months***

If ET_p exceeds effective precipitation, the month is rather dry. In addition to the amount of effective precipitation a certain portion of the soil water evaporates (equation (3.17)). The water content of the soil decreases following the empirical e-function of equation (3.15). As the parameter a_{Thorn} in the exponent of the e-function is always positive (equation (3.16)), the new soil storage at the end of the actual month will be lower than at the end of the previous month. Percolation of soil water from the unsaturated zone to the groundwater is set to zero.

$$S_i = S_{i-1} \cdot e^{\left(-a_{Thorn}\left|P_{eff_i} - ET_{p_i}\right|\right)} \tag{3.15}$$

$$a_{Thorn} = \frac{\ln WHC}{(1.1282 \cdot WHC)^{1.2756}} \tag{3.16}$$

[3] Rivers are mostly too narrow to be represented by pixels in the resolution of the USGS landuse data set.

$$ET_{a_i} = P_{eff_i} + (S_i - S_{i-1}) \quad (3.17)$$

with
- S_{i-1} soil storage at the end of the previous month [mm]
- S_i soil storage at the end of the current month [mm]
- $P_{eff, i}$ effective precipitation of the current month [mm]
- $ET_{p, i}$ potential evapotranspiration of the current month [mm]
- $ET_{a, i}$ actual evapotranspiration of the current month [mm]
- WHC water holding capacity of the grid cell [mm]
- a_{Thorn} empirical parameter after Thornthwaite

→ ***Case B: Moist months***

Months in which effective precipitation exceeds ET_p are moist so that actual evapotranspiration can be equated to potential evapotranspiration (equation (3.18)).

$$ET_{a_i} = ET_{p_i} \quad (3.18)$$

The surplus of effective precipitation over actual evapotranspiration infiltrates into the soil and enlarges the soil water content. If the sum of the soil water content of the end of the previous month and the amount of infiltrating water exceeds the water holding capacity of the soil, percolation to the groundwater occurs (equation (3.20)) and the soil storage will be filled up to its water holding capacity at the end of the current month (equation (3.19)).

$$S_i = WHC \quad (3.19)$$

$$PERC_i = S_{i-1} + (P_{eff_i} - ET_{a_i}) - WHC \quad (3.20)$$

If the soil is able to hold the infiltrating water against its gravity (equation (3.21), percolation is zero as in the case of the dry soil. The meaning of the variables is the same as in the dry case.

$$S_i = S_{i-1} + (P_{eff_i} - ET_{a_i}) \quad (3.21)$$

3.1.7 Module 6: Base flow

BAUMGARTNER & LIEBSCHER (1990: 454) define base flow as that part of groundwater runoff that drains from a certain region into a receiving water and that can be recorded there together with other runoff components by a measuring device. Groundwater leaving the area subterranean is explicitly excluded in this definition.

The base flow module of the model requires information about the groundwater recharge (percolation) which has been determined in module 5 (chapter 3.1.6), the base flow of the last day of the previous month and the daily recession constant k as input data. In order to understand the model equations determining monthly base flow, the theory of the linear storage must first be explained in a short digression.

According to the theory of the linear storage, the emptying of the storage only depends on the storage content. In the case of zero groundwater recharge (percolation = 0 mm) outflow

of a storage Q and the corresponding storage content V are said to be proportional which is expressed by equation (3.22)[4]. The proportionality factor α can be interpreted as a depletion constant [DEMUTH 1993].

$$Q(t) = \alpha \cdot V(t) \tag{3.22}$$

with Q (t) base flow at time t [mm]
V (t) groundwater storage content at time t [mm]
t time [days]
α depletion constant [days^{-1}]

If no percolation of soil water into the groundwater occurs, the outflow Q(t) diminishes in relation to a certain starting value Q_0 according to the e-function of equation (3.23). According to DEMUTH (1993), AGUNG (1995), FEDERAL INSTITUTE OF HYDROLOGY (1997) and KRAHÉ ET AL (1997), this equation has first been published by BOUSSINESQ (1904) and is therefore called Boussinesq-equation. Other authors [HÖLTING 1996, BAUMGARTNER & LIEBSCHER 1990] put the formula down to MAILLET (1905). On a daily time step the term $e^{-\alpha}$ is substituted by k, which is a dimensionless parameter called daily recession constant. It represents the relation of the base flow of two successive days.

$$Q(t) = Q_0 \cdot e^{-\alpha \cdot t} = Q_0 \cdot k^t \tag{3.23}$$

Turning back from the digression to the model, equation (3.24) becomes understandable, determining base flow for each day of the current month with this assumption of a linear storage. In this case the amount of percolation is taken into account as well [FEDERAL INSTITUTE OF HYDROLOGY 1997: 34][5], assuming that the total monthly percolation $PERC_i$ is distributed equally among all days of that month.

$$BF_{i,j} = BF_{i,j-1} \cdot k + \frac{PERC_i}{d_i} \cdot (1-k) \qquad \forall j = 1, d_i \tag{3.24}$$

with k daily recession constant [dimensionless]
$Bf_{i,j}$ base flow at the j-th day (of the i-th month) [mm]
$PERC_i$ percolation in the i-th month [mm]
d_i number of days of the i-th month

Base flow of the i-th month BF_i is finally equal to the sum of all daily base flows $BF_{i,j}$ of that month:

$$BF_i = \sum_{j=1}^{d_i} BF_{i,j} \tag{3.25}$$

---

[4] According to Wittenberg (1997: 570), the relation between the storage content V(t) and base flow Q(t) is non-linear in general and can be described as follows: $V(t) = a \cdot Q(t)^b$. Only for the special case of b = 1 the storage becomes linear.

[5] THORNTHWAITE & MATHER (1957) in their original version of the water balance model also determined the current base flow in dependence of the base flow of the previous time step and the amount of monthly percolation. But they did not introduce recession constants depending on watershed conditions like hydrogeology, geology or soil texture. Instead they used constant factors of 0.5, invariant with time and space: $BF_i = 0.5 \cdot BF_{i-1} + 0.5 \cdot PERC$

3.1.8 Starting values and iterations

Computations begin with *provisional* starting values which are summarized in Table 3-5. *Final* starting values are derived iteratively, as shown in Figure 3-2 on page 11. After the six program modules have been run through for all twelve months, the difference of the soil storage of December and the provisional soil storage is investigated. As long as the difference exceeds 1 mm, a further iteration is necessary. December values serve as new starting values for the following iteration. If the difference is lower than 1 mm, December values serve as final starting values for the model application. After the final starting values have been found, the results of the next run are interpreted as model predictions and written to the output files.

Table 3-5: Provisional starting values for all model applications.

soil water storage [mm]	90 % of water holding capacity
snow storage [mm]	0.0
number of successive months without snowfall	0
base flow of the previous month [mm]	10.0

3.1.9 Summary of introduced model extensions

Table 3-6 gives a brief summary of the extensions that have been introduced step by step during the work with the model. For a deeper discussion see chapters 3.1.3 to 3.1.6.

Table 3-6: Summary of all introduced extensions of the model structure.

Module	***extension***	***reason***
Module 2: building of snow cover	snow cover only built if the mean temperature of the actual as well as the previous month is lower than the limit temperature plus 2 degrees	otherwise soil temperature is too high for the snow to remain for a whole month
Module 3: surface runoff	different computation of the surface runoff for the land use classes “water bodies“ and “snow & ice“	almost all precipitation becomes surface runoff in these regions
	introduction of three slope classes with different runoff factors	surface runoff depends on the steepness of a slope
Module 4: snow melt	snow melt calculation differentiated in three instead of only two elevation classes	faster snow melt in the lowland
	last 30 mm of the melting snow cover are added to the effective precipitation (→ snow melt runoff decreased; infiltration into the soil, percolation to the groundwater and base flow increased)	snow melt obviously does not only drain on the surface because soils are wet in the end of melting processes
Module 5: Soil water balance	different computation of infiltration/percolation and the actual evapotranspiration for the land use classes “water bodies“ and “snow & ice“; introduction of lake evaporation	obviously different processes than in vegetated areas

Normal distribution of temperatures

In the present version of the model the differentiation of months with a mean temperature lower or higher than the limit temperature is very rough. For months with a mean temperature that is five or more degrees lower or higher than the limit temperature this approach might be sufficient. But especially in the seasons with a mean temperature around the limit temperature, precipitation can fall as rain or snow depending on the actual temperature of the day. In those months the snow cover might be increased and decreased alternately. If the mean temperature is only one degree lower than the limit temperature, the increase of the snow coverage will be overestimated. In months with a mean temperature that is slightly over the limit temperature snow melt and surface runoff might be overestimated.

This problem gave grounds to test whether the assumption of a normal distribution of temperatures can improve the model. For a mean temperature equal to the limit temperature it is assumed that 50 % of the precipitation falls as rain and 50 % as snow. In all months with a mean temperature below the limit temperature the portion of snow exceeds the portion of rain and the other way around. As normal distributions require a mean and a standard deviation as parameters but only mean temperatures are given, the standard deviation is used as a calibration parameter and applications with a standard deviation of 1 and 2 (Table 3-7) are tested. Assuming a limit temperature of -1°C and a standard deviation of 2°C, the probability of exceeding the limit temperature is 69.15 % if the mean monthly temperature is -2°C. If, in addition, precipitation is assumed to be distributed equally on all days of the month[6], it can be derived that the probability of precipitation falling as snow is 69.15 % and as rain 30.85 %.

Table 3-7: Portions of snow and rain for different mean monthly temperatures (limit temperature = -1°C).

mean monthly temperature in °C	***standard deviation = 1°C***		***standard deviation = 2°C***	
	portion of snow [%]	*portion of rain [%]*	*portion of snow [%]*	*portion of rain [%]*
-5			97.72	2.28
-4			93.32	6.68
-3	97.72	2.28	84.13	15.87
-2	84.13	15.87	69.15	30.85
-1	50.00	50.00	50.00	50.00
0	15.87	84.13	30.85	69.15
1	2.28	97.72	15.87	84.13
2			6.68	93.32
3			2.28	97.72

[6] This assumption is very questionable, since the amount of precipitation varies extremely with time. It is possible that the whole amount of precipitation in that month has fallen in a few days with a temperature above the limit temperature, so that precipitation might have fallen completely as rain.

Unfortunately, this approach did not lead to an improvement of the model efficiency. Especially in the autumn months October and November residuals were even enlarged, since apart from the snow melt in spring the model generally produced a second snow melt peak in autumn.

3.2 Sensitivity of the calibration parameters

3.2.1 Limit temperature

The limit temperature can take on values between -2.5°C and -1°C. There is a reason for the fact that this interval is not symmetric around 0°C, the melting temperature of ice. In months with a positive mean temperature, there might be some days with the precipitation falling as snow which will, however, not remain until the end of the month. It will melt in the warmer days of the current month.

The lower / higher the limit temperature is set,

- the lower / higher the number of months with snow accumulation is,
- the earlier / later in the year snow melt starts and
- the lower / higher the total sum of snow melt is.

As for the European application temperatures are only given as integers, calibration is only performed for limit temperatures of the set {-2; -1}. For the regional application temperatures are given with one decimal place, so that calibration is carried out for values of {-2.5; -2.3; -2.0; -1.5; -1.0}.

3.2.2 Runoff factors

Runoff factors of the steeper relief classes (2° < slope ≤ 10° and slope > 10°) are determined with the help of the calibration parameters *slope_fac1* and *slope_fac2* which have to fulfil the following condition:

$$1.0 \leq slope\_fac1 \leq slope\_fac2$$

During the calibration process they are assigned all 20 possible value combinations resulting from Table 3-8.

Table 3-8: Calibration of slope_fac1 and slope_fac2.

slope_fac1 (2° < slope ≤ 10°)	*slope_fac2 (slope > 10°)*
1.0	1.5
1.1	2.0
1.3	2.5
1.5	3.0
1.7	

3.2.3 Melting percentages

The nine melting percentages *low1*, *low2*, *low3*, *mid1*, *mid2*, *mid3*, *high1*, *high2* and *high3*, which are used as calculation parameters, can take on values of the interval [0.0; 1.0] with rising values from the first to the third month of snow melt:

$$low1 \leq low2 \leq low3 \quad \wedge \quad mid1 \leq mid2 \leq mid3 \quad \wedge \quad high1 \leq high2 \leq high3$$

A melting percentage in the second or third month of snow melt can only be set to 0.0 if the one of the previous month has been set to 1.0. Otherwise there might be a non-meltable snow storage in the model. Among various possible shapes of hydrographs with a snow melt component two extreme types can be distinguished:

- If the rise of a hydrograph indicating snow melt is steep and sudden with a very pointed peak, this indicates that a high melting percentage for the first month can approximate measured values best. If the curve of measured monthly runoff shows a snow melt peak of just one month, the melting percentage of the first month should be 1.0, and 0.0 for all following months.
- If, however, the increase of observed runoff is flat and the snow melt peak has the form of a "convex hill", melting percentages should increase slowly for successive months. The percentages of melting snow will generally be smaller than in the first case.

Table 3-9 shows all melting percentages that have been tested during calibration. Sensitivity analysis has revealed that *low3* is actually not required in the model since the snow storage is already emptied within the first two months of snow melt. Since it is assumed that snow in higher elevation classes melts more slowly than in lower regions, only those combinations of Table 3-9 were used that meet all of the following conditions:

$low1 \geq mid1 \geq high1$

if $low1 = mid1$, then: $low2 \geq mid2$

if $mid1 = high1$, then: $mid2 \geq high2$

if $mid2 = high2$, then: $mid3 \geq high3$

Table 3-9: Calibration of the melting percentages (indices stand for 1., 2. and ≥ 3. month of snow melt).

elevation ≤ 500 m			**500 m < elevation ≤ 1600 m**			**elevation > 1600 m**		
low1	low2	low3	mid1	mid2	mid3	high1	high2	high3
1.0	0.0	0.0	0.0	0.2	0.3	0.0	0.2	0.3
0.9	1.0	0.0	0.0	0.2	0.4	0.0	0.3	0.5
0.8	1.0	0.0	0.0	0.2	0.5	0.1	0.2	0.3
0.7	1.0	0.0	0.0	0.2	0.7	0.1	0.3	0.5
0.6	1.0	0.0	0.1	0.2	0.3	0.2	0.4	0.5
0.5	1.0	0.0	0.1	0.3	0.5	0.3	0.5	0.6
0.4	1.0	0.0	0.2	0.4	0.6			
0.3	1.0	0.0	0.3	0.5	0.7			
0.2	1.0	0.0	0.3	0.6	1.0			
0.1	1.0	0.0	0.4	0.6	0.8			
			0.4	0.7	1.0			
			0.5	0.7	0.9			
			0.5	0.8	1.0			
			0.6	0.8	1.0			
			0.6	1.0	0.0			
			0.7	1.0	0.0			
			0.8	1.0	0.0			
			0.9	1.0	0.0			

3.2.4 Recession constant

Although the daily recession constant k of some test catchments is derived from hydrograph analysis (chapter 4.2.3), this is impossible for the majority of the grids. Therefore, it makes sense to investigate the impacts of different k-values and to use k as a calibration parameter as well.

According to equation (3.24), a high k increases the first summand $BF_{j-1} \cdot k$, a lower k increases the second summand $PERC_i / d_i \cdot (1-k)$. For this reason a high k produces a relatively uniform base flow curve. The difference between the maximum value in winter or spring and the minimum value in summer or autumn (range) is rather low since base flow of the actual month is mainly orientated towards the one of the previous month. As a consequence, the mean base flow level is more strongly influenced by the starting value than in the case of a low k. If the second summand increases due to a low recession constant, the range of base flow values rises because of the greater influence of percolation. As values of k usually vary within the interval of 0.91 and 0.99 (see Table 3-10), calibration runs are carried out with $k_1 = 0.91$, $k_2 = 0.92$ up to $k_9 = 0.99$.

Table 3-10: Upper and lower limits of the depletion constant α and the daily recession constant k.

	depletion constant α	daily recession constant k
high retention capacity	0.02	0.99
low retention capacity	0.10	0.91

4 DATA FOR MODEL INPUT AND VALIDATION

4.1 Data sources

Table 4-1 gives an overview of all GIS data used. All data sets from the US Geological Survey – land use data, the Digital Elevation Model and all derived data sets including the slope data set – are provided via internet in Lambert Azimuthal Equal Area projection. These data sets were reprojected to geographic coordinates (cell size 0.01°) with the help of the Geographic Information System Arc/Info. Regions outside the study area of 25°W-60°E and 34°-73°N were cut. Area-weighted means of elevation and slope were determined for each 0.5° x 0.5° grid cell with the help of the grid module of Arc/Info and saved as model input files. Soil texture data are already provided in geographic coordinates and did not have to be reprojected. But since the soil data set is delivered as a set of polygon coverages the relevant coverages had to be merged. Table 4-2 shows the sources of climatological model input data – temperature and precipitation – and hydrological data required for model validation.

4.2 Model input data

Model predictions are performed on a 0.5° x 0.5° raster with the grid cells covering different areas in longitudinal direction (see Table 2-1). Analyses in Arc/Info are performed in geographic coordinates as well, partly on a 0.01° x 0.01° resolution and partly on a 0.5° x 0.5° resolution. In various steps area-weighted means or sums had to be calculated so that grids with attribute information about the size of each grid cell in km were constructed (see Appendix C).

Model calculations are only performed for land surface cells, the oceans are generally excluded. A problem rises for all 0.5° x 0.5° grid cells which partly cover land areas and partly non-land areas. If those mixed land-ocean cells are excluded, some typical climatological and hydrological aspects of coasts, e. g. West-side climates in Scandinavia, cannot be investigated. Therefore, on the one hand, all 0.5° x 0.5° grid cells with a land surface area of more than 0 % should be included. On the other hand, runoff can only be predicted for all grid cells, for which all necessary input data are available. A grid called “land_mask“ containing all 0.5° x 0.5° grid cells fulfilling these two conditions is derived in Arc/Info (see Appendix C).

Portions of water bodies, of areas covered by snow and ice during the whole year and of urbanized areas are required as input data for the model. For details on their derivation see again Appendix C.

Table 4-1: Sources of GIS-data.

Data set	***Data source***	***Spatial resolution / scale***	***Original projection***	***Year of publication***	***Data format***	***Notes***
Digital elevation model (DEM)	United States Geological Survey (Eros Data Centre)	1 km	Lambert azimuthal equal area	--	Arc/Info raster image	downloadable from the internet: http://edcwww.cr.usgs.gov/landdaac/glcc/tablambert_euras_eur.html
Hydrologically correct DEM and derived data sets: • ***flow direction*** • ***flow accumulation*** • ***stream net*** • ***slope***	United States Geological Survey (Eros Data Centre)	1 km	Lambert azimuthal	Nov. 1998	Arc/Info raster image	downloadable from the internet: http://edcwww.cr.usgs.gov/landdaac/gtopo30/hydro/europe.html
Land use data	United States Geological Survey (Eros Data Centre)	1 km	Lambert azimuthal equal area	--	Arc/Info raster image	derived from satellite pictures spanning April 1992 through March 1993 downloadable from the internet: http://edcwww.cr.usgs.gov/landdaac/glcc/tablambert_euras_eur.html
Soil texture data	Food and Agriculture Organization (FAO) of the United Nations	--	Geographic coordinates	May 1994	Arc/info polygon coverages	digitized version of the Soil Map of the World published 1974-78 at 1:5.000.000 scale
Hydrogeological data	Bundesanstalt für Geowissenschaften und Rohstoffe (BGR) and Unesco	1:1.500.000		first sheet 1970 (not all sheets available yet)	analogous maps	received from the Geo-Center – Internationales Landkartenhaus (ILH)

Table 4-2: Sources of climatological and hydrological data for the Europe application.

Data set	***Data source***	***Spatial resolution***	***Time period***	***Temporal resolution***	***Data format***
Grid-based temperature and precipitation (long-term means)	International Institute for Applied System Analysis (IIASA) see LEEMANS & CRAMER (1990)	0.5° x 0.5°	1961 - 90	months	digital tables
Observed runoff at 29 gauging stations (time series)	Global Runoff Data Centre (GRDC)	--	1961 - 90 (partly missing)	months	digital tables
Observed runoff at 11 gauging stations (time series)	Global Runoff Data Centre (GRDC)	--	1961 - 90 (partly missing)	days	digital tables

4.2.1 Deduction of the watersheds from the Digital Elevation Model

In order to derive a stream net and watersheds from a Digital Elevation Model (DEM) the sinks in a DEM first have to be removed. A sink is an area surrounded by higher elevation values [ESRI 1994]. Some of these sinks, being areas of internal drainage, can be natural especially in glacial or karst areas [MARK 1988], but most of them represent imperfections in the DEM. The latter ones have to be filled to their pour point, the minimum elevation along their watershed boundary. The boundary of the filled area may create new sinks which then have to be filled in an iterative process. The version of the DEM with all unnatural sinks filled is called “hydrologically correct“ or “depressionless“.

In a second step, the direction of flow of each grid cell of the depressionless DEM is determined by finding the direction of steepest descent or maximum drop in a 3x3 cell neighbourhood. If the descent from all adjacent cells is the same, the neighbourhood is enlarged until the steepest descent is found [ESRI 1994]. This flow direction grid is then used to calculate the accumulated flow. The value of each output grid cell is the number of cells flowing into each cell. Cells with a high flow accumulation are used to identify stream channels.

Since November 1998 the US Geological Survey (USGS) offers a hydrologically correct DEM for Europe as well as the derived grids of flow direction and flow accumulation. The grids are in Lambert Azimuthal Equal Area projection with a spatial resolution of 1 km. Therefore a grid cell with a flow accumulation of 150 has a contributing area of exactly 150 km². On the basis of their flow accumulation grid river basins were delineated for all gauging stations of the European test catchments (see Appendix C).

4.2.2 Derivation of the water holding capacity

According to ROWELL (1997), DUNNE & WILLMOTT (1996), DVWK (1980) and THORNTHWAITE & MATHER (1957) the water holding capacity (WHC) is determined as the product of the available water capacity (aWC) and the rooting depth (see equation (4.26)) for each 0.01° x 0.01° grid cell.

$$WHC\,[mm] = aWC\left[\frac{mm}{dm}\right] \cdot depth\,[dm] \tag{4.26}$$

Estimations for the available water capacity are deduced from soil texture information. Rooting depths are derived from a combination of land use and soil texture. Different rooting depths are estimated for the summer and winter months, since especially the rooting depth of crops differs in these seasons. So two maps of WHC – one for summer and one for winter – are deduced as well (Figure 4-2).

Step 1: Preparation of the FAO soil texture information

Figure 4-1(a) shows the three FAO texture classes in relation to the USDA scheme:

a) *coarse (1)*: sands, loamy sands and sandy loams with < 18 % clay and > 65 % sand;
b) *medium (2)*: sandy loams, loams, sandy clay loams, silt loams, silt, silty clay loams and clay loams with < 35 % clay and < 65 % sand; the sand fraction may be as high as 82 % if a minimum of 18 % clay is present;
c) *fine (3)*: clay, silty clays, sandy clays, clay loams, with > 35 % clay.

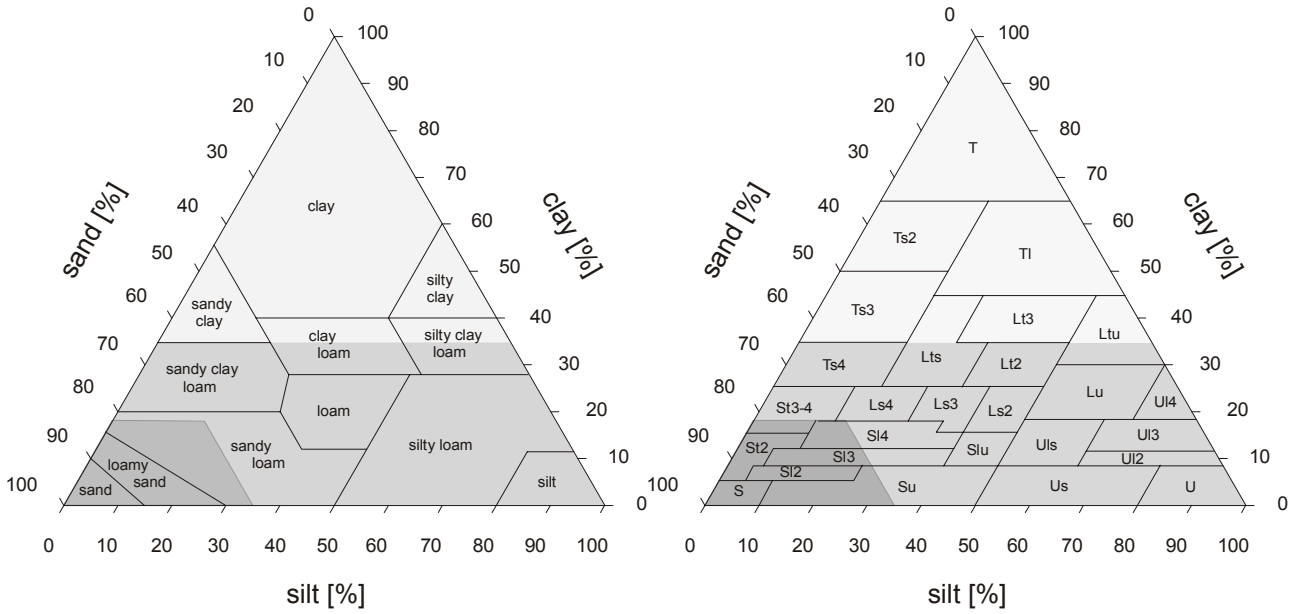

Figure 4-1: Comparison of texture triangles (a) USDA and FAO [after BMU 1995: 6.2-26], (b) DVWK and FAO [after DVWK 1980: 9-10, Arbeitsgemeinschaft Bodenkunde 1971: 36-38].

Strictly speaking, the German and the FAO classification schemes given in Figure 4-1(b) are not directly comparable since definitions of silt and sand differ slightly from each other in the Anglo-Saxon and German language areas (see Table 4-3). While being conscious of this methodical problem, the separates clay, silt and sand are treated the same.

Table 4-3: Upper and lower limits of separates clay, silt and sand (differences marked bold).

	Particle sizes in mm	
	FAO/USDA	Germany
clay	< 0.002	< 0.002
silt	0.002 – **0.05**	0.002 – **0.063**
sand	**0.05** – 2	**0.063** – 2

The textural class given in the mapping unit refers to the upper 30 cm of the dominant soil. When the soil of a digitized polygon is not homogeneous, it is regarded as being composed of one *dominant* soil and up to seven *component* soils. The latter are *associated* soils, covering at least 20 % of the area, and *inclusions*, important soils covering less than 20 % of the area. For each dominant and component soil the percentage of area is provided. Where two or three texture classes are indicated within one dominant or component soil, each is taken to apply to 50 or 33 % respectively of the soil unit. The separates of each

dominant and component soil had to be summed up in an area-weighted manner in order to get total percentages of coarse, medium and fine soils within a polygon.

Step 2: Derivation of the available water capacity grid from soil texture

The **field capacity (FC)** is the amount of water that a soil can hold against gravity after complete water saturation [SEMMEL 1983: 19]. The **permanent wilting point (PWP)** is the amount of water that is still in the soil when the turgidity of the plant does not return after water supply [SCHEFFER & SCHACHTSCHABEL 1992: 192]. The **available water capacity (aWC)** is defined as the difference of water amounts between the field capacity and the permanent wilting point [SCHEFFER & SCHACHTSCHABEL 1992: 197]:

$$aWK = FK - PWP \tag{4.27}$$

Valid units of field capacity, permanent wilting point and available water capacity are mm/dm, Vol.-%, Weight-% or l/m³ [SCHEFFER & SCHACHTSCHABEL 1992: 191/192, ARBEITSGEMEINSCHAFT BODENKUNDE 1971: 72/73].

The available water capacity depends on soil texture, bulk density, kind of peat, volume of substances, degree of decomposition and humus content and is different for gravels, grits and rocks [NIEDERSÄCHSISCHES LANDESAMT FÜR BODENFORSCHUNG 1992: VERKNÜPFUNGSREGEL 1.7]. Information are only available on soil texture in the three FAO classes “fine“, “medium“ and “coarse“. All soils are assumed to have a middle bulk density of 3. Humus content is assumed to be generally lower than 15 %. All other mentioned parameters cannot be considered at all.

The NIEDERSÄCHSISCHES LANDESAMT FÜR BODENFORSCHUNG (1992), DVWK (1982) and ROWELL (1997) published tables of mean FC and aWC depending on soil texture, with a diminishing degree of detail in the order of enumeration, but all based on the German texture triangle. Estimates of aWC vary within the interval of 6-25 mm/dm for mineral soil with organic matter of less than 15 %.

DUNNE & WILLMOTT (1996) published a table of estimated PWP, FC and aWC, based on the USDA texture triangle. They computed their estimates using linear regression equations of RAWLS ET AL (1982) and resulted in the interval of 4.3-17.6 mm/dm. In contrast to the publications above, they assumed zero organic matter. But since FC increases stronger with the content of organic matter than PWP does (presuming a constant soil texture), aWC increases with the content of organic matter as well [DUNNE & WILLMOTT 1996, RAWLS ET AL 1982]. This should be one reason for the fact that aWC estimates given by Dunne & Willmott are generally lower, varying in the interval of 4.3-17.6 mm/dm.

Estimations of DVWK (1982) are used for further investigations. Table 4-4 and Table 4-5 show the assignment of aWC to the German and FAO soil texture classes.

Table 4-4: Assignment of available water capacity to soil texture classes [after DVWK 1982: 3].

German soil texture		available water capacity [mm/dm]	FAO soil texture	
Sand	S			
Grobsand	gS	6	coarse	1
Mittelsand	mS	9	coarse	1
Feinsand	fS	12	coarse	1
schluffiger Sand	Su	18	medium/coarse	1/2
lehmiger Sand	Sl			
schwach lehmiger Sand	Sl2	16	coarse	1
schluffig-lehmiger Sand	Slu	19	medium	2
mittel lehmiger Sand	Sl3	17	coarse/medium	1/2
stark lehmiger Sand	Sl4	16	coarse/medium	1/2
toniger Sand	St			
schwach toniger Sand	St2	14	coarse	1
mittel-stark toniger Sand	St3	15	coarse/medium	1/2
Schluff	U	25	medium	2
sandiger Schluff	Us	22	medium	2
lehmiger Schluff	Ul			
schwach lehmiger Schluff	Ul2	25	medium	2
sandig-lehmiger Schluff	Uls	22	medium	2
mittel lehmiger Schluff	Ul3	24	medium	2
stark lehmiger Schluff	Ul4	21	medium	2
toniger Schluff	Ut			
schwach toniger Schluff	Ut2	25	medium	2
mittel toniger Schluff	Ut3	24	medium	2
starl toniger Schluff	Ut4	21	medium	2
sandiger Lehm	Ls			
schwach sandiger Lehm	Ls2	17	medium	2
mittel sandiger Lehm	Ls3	17	medium	2
stark sandiger Lehm	Ls4	17	medium	2
schluffiger Lehm	Lu	19	medium	2
toniger Lehm	Lt			
schwach toniger Lehm	Lt2	15	medium	2
mittel toniger Lehm	Lt3	15	fine	3
schluffig-toniger Lehm	Ltu	17	medium/fine	2/3
sandig-toniger Lehm	Lts	16	medium/fine	2/3
schluffiger Ton	Tu			
schwach schluffiger Ton	Tu2	14	fine	3
mittel schluffiger Ton	Tu3	15	fine	3
stark schluffiger Ton	Tu4	17	medium	2
lehmiger Ton	Tl	14	fine	3
Ton	T	15	fine	3

Table 4-5: Assignment of available water capacity to FAO soil texture classes resulting from Table 4-4.

Soil texture	Available water capacity in mm/dm
coarse	13.0
medium	20.0
fine	15.0

The available water capacity of each polygon is determined by an area weighted mean. For a polygon with total textural percentages of “coarse“ = 50 %, “medium“ = 30 % and “fine“ = 20 % aWC is computed as:

$$aWC = 0.5 \cdot 13.0 \frac{mm}{dm} + 0.3 \cdot 20.0 \frac{mm}{dm} + 0.2 \cdot 15.0 \frac{mm}{dm} = 15.5 \frac{mm}{dm} \quad (4.28)$$

An Arc/Info table containing the aWC value of each polygon is produced and joined with the soil coverage. Afterwards the coverage is converted to a grid with a cell size of 0.01°.

Step 3: Derivation of the routing depth grids from soil texture and land use

The *effective rooting depth* is the depth up to which the available water capacity is exhausted completely [DVWK 1980: 15]. This may be less than the total soil depth and even less than the depth of the rooted soil.

In order to derive a rooting depth grid, grids of soil texture and land use are required. Unfortunately, the soil texture polygon coverage cannot directly be converted to a grid, since it contains three attributes concerning texture: area percentages of coarse, medium and fine soil. Therefore a key summarized in Table 4-6 had to be found to represent each polygon by its dominant texture classes. All polygons can be assigned unambiguously. A polygon with 45 % coarse, 55 % medium and 0 % fine soils, is assigned to texture class 2 (coarse / medium) for example. But a polygon with 20 % coarse, 30 % medium and 50 % fine soils is assigned class 5 (fine). Grids of soil texture and land use are prepared – each in geographic coordinates and with a cell size of 0.01°.

Table 4-6: Definition of texture classes.

Texture class		***Description***
0	no soil	percentages of all three texture classes are zero (no soil, but water bodies, glaciers or bare rock)
1	coarse	percentage of texture class “coarse“ is maximum and at least 20 % higher than the second biggest texture class
2	coarse / medium	maximum difference between texture classes “coarse“ and “medium“ is 15 %; difference between the second and third biggest texture percentage is at least 10 % higher than the difference between the first and second biggest texture class
3	medium	percentage of texture class “medium“ is maximum and at least 20 % higher than the second biggest texture class
4	medium / fine	maximum difference between texture classes “medium“ and “fine“ is 15 %; difference between the second and third biggest texture percentage is at least 10 % higher than the difference between the first and second biggest texture class

5	fine	percentage of texture class “fine“ is maximum and at least 20 % higher than the second biggest texture class
6	coarse / fine	maximum difference between texture classes “coarse“ and “fine“ is 15 %; difference between the second and third biggest texture percentage is at least 10 % higher than the difference between the first and second biggest texture class
7	coarse / medium / fine	rest

Tables of crop rooting depth varying with soil texture are published by SCHEFFER & SCHACHTSCHABEL (1992: 199, TABLE 63), NIEDERSÄCHSISCHES LANDESAMT FÜR BODENFORSCHUNG (1992: VERKNÜPFUNGSREGEL 1.6) and DVWK (1980: 18, TABLE 17). They agree with each other that crops root to a depth of 5-7 dm in sands, 8-9 dm in silty or clay sands and 10-11 dm in silts, loams and clays. Thus, especially in sands rooting depth is reduced.

Tables of *effective* rooting depth varying with land use are published by BMU (1995: 6.2 - 27, TABLE 4) and WEBB & ROSENZWEIG (1993: 105, TABLE 4). BMU estimates rooting depth of pastures as 4.5 dm, of cropland as 5.5 dm and of forests as 12.5 dm, whereas Webb & Rosenzweig give higher estimates for forests. According to them, woodland, deciduous and evergreen forests have a rooting depth of 20 dm. They do not provide values for cropland or pasture. The rooting depth of Tundra is estimated at 1 dm. No differentiation is made, however, concerning herbaceous, wooded or bare ground tundra.

CANADELL ET AL (1996) published *maximum* (not effective) rooting depths across 11 terrestrial biomes at the global scale after compiling a total of 290 observations of rooting depth which covered 253 different plant species. Table 4-7 summarizes their findings that can only serve as a relative clue for effective rooting depths. For example it is important to know that roots of boreal forests are less deep than those of temperate forests and that shrubs are deeper rooted than temperate trees.

Table 4-7: Maximum rooting depths of several biomes and functional groups according to CANADELL ET AL (1996).

Biome or functional group	maximum rooting depth in dm (mean and standard error)
Cropland	21 ± 2
Temperate grassland	26 ± 2
Boreal forests	20 ± 3
Temperate coniferous forests	39 ± 4
Temperate deciduous forests	29 ± 2
Tundra	5 ± 1
Shrubs	51 ± 8
Herbaceous plants	26 ± 1

Table 4-8: Rooting depth in summer (in dm) – depending on land use and soil texture.

texture class / USGS land use class	1 coarse	2 coarse / medium	3 medi-um	4 medium / fine	5 fine	6 coarse / fine	7 mix
1 Urban and built-up land	0	0	0	0	0	0	0
2 Dryland cropland and pasture	5	7	11	10	10	6.5	8
3 Irrigated cropland and pasture	5	7	11	10	10	6.5	8
5 Cropland/grassland mosaic	7.5	9.5	11.5	11	11	8.5	10
6 Cropland/woodland mosaic	8.5	12.5	18	17.5	15.5	11	13
7 Grassland	10	11	12	12	12	11	11
8 Shrubland	10	12	15	15	14	11.5	12.5
9 Mixed shrubland/grassland	10	11.5	13.5	13.5	13	11	12
10 Savanna	4	4	4	4	4	4	4
11 Deciduous broadleaf forest	12	18	25	23	21	16	19
12 Deciduous needleleaf forest	10	12	18	17	15	11	13
13 Evergreen broadleaf forest	12	18	25	23	21	16	19
14 Evergreen needleleaf forest	10	12	18	17	15	11	13
15 Mixed forest	12	18	25	23	21	16	19
16 Water bodies	0	0	0	0	0	0	0
17 Herbaceous wetland	5	8	10	10	9	7	8.5
18 Wooded wetland	10	15	20	20	18	14	15.5
19 Barren or sparsely vegetated	0.5	0.5	0.5	0.5	0.5	0.5	0.5
20 Herbaceous tundra	1	2	3	3	2.5	2	2
21 Wooded tundra	3	4	5	5	4.5	4	4
22 Mixed tundra	2	3	4	4	3.5	3	3
23 Bare ground tundra	0	0	0	0	0	0	0
24 Snow or ice	0	0	0	0	0	0	0

Table 4-9: Rooting depth in winter (in dm) – depending on land use and soil texture.

texture class / USGS land use class	1 coarse	2 coarse / medium	3 medi-um	4 medium / fine	5 fine	6 coarse / fine	7 mix
1 Urban and built-up land	0	0	0	0	0	0	0
2 Dryland cropland and pasture	2	2	2	2	2	2	2
3 Irrigated cropland and pasture	2	2	2	2	2	2	2
5 Cropland/grassland mosaic	2.5	3	4	4	3.5	3	3
6 Cropland/woodland mosaic	5	7	10	10	9	7	8
7 Grassland	10	11	12	12	12	11	11
8 Shrubland	10	12	15	15	14	11.5	12.5
9 Mixed shrubland/grassland	10	11.5	13.5	13.5	13	11	12
10 Savanna	4	4	4	4	4	4	4
11 Deciduous broadleaf forest	12	18	25	23	21	16	19
12 Deciduous needleleaf forest	10	12	18	17	15	11	13
13 Evergreen broadleaf forest	12	18	25	23	21	16	19
14 Evergreen needleleaf forest	10	12	18	17	15	11	13
15 Mixed forest	12	18	25	23	21	16	19
16 Water bodies	0	0	0	0	0	0	0
17 Herbaceous wetland	5	8	10	10	9	7	8.5
18 Wooded wetland	10	15	20	20	18	14	15.5
19 Barren or sparsely vegetated	0.5	0.5	0.5	0.5	0.5	0.5	0.5
20 Herbaceous tundra	1	2	3	3	2.5	2	2
21 Wooded tundra	3	4	5	5	4.5	4	4
22 Mixed tundra	2	3	4	4	3.5	3	3
23 Bare ground tundra	0	0	0	0	0	0	0
24 Snow or ice	0	0	0	0	0	0	0

According to THORNTHWAITE & MATHER (1957: 244, TABLE 10), alfalfa, pastures and shrubs have deep roots of 10 dm or more. Corn, cotton, tobacco and cereal grains have a medium root depth of 5-10 dm and crops like spinach, peas, beans, beets and carrots shallow roots of 2.5-6.2 dm depth, always varying with soil texture. According to ROWELL (1997: 436, TABLE 12.2) roots of crops like barley, maize and wheat are deeper than 10 dm, followed by peanuts, beans, grasses, potatoes and vegetables, the latter with a root depth of 3-6 dm. DARDANELLI ET AL (1997) studied rooting depth of different crops like maize, peanut, soybean, sunflower and alfalfa, ranging from 13 (soybean) to 29 dm (sunflower).

Table 4-8 and Table 4-9 show rooting depths that have been assigned for the current study here. Rooting depth in urban and built-up land, water bodies and snow and ice (land use classes 1, 16 and 24) are generally set to zero. USGS land use class 4 (mixed dryland / irrigated cropland and pasture) does not occur in the study area and is therefore not listed.

For vegetated areas higher values of rooting depth are assigned for medium and fine texture classes, lower for coarse textures. Following Webb & Rosenzweig and BMU, forests are assigned a rooting depth of 12-25 dm, with lower values in the interval of 10-18 dm for boreal forests, which are mainly summed up as evergreen and deciduous needleleaf forests in the USGS classification (land use classes 12 and 14). Central European forests are considered as woodland (land use class 6 = “Cropland/Woodland mosaic“). Unfortunately, cropland and pasture were not isolated in separate land use classes by the USGS. Therefore, mixed cropland and pasture are assigned values between 5-11 dm in accordance with Thornthwaite & Mather and Rowell. Rooting depth of Tundra vegetation classes is assigned 1-5 dm following Webb & Rosenzweig and Canadell et al. Rooting depths of summer and winter only differ from each other in land use classes with cropland (classes 2, 3, 5 and 6), since most crops are only cultivated in summer.

Step 4: Derivation of the water holding capacity grid from aWC and rooting depth

The WHC grid is computed by a simple multiplication of the aWC grid and the rooting depth grid (see equation (4.26)). Afterwards a resampling to a cell size of 0.5° is performed in an area-weighted manner considering that the 0.01° x 0.01° grid cells have different areas in longitudinal direction. Figure 4-2 shows the results.

Maximum WHC values of more than 300 mm – regionally up to 450 mm – are predominant in the taiga belt with its evergreen Boreal Forests and in needleleaf forests of High Mountains (land use classes 13 and 14) like the Alps or in the south of Norway.

In the barren or sparsely vegetated deserts, semideserts and steppes (land use class 19) in the region north of the Caspian Sea and between the Caspian and the Aral Sea as well as in the Iranian salty deserts, *minimum* WHC values of mostly lower than 5 mm can be found during the whole year. In the ice-covered central part of Iceland the WHC is always zero.

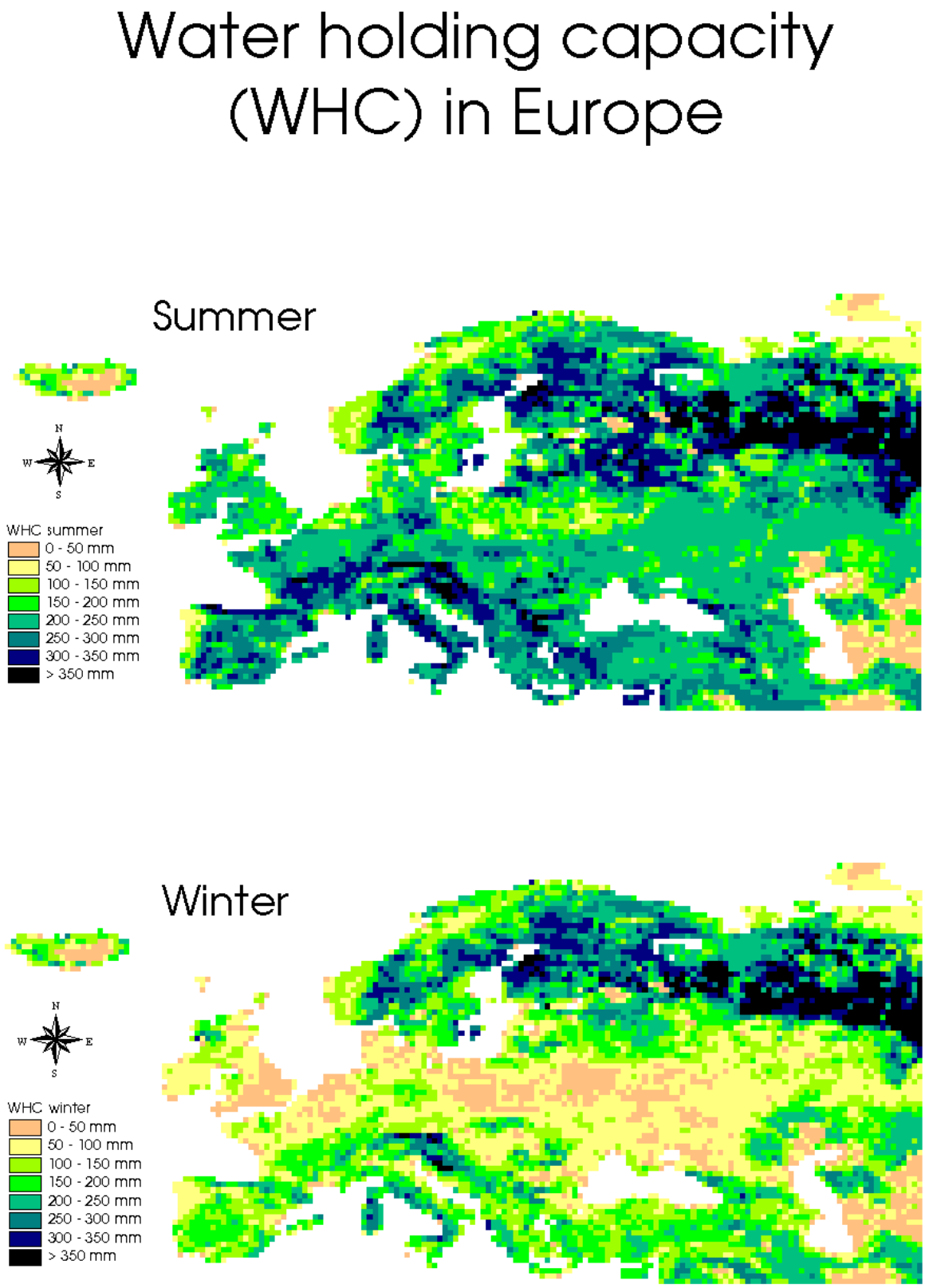

Figure 4-2: Derived water holding capacities (WHC) for summer and winter seasons.

Especially in regions with predominant cropland and pasture (land use class 3) – which is the flatland belt from the South of England passing the North of France and Germany till Belarus and the regions north of the Black Sea – WHC values differ strongly between summer and winter. In winter minimum values of lower than 50 mm are prevalent. In summer the soil's WHC rises up to 200 mm in these regions.

Less extreme differences between summer and winter WHC values can be found in regions with mixed cropland and woodland (land use class 6) like large parts of Spain, the South of France, Italy, Ex-Yugoslavia, Western Turkey and a broad latitudinal belt directly south of the Boreal Forests in Russia. Low differences between summer and winter WHC can additionally be found in regions with mixed cropland and grassland (land use class 5) like Ireland, several parts of Southern Germany and areas north-east of the Carpathians.

Conspicuously, the north-west of the Iberian Peninsula shows a rather low WHC of 50 - 100 mm during the whole year. This region has falsely been designated as "savanna" in the USGS land use classification. In fact, its acid brown soils are rather infertile and unproductive and most of them can only be used as pastures. However, it is by no means a "savanna". But it is in accordance with reality that WHC values are lower there than in the rest of Spain and Portugal.

Discussion of the resulting WHC estimates

DUNNE & WILLMOTT 1996 have published a global data set of plant-extractable water capacities of soil for the whole world. In contrast to Figure 4-2, summer and winter situations have not been distinguished. According to their estimates for the European continent, WHC is lower than 50 mm in Norway, Northern Ireland, the Russian tundra and in some areas between the Black and Caspian Seas. WHC values of 50-100 mm are found to be predominant in Sweden, Southern Finland, in the High Mountains of the Alps and north and east of the Caspian Sea. A large belt south of the Russian Boreal Forests, the middle part of Spain, Turkey, Greece and some regions north of the Black Sea are marked to have a WHC of 100-150 mm. The soils of all remaining parts of Europe, especially the Russian taiga belt with its Boreal Forests, are estimated to hold more than 150 mm of plant-extractable water [DUNNE & WILLMOTT 1996: 852].

Comparing these results with those of Figure 4-2, it can be recognized that the estimates of Figure 4-2 are generally higher. Cropland where even the mean values of estimated summer and winter WHCs of Figure 4-2 still fall below those of Dunne & Willmott represent an exception. But both studies are in accordance with each other that maximum WHC values of the European continent can be found in the Russian taiga belt.

A possible overestimation of available water capacity and / or rooting depth leads to an overestimation of the size of maximum soil water storage respectively. This has several consequences on the hydrological cycle. Looking upwards into the atmosphere, it can be said that the soil water storage controls how much precipitation can potentially be transpired back into the atmosphere via plants or directly from the soil surface [MILLY & DUNNE 1994]. ZUBENOK (1978) found that a given percentage change of storage capacity typically gives a percentage change in evaporation that is an order of magnitude smaller. Increased evapotranspiration leads to an enlarged relative humidity, an increased latent heat flux from the soil into the atmosphere and a reduction of sensible heat at the soil surface that is equivalent to cooling [KLEIDON & HEIMANN 1998a]. MILLY & DUNNE 1994 show that precipitation increases with enlarged evaporation. Looking downwards into the deeper soil, it can be recognized that an overestimation of the soil‘s storage capacity reduces percolation, groundwater recharge and base flow step by step [KLEIDON & HEIMANN 1998a and 1998b, MILLY & DUNNE 1994].

4.2.3 Derivation of the recession constant from measured daily runoff

Theoretical background for the derivation of the daily recession constant by hydrograph analysis builds equation (3.23). Finding the logarithm transforms equation (3.23) into the linear equation (4.29). The depletion constant α can then be interpreted as the slope of a straight line in a simple logarithmic co-ordinate system with t on the abscissa and ln Q (t) on the ordinate [DEMUTH 1993: 80].

$$\ln Q(t) = \ln Q_0 - \alpha \cdot t \tag{4.29}$$

with

	Q (t)	base flow at time t [mm]
	Q_0	base flow starting value [mm]
	t	time [days]
	α	depletion constant [$days^{-1}$]
	k	daily recession constant [dimensionless]
	K	monthly recession constant [dimensionless]

DEMUTH (1993) developed a method called DEREC2 to separate depletion segments from hydrographs of time series of daily runoff. These segments must fulfil the following conditions:

- Runoff must always be lower than the mean runoff MQ.
- The starting value of the segment must be at least two days later than the peak of the last ascent.
- All depletion curves (segments) must have a minimum duration of seven successive days with at least three decreasing runoff values at the beginning. Small peaks are smoothed.

The segments are sorted by their length and then aggregated to classes of depletion curves having the same length. A middle depletion curve **A*** is estimated by a regression model minimizing residual squares. Curve A* is moved in positive y-direction to the maximum starting value of the depletion segments and is now called **A‘**. Each individual depletion curve is then shifted in positive x-direction, until their starting values intersect A‘. The distance t_k between the original position of a segment‘s starting point $Q_{0,k}$ and the depletion curve A‘ is calculated by equation (4.30) [DEMUTH 1993: 85].

$$t_k = \frac{\ln\left(\frac{Q_{0_k}}{Q'(t)}\right)}{\alpha'} \tag{4.30}$$

with $Q_{0,k}$ starting value of segment k
$Q'(t)$ runoff at time t according to the depletion curve A‘
α' depletion constant according to the depletion curve A‘
t_k distance between starting point of segment k and the destination curve A‘

In a last step, a depletion curve **A** is determined by a new regression model based on the repositioned segments. The starting value Q_0 of the depletion curve A is equal to the maximum starting point of the segment.

The described algorithm has been programmed in Fortran by Christoph Franzen of the Federal Institute of Hydrology in Koblenz. His programs “Ast Version 4.1“ and “Trck Version 3.2“ were used to determine depletion curves for eleven European test catchments. The corresponding depletion constants α are required to compute the daily recession constants defined in equation (4.31). A daily recession constant k represents the relation of the base flow of two successive days. The half-time is equal to the time $t_{0.5}$, after that base flow is half the value of its starting value (see equation (4.33)). The higher α is, the lower k and $t_{0.5}$ get and the steeper the depletion curve becomes. A steep depletion curve is a hint at a low, a shallow curve is a hint at a high retention capacity of the aquifer.

Table 4-10 gives an overview of all base flow parameters for the Europe model applications.

$$e^{-\alpha} = k \tag{4.31}$$

$$Q(t) = Q_0 \cdot k^t \tag{4.32}$$

$$t_{0.5} = \frac{\ln 2}{\alpha} \tag{4.33}$$

Table 4-10: Depletion constants, half-times and daily recession constants derived after DEREC2.

catchment (gauging station)	***considered time period***	***starting value***	***depletion constant***	***daily recession constant***	***half-time***	***root mean square***
		Q_0 [m³/s]	α	$k_2 = e^{-\alpha}$	$t_{0.5} = \frac{\ln 2}{\alpha}$	RMS
Weser (Vlotho)	01.01.1961 - 31.12.1990	157	0.02492	0.9754	27.815	49.71
Rhine (Rheinfelden)	01.01.1961 - 31.12.1990	969	0.02588	0.9745	26.783	222.05
Mosel (Cochem)	01.01.1961 - 31.12.1990	313	0.06053	0.9413	11.451	90.6
Maas (Borghaven)	01.01.1961 - 31.12.1990	222	0.08653	0.9171	8.010	60.48
Kymijoki (Anjala)	01.01.1961 - 31.12.1990	292	0.02542	0.9749	27.268	56.68
Kenijoki (near mouth)	01.01.1961 - 31.12.1990	541	0.04647	0.9546	14.916	23.26
Weser (Intschede)	01.01.1961 - 31.12.1990	318	0.03161	0.9689	21.928	72.87
Inn (Passau-Ingolstadt)	01.01.1961 - 31.10.1989	680	0.04043	0.9604	17.144	153.13
Garonne (Mas-D'agenais)	01.01.1961 - 31.12.1979	567	0.04845	0.9527	14.306	232.44
Rhône (Chancy)	01.01.1961 - 31.12.1990	277	0.02516	0.9752	27.550	80.94
Rhône (Beaucaire)	01.01.1961 - 31.12.1979	1598	0.05126	0.9500	13.522	384.13

4.2.4 Derivation of the recession constant from hydrogeology

For the remaining test catchments, for which daily runoff is not available, the recession constant is tried to be estimated from hydrogeological information. Several authors have stressed that the role of geology is important for the estimation of base flow and recession constants, e.g. WRIGHT (1970) and (1974) for Scotland and south-east England, PEREIRA & KELLER (1982) for the Pre-Alps, GUSTARD ET AL (1992) for the United Kingdom.

DEMUTH & HAGEMANN 1994a, 1994b and DEMUTH 1993 have published a hydrogeological index for use in statistical regionalization models to estimate low flow parameters at ungauged sites. They carried out a multiple regression analysis relating known recession constants, which had been determined by analysis of daily measured runoff, to hydrogeological classes. Daily recession constants for summer and winter, k_s and k_w, are understood as a function of 14 independent input variables, the hydrogeological classes HG_1 to HG_{14}. They were derived from the Hydrogeology Map (scale 1:500.000) and the Geology Map (scale 1:600.000) of Baden-Württemberg. Table 4-11 describes the original hydrogeological classes defined by Demuth & Hagemann. The resulting regression equations for the summer (4.34) and winter (4.35) season have the following form:

$$k_s = 0.84 \cdot (HG_1 + 1)^{-2.67} \cdot (HG_2 + 1)^{0.28} \cdot (HG_3 + 1)^{0.16} \cdot (HG_4 + 1)^{-0.19} \cdot (HG_5 + 1)^{0.18} \cdot (HG_6 + 1)^{0.05} \cdot (HG_7 + 1)^{0.12} \cdot (HG_8 + 1)^{0.39} \cdot (HG_9 + 1)^{0.18} \cdot (HG_{10} + 1)^{0.08} \cdot (HG_{11} + 1)^{0.10} \cdot (HG_{12} + 1)^{0.15} \cdot (HG_{13} + 1)^{0.17} \cdot (HG_{14} + 1)^{0.16} \quad (4.34)$$

$$k_w = 0.87 \cdot (HG_1 + 1)^{0.72} \cdot (HG_2 + 1)^{0.05} \cdot (HG_3 + 1)^{0.12} \cdot (HG_4 + 1)^{-0.09} \cdot (HG_5 + 1)^{0.15} \cdot (HG_6 + 1)^{0.08} \cdot (HG_7 + 1)^{0.08} \cdot (HG_8 + 1)^{0.16} \cdot (HG_9 + 1)^{0.11} \cdot (HG_{10} + 1)^{0.07} \cdot (HG_{11} + 1)^{0.08} \cdot (HG_{12} + 1)^{0.09} \cdot (HG_{13} + 1)^{0.11} \cdot (HG_{14} + 1)^{0.12} \quad (4.35)$$

In order to derive daily recession constants for ungauged European catchments, the International Hydrogeological Map of Europe with the much lower scale of 1:1.500.000 was utilized. This map contains hydrological information concerning groundwater occurrence and productivity and geological information on the rock formation of the aquifer. But the definition of the hydrogeological classes is generally different from that of the Hydrogeology Map of Baden-Württemberg so that the 14 classes cannot be transmitted directly. The daily available water yield, for example, was one criteria for the separation of the original 14 HG classes. But the International Hydrogeological Map does not contain any figures of daily available water yield as does the Hydrogeology Map of Baden-Württemberg.

Two ways of solving this problem have been thought through: The first possibility is to keep the given regression equations and find a key to relate the 14 hydrogeological classes to those of the International Hydrogeological Map by uniting some classes and simplifying the original regression equations accordingly. For example HG_{13} and HG_{14} could be combined to a hydrogeological class called $HG_{13;14}$. The exponents of the last two factors in equation (4.34) are first replaced by their arithmetic mean, which is a legal approximation:

$$(HG_{13} + 1)^{0.165} \cdot (HG_{14} + 1)^{0.165} \quad (4.36)$$

In order to be able to insert the sum of HG_{13} and HG_{14} together into the equation, it was thought to substitute these two factors by one in a second step:

$$(HG_{13;14} + 1)^{0.165} \quad (4.37)$$

But this simplification is mathematically inadmissible and leads to arbitrary results, since:

$$a^x \cdot b^x = (a \cdot b)^x \neq (a + b)^x \quad (4.38)$$

Besides if $a = (HG_{13} + 1)$, $b = (HG_{14} + 1)$, and $HG_{13} + HG_{14} = HG_{13;14}$, then is

$(a + b)^x = (HG_{13;14} + 2)^x \neq (HG_{13;14} + 1)^x$

It has to emphasized, that even if a simplification of the original regression equations was possible, the assignment of HG classes of the map of Baden-Württemberg to the international map would be rather daring. On the one hand, some symbols of the international map could be assigned to different hydrogeological classes. On the other hand, the international map contains several geological rock formations – like slates, gneisses or other metamorphic rocks, extrusive and intrusive rocks or dolomites – which are not mentioned at all in the description of the original 14 hydrogeological classes. Rock formations that do

not exist in the south-west of Germany could not be considered in the regression analysis of Demuth & Hagemann of course.

The second possibility is to carry out an own multiple regression analysis relating the recession constants determined in chapter 4.2.3 to the hydrogeological classes of the legend of the International Hydrogeological Map. Only the methodical approach of Demuth & Hagemann would be taken over, but one (for the whole year) or two (for summer and winter) new regression equations would have to be derived. Since daily recession constants could only be determined for 11 catchments in chapter 4.2.3 due to lack of daily measured runoff data of the other catchments, an own regression analysis will probably result in equations of insufficient statistical certainty. Nevertheless, the second method is at least tested. The number of 14 classes is reduced to 9 by uniting

- HG_6 and HG_9 to $HG_{6;9}$
- HG_5 and HG_7 to $HG_{5;7}$
- HG_{10}, HG_{11} and HG_{12} to $HG_{10;11;12}$
- HG_{13} and HG_{14} to $HG_{13;14}$.

Table 4-11 shows the original HG classes and Table 4-12 the utilized key relating hydrogeological information of reclassified hydrogeological classes to those of the international map. The hydrogeological proportions of all European test catchments are determined from the analogous map with the help of a planimetre. Table 4-13 summarizes the results. The very right column contains the recession constants as derived from hydrological flow data in chapter 4.2.3.

A multiple linear regression analysis is carried out with the help of the statistic program SPSS. The HG classes serve as independent variables, the recession constants derived from hydrograph analysis as dependent variable. First the correlation matrix is investigated to check if any pair of two independent variables is correlated to each other too strongly [BACKHAUS ET AL 1996: 33, JANSSEN & LAATZ 1994: 366]. But since all correlation coefficients are lower than 0.6, there is no hint at strong collinearity so that all nine HG classes can be included into the analysis.

Table 4-11: Original hydrogeological classes after DEMUTH & HAGEMANN (1994a: 88).

HG class	Groundwater	Rock formation of the aquifer
HG_1	high storage at shallow depth	sand and gravel
HG_2	good storage at shallow depth	sand and gravel, local impermeable loam cover
HG_3	low storage at shallow depth	sand and gravel, local impermeable loam cover
HG_4	low storage at great depth	sandstone, marl and clay in karsted limestone
HG_5	low storage at great depth	chalk and marl in sandstone
HG_6	scarce at shallow depth	deposits of gravel, sand and loam
HG_7	scarce at different depth in sandstone	old terrace gravel, sandstone or chalk
HG_8	scarce	karsted chalk
HG_9	very scarce – mostly at shallow depth	gravel deposits, sand and loam
HG_{10}	very scarce	chalk, sandy deposits of loam and marl
HG_{11}	very scarce	sandstone alternating with clay and marl
HG_{12}	very scarce	local hard sandstone alternating with clay and marl
HG_{13}	very scarce	weathered debris, irregular cracks in massive rocks
HG_{14}	occasional or no storage	karsted chalk, local alternating marl and clay

Table 4-12: Reclassified hydrogeological classes and their description according to the legend of the International Hydrogeological Map of Europe 1:1.500.000.

Merged classes	Occurrence of groundwater	Rock formation of the aquifer
HG_1	extensive and highly productive aquifers in porous commonly unconsolidated rocks	gravel, coastal sand, coarse or fine sand, silt, clay (no impermeable cover)
HG_2		gravel, coastal sand, coarse or fine sand, silt, clay with low permeable layers of clay, loam or peat
HG_3	local or discontinuous productive aquifers, rsp. extensive but only moderately productive aquifers in porous commonly unconsolidated rocks	gravel, coastal sand, coarse or fine sand, silt, clay with low permeable layers of clay, loam or peat
$HG_{6;9}$		gravel, coastal sand, coarse or fine sand, silt, clay (no impermeable cover)
HG_4	extensive and highly productive aquifers, often at great depth only	limestone, calcarenite, dolomitic limestone, dolomite, partially jointed and karstified
HG_8		chalk, partially jointed and karstified
$HG_{5;7}$	local or discontinuous productive aquifers, rsp. extensive but only moderately productive aquifers	alternating sandstones, marls, siltstones, claystones, limestones (locally with dolomites, gypsum, rock salt, coal)
$HG_{10;11;12}$	local occurrence of groundwater, especially in zones of fractured and weathered solid rocks	sands, silts, clays, marls, sandstone, siltstone, claystone, limestone, slates, pyroclastics, phyllites, quartzites, effusive rocks
$HG_{13;14}$	no groundwater resources worth mentioning, even at depth	metamorphic rocks, intrusive and extrusive rocks, slates, gneisses, graywackes, quartzites, phyllites, with claystones, siltstones and sandstones

Table 4-13: Proportions of the hydrogeological components for all catchments (%) and daily recession constants derived by hydrograph analysis.

Catchment	Gauging station	HG_1	HG_2	HG_3	$HG_{6;9}$	HG_4	HG_8	$HG_{5;7}$	$HG_{10;11;12}$	$HG_{13;14}$	daily recession constant k
Bug	Wyszkow	4.7	3.6	19.9	27.1	18.2	-	21.8	4.7	-	-
Drava	Donij Miholjac	map sheet with Hungary and Slawonia not yet published									-
Duero	Tore	12.9	-	-	9.2	7.1	-	7.7	60.6	2.5	-
Ebro	Zaragoza	10.0	-	-	7.9	14.5	-	2.4	65.1	0.2	-
Garonne	Mas D'agenais	19.1	-	-	0.4	14.6	-	11.2	26.3	28.4	0.95270
Gloma	Langnes	0.2	-	-	4.2	-	-	0.4	47.0	48.2	-
Guadalquivir	Alcala del Rio	map sheet of South West Spain not yet published									-
Inn	Passau-Ingolstadt	5.7	-	-	17.2	19.5	-	1.6	12.8	43.3	0.96038
Júcar	Masia de Pompo	6.1	-	-	17.3	30.0	-	5.2	41.4	-	-
Kenijoki	near the mouth	-	-	-	5.0	-	-	-	64.1	30.9	0.95459
Kymijoki	near the mouth	2.6	-	-	2.1	-	-	-	40.9	54.4	0.97490
Loire	Blois	8.4	-	-	0.1	2.8	5.4	11.2	23.9	48.1	-
Maas	Borghaven	3.8	-	-	-	8.4	20.6	6.5	6.4	54.2	0.91711
Mosel	Cochem	4.4	-	-	1.2	24.3	6.0	10.8	36.6	16.8	0.94127
Mures	Arad	map sheet with Transsylvania (Romania) not yet published									-
Oka	Kaluga	0.5	-	0.8	18.4	35.4	-	13.4	0.2	31.3	-
Po	Piacenza	2.8	34.2	-	5.1	3.0	-	4.7	9.3	41.0	-
Po	Boretto	1.7	32.3	-	1.6	8.4	-	6.3	-	49.6	-
Po	Pontelagoscuro	-	50.0	-	11.0	8.2	-	2.0	1.8	27.0	-
Rhine	Rheinfelden	6.7	-	-	8.8	11.8	6.5	6.3	49.1	10.8	0.97445
Rhône	Chancy	3.2	4.2	-	1.7	20.8	3.4	2.7	30.8	33.3	0.97515
Rhône	la Mulatière	9.5	0.3	-	25.3	27.0	19.2	2.0	9.5	7.2	-
Rhône	Beaucaire	12.9	-	-	12.2	18.0	4.2	12.5	22.6	17.7	0.95003
Seine	Paris	17.5	-	-	-	15.8	32.1	14.5	15.4	4.7	-
Thames	Teddington	4.6	-	-	8.1	13.2	28.1	-	27.9	18.1	-
Warta	Gorzow	4.7	3.0	25.3	39.1	3.8	-	18.1	5.9	0.2	-
Weser	Vlotho	5.9	-	1.2	-	57.6	-	9.9	13.4	12.0	0.97539
Weser	Intschede	37.1	-	-	10.4	18.9	1.1	3.2	24.8	4.5	0.96888
Western Dvina	Daugavpils	4.6	4.5	38.2	6.7	17.2	-	13.6	9.5	5.7	-

The resulting regression coefficients are summarized in Table 4-14c. The function reaches an R square of 0.786 (see Table 4-14a), which means that 78.6 % of the variance of the daily recession constant k can be explained by the variance of the proportions of the HG classes.

Although there were no strong correlations between two independent variables, HG_4 is excluded from regression analysis due to collinearity as reported in Table 4-14d. The reason is that all coefficients of the correlation matrix can only find correlations in pairs of variables, not more complex dependencies among three or more explaining variables. SPSS computes one R square for each independent variable, that would result in a regression between itself and all remaining independent variables. $R^2 = 1$ means that the corresponding variable can be produced by a linear combination of the other independent variables. Since such a variable does not contain any additional information, it cannot contribute to the explanation of the dependant variable. In contrast it increases the standard deviation of the regression coefficients leading to more unsure estimates. The same is valid for values of R square near 1. For this reason SPSS excludes independent variables if their tolerance, defined as $1-R^2$, is lower than 0.0001 [BACKHAUS ET AL 1996: 41, JANSSEN & LAATZ 1994: 381-382].

The model itself is tested on significance by an F-test (see Table 4-14b). The regression coefficients are individually tested on significance by t-tests (see Table 4-14c). Neither the regression function as a whole nor a regression coefficient is found to be significant. As expected, the sample of only 11 cases is far too small to produce significant results. It is abstained from further analyses proving other premises of regression analyses like auto-correlation (Durbin/Watson-Test) and heteroscedasticity (Geldfeld/Quandt-Test), because the function is not usable for further investigation anyway.

Table 4-14: SPSS results of a linear multiple regression analysis. Nine HG classes serve as independents and the daily recession constant as dependant variable. (a) Model summary, (b) ANOVA statistics, (c) regression coefficients, (d) excluded coefficients.

Model Summary

Model	R	R Square	Adjusted R Square	Std. Error of the Estimate
1	.886[a]	.786	-.072	1.889E-02

a. Predictors: (Constant), HG13;14, HG2, HG10;11;12, HG6;9, HG8, HG1, HG5;7, HG3

ANOVA[b]

Model		Sum of Squares	df	Mean Square	F	Sig.
1	Regression	2.614E-03	8	3.267E-04	.916	.619[a]
	Residual	7.137E-04	2	3.569E-04		
	Total	3.328E-03	10			

a Predictors: (Constant), HG13;14, HG2, HG10;11;12, HG6;9, HG8, HG1, HG5;7, HG3

b Dependent Variable: daily recession constant after DEREC2

Coefficients[a]

Model		Unstandardized Coefficients		Standardized Coefficients	t	Sig.
		B	Std. Error	Beta		
1	(Constant)	.919	.132		6.963	.020
	HG_1	6.669E-04	.002	.389	.398	.729
	HG_2	6.790E-03	.008	.467	.838	.490
	HG_3	3.706E-02	.056	.710	.660	.577
	$HG_{6;9}$	1.142E-03	.002	.369	.464	.688
	HG_8	-8.607E-04	.002	-.289	-.470	.684
	$HG_{5;7}$	-2.046E-04	.003	-.052	-.064	.955
	$HG_{10;11;12}$	5.939E-04	.001	.555	.451	.696
	$HG_{13;14}$	2.606E-04	.001	.247	.190	.867

a Dependent Variable: daily recession constant after DEREC2

Excluded Variables[b]

Model		Beta In	t	Sig.	Partial Correlation	Collinearity Statistics
						Tolerance
1	HG_4	.[a]	.	.	.	.000

a Predictors in the Model: (Constant), HG13;14, HG2, HG10;11;12, HG6;9, HG8, HG1, HG5;7, HG3

b Dependent Variable: daily recession constant after DEREC2

4.3 Data for model validation

Selection and description of the test catchments

The sample of test catchments has to be selected representatively in order to be able to conclude from model results of the test catchments to the model quality in general. A sample can only be representative, if all cases are selected by chance. But since data are not available for any European catchment whatsoever, this condition cannot be fulfilled. So dependent upon the availability of validation data, test catchments are selected ensuring that each climatological, morphological, runoff regime, hydrogeological, land use, and soil types are represented as far as possible. See Figure 4-3 for an overview of the catchment characteristics[7]. Hydrological characteristics of the European test catchments have already been summarized in Table 4-13 on page 49. For a visual overview of the geographical locations of the introduced 29 test catchments see Figure 4-3.

Three shortcomings are connected with this choice of test catchments due to lack of further measured runoff data:

- High mountainous basins are over-represented.
- The climatological and land use situation of the dry and hot deserts, semideserts and steppes around the Caspian Sea is not represented.
- Soil types covering larger regions of Europe but not represented are:
  - Xerosols, which are prevalent in Turkey and around the Caspian Sea,
  - Kastanozems and Chernozems (Black earth), building two parallel east-west-directed belts north of the Black Sea and the Caspian Sea and
  - Phaeozems covering larger areas in the Balkans.

[7] **Climate**: assigned after the effective climate classification of KÖPPEN & GEIGER (1932). Used abbreviations are explained in Appendix D.

Runoff regime: According to KELLER (1961), *nival* regimes are dominated by snow melt, in *nivo-pluvial* regimes the snow melt peak is higher than the peak resulting from rainfalls, in *pluvio-nival* regimes rainfall peaks exceed the snow melt peak, and *pluvial* regimes are only influenced by rainfall.

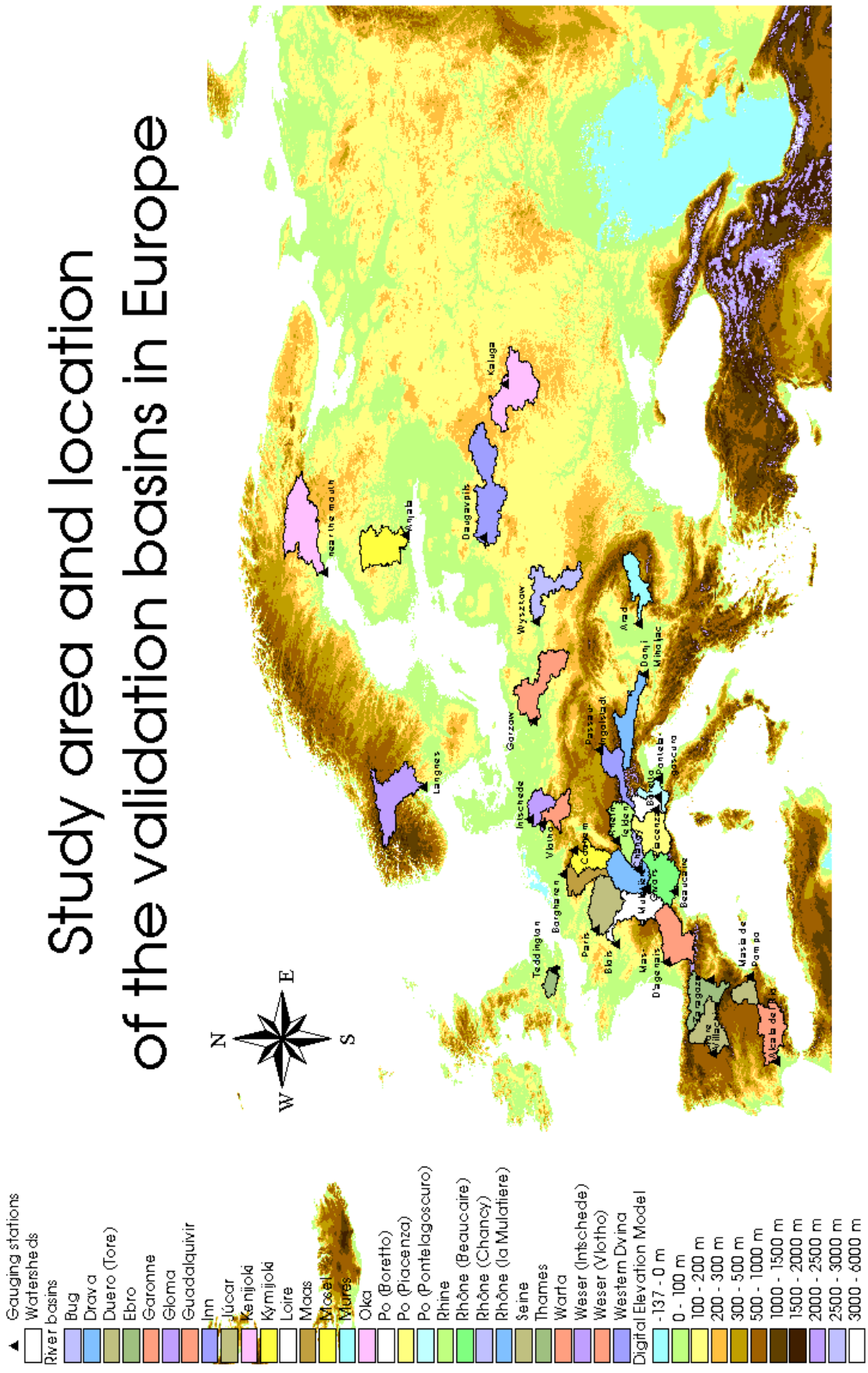

Figure 4-3: Geographical location of the 29 European test catchments.

Table 4-15: Climate, elevation, runoff regime, predominant land use and soil type of all 29 European test catchments.

River	Main countries	Climate	Elevation Min-Max (Mean)	Runoff regime	Land use	Soil types
Bug	Ukraine, Belarus, Poland	snow climate (Dfb)	87-445m (259m)	nival (snow melt March-May)	mainly cropland / pasture, partly woodland	Podzol, Luvisol, Podzoluvi-sols
Drava	Austria, Slovenia, Croatia, Serbia	warm-temperate climate (Cfb)	84-3428m (1477m)	nival (summer snow melt)	forests and snow & ice in the moun-tains (glaciers of Hohe Tauern), cropland / pastures in the lowland	Cambisols, Luvisols, Fluvisols
Duero	Spain, Portugal	warm-temperate climate (Cfb, Csb)	620-2302m (1286m)	Pluvial (runoff maximum in winter)	Mediterranean cropland / pastures	Cambisols, Luvisols
Ebro	Spain	warm-temperate climate (Csa, BSk)	178-2500m (1081m)	Pluvial (runoff maximum in winter)	mainly Mediter-ranean cropland / pastures, partly forests	Cambisols
Garonne	France	warm-temperate climate (Cfb)	20-2941m (1239m)	Pluvial (runoff maximum in winter)	cropland / pastures	Cambisols
Gloma	Norway	snow and ice climate (Dfc, E)	101-2237m (1239m)	nivo-pluvial (summer snow melt, second peak in October)	forests, arctic tundra, snow & ice (glaciers of Jostedalsbre)	Podzols, Lithosols
Guadal-quivir	Spain	warm-temperate climate (Csa)	2-3361m (1079m)	pluvial (runoff maximum in winter)	mainly Mediterra-nean cropland / pastures, partly forests	Cambisols
Inn	Austria, Germany	snow climate in alpine mountains (Dfb), warm-temperate climate elsewhere (Cfb)	299-3589m (1723m)	nivo-pluvial (summer snow melt)	pastures, forests, snow & ice (gla-ciers of Bernina Alps, Ötztal Alps, Zillertal Alps, Hohe Tauern)	Luvisols, Rendzinas, Podzols
Júcar	Spain	dry climate (BSk)	273-1796m (1031m)	relatively con-stant throughout the year (influ-enced by three reservoirs)	Mediterranean mainly cropland / pastures, partly forests	Cambisols
Kenijoki	Finland	snow climate (Dfc)	6-642m (272m)	nival (snow melt peak in May)	Boreal Forests, arctic tundra, glaciers	Histosols, Podzols
Kymijoki	Finland	snow climate (Dfc)	2-266m (132m)	relatively con-stant throughout the year (due to the vast areas of lakes)	Boreal Forests, vast areas of water bodies	Podzols
Loire	France	warm-temperate climate (Cfb)	74-1756m (777m)	pluvial (runoff maximum in winter)	mainly cropland / pasture, partly woodland	Cambisols, Luvisols

River	Main countries	Climate	Elevation Min-Max (Mean)	Runoff regime	Land use	Soil types
Maas	France, Belgium, Nether-lands	warm-temperate climate (Cfb)	47-687m (344m)	pluvial (runoff maximum in winter)	mainly cropland / pasture, partly woodland	Cambisols
Mosel	France, Germany	warm-temperate climate (Cfb)	88-1147m (535m)	pluvial (runoff maximum in winter)	mainly cropland / pasture, partly woodland	Cambisols
Mures	Romania	snow climate (Dfb)	109-2428m (1013m)	nival (snow melt March-June)	cropland / pastures in the lowland, forests in the mountains	Cambisols, Luvisols
Oka	Russia	snow climate (Dfb)	113-334m (216m)	nival (snow melt peak in April)	Mainly cropland / pastures, partly forests	Podzoluvi-sols, Luvi-sols, Cherno-zems, Grey-zems
Po, station Piacenza	Italy	snow climate in alpine mountains (Dfb), warm-temperate climates elsewhere (upstream part: Cfb; middle part: Cfb, Cfa, Csa; downstream part: Cfb, Cfa)	35-4440m (1671m)	Mainly pluvial (three runoff peaks in March, May and Oct.)	Mediterranean cropland in the lowland, forests in the mountains, snow & ice in High Mountains (glaciers of Berni-na Alps, Ortles mountain group, Adamello moun-tain group, Pennine Alps, Mont Blanc)	Cambisols, Luvisols, Rendzinas, Gleysols, Podzols, Lithosols
Po, station Boretto			21-3798m (1494m)	Pluvial (runoff peaks in spring and autumn)		
Po, station Pontela-goscuro			2-3333m (1149m)	Complex, mainly pluvial (runoff peaks in spring and autumn)		
Rhine	Switzer-land	snow climate (Dfb)	274-3852m (1660m)	nival (summer snow melt)	Pastures, forests, snow & ice (glaciers of Bernese Alps, Dammastock, Glarus Alps)	Cambisols, Luvisols, Rendzinas, Gleysols, Podzols, Lithosols
Rhône, station Chancy	Switzer-land	snow climate (Dfb)	333-4222m (1903m)	nival (summer snow melt)	Pastures, grass-land, forests, snow & ice (glaciers of Bernese Alps, Pennine Alps, Mont Blanc)	Luvisols, Rendzinas, Gleysols, Lithosols
Rhône, station la Mulatière /Givors	France	warm-temperate climate (Cfb)	169-2283m (872m)	pluvial (runoff maximum in winter)	Cropland	Luvisols, Cambisols, Rendzinas, Fluvisols
Rhône, station Beaucaire	France	snow climate in alpine mountains (Dfb), warm-tem-perate climate else-where (Cfb)	5-3676m (1582m)	complex nivo-pluvial (summer snow melt, second runoff peak in autumn)	Mediterranean cropland, partly woodland	Luvisols, Cambisols, Rendzinas, Fluvisols, Lithosols
Seine	France	warm-temperate climate (Cfb)	25-780m (349m)	pluvial (runoff maximum in winter)	Mainly cropland / pastures, partly woodland; city of Paris included	Luvisols, Rendzinas, Cambisols

River	Main countries	Climate	Elevation Min-Max (Mean)	Runoff regime	Land use	Soil types
Thames	Great Britain	warm-temperate climate (Cfb)	1-277m (134m)	pluvial (runoff maximum in winter)	pastures, cropland, city of London included	Cambisols, Gleysols, Rendzinas, Luvisols, Podzols
Warta	Poland	warm-temperate climate (Cfb)	18-422m (215m)	small snow melt peak in spring	mainly cropland / pasture, partly woodland	Podzols, Luvisols, Podzoluvi-sols, Areno-sols
Weser, station Intschede	Germany	warm-temperate climate (Cfb)	7-904m (352m)	pluvial (runoff maximum in winter)	mainly cropland / pasture, partly woodland	Luvisols, Podzoluvi-sols, Podzols, Fluvisols, Cambisols
Weser, station Vlotho	Germany	warm-temperate climate (Cfb)	45-931m (430m)	pluvio-nival (runoff maxi-mum in winter, snow melt in spring)	Cropland / pasture, woodland	Cambisols
Western Dvina	Russia, Belarus, Latvia	snow climate (Dfb)	82-293m (187m)	nival (snow melt peak in April)	mainly cropland / pasture, partly woodland	Podzoluvi-sols

Data completeness

Table 4-16 shows all included gauging stations, their basin area and the years for which measured discharge data are available within the time period of 1961-90. Unfortunately, full time series are only available for the rivers Guadalquivir, Kenijoki, Kymijoki, Maas, Mosel, Rhine and Warta. All other time series end 1979 or in the 80s. Time series of the gauging stations Boretto (river Po), Chancy (Alpine part of the river Rhône), Teddington (river Thames) and Daugavpils (river Western Dvina) do not begin until 1965.

The gauging station of the river Duero at Villachica was moved to Tore at the end of 1979. Tore is only a few kilometres upstream so that the corresponding catchment has been reduced by only 48 km². The time series of Villachica and Tore are treated as one. The same goes for the stations la Mulatière and Givors of the river Rhône, although the difference of their corresponding catchment areas is more than 700 km². The gauging station at la Mulatière was shifted to Givors at the end of 1972.

Table 4-16: Available and missing measured runoff data.

GRDC-Code	***River***	***Gauging station***	***basin area [km²]***	***Available data within the period of 1961-90***	***Number of missing months***
6458550	Bug	Wyszkow	39119	1961 – 87	2
6546800	Drava	Donji Miholjac	37142	1961 – 84	24
6212400	Duero	Villachica	41856	1961 – 79	–
6212410	Duero	Tore	41808	1980 – 84	–
6226400	Ebro	Zaragoza	40434	1961 – 84	39
6125100	Garonne	Mas-D'agenais	52000	1961 – 79	–
6731400	Gloma	Langnes	40221	1961 – 84	–
6217100	Guadalquivir	Alcala del Rio	46995	1961 – 90	–
6343900	Inn	Passau-Ingolstadt	26084	1961 – 89	2
6227500	Júcar	Masia de Pompo	17876	1961 – 87	20
6854700	Kenijoki	near the mouth	50900	1961 – 90	–
6855200	Kymijoki	Anjala	36305	1961 – 90	–
6123300	Loire	Blois	38240	1961 – 79	12
6421500	Maas	Borghaven	21300	1961 – 90	–
6336050	Mosel	Cochem	27100	1961 – 90	–
6744200	Mures	Arad	27061	1961 – 88	–
6975140	Oka	Kaluga	54900	1961 – 85	–
6348400	Po	Piacenza	42030	1961 – 79	–
6348500	Po	Boretto	55183	1965 – 79	–
6348800	Po	Pontelagoscuro	70091	1961 – 79	–
6335400	Rhine	Rheinfelden	*34600	1961 – 90	–
6139100	Rhône	Beaucaire	95590	1961 – 79	12
6139390	Rhône	la Mulatière	50200	1961 – 72	–
6139400	Rhône	Givors	51080	1973 – 79	12
6939050	Rhône	Chancy	10299	1965 – 82	–
6122300	Seine	Paris	44320	1961 – 79	15
6607700	Thames	Teddington	9950	1965 – 84	–
6457800	Warta	Gorzov	52404	1961 – 90	–
6337100	Weser	Vlotho	17618	1961 – 86	2
6337200	Weser	Intschede	37788	1961 – 84	–
6973300	Western Dvina	Daugavpils	64500	1965 – 84	–

* The size of this basin is missing in the GRDC data set. It is taken from the Internat. Hydrogeological Map of Europe.

Data preparation

There are three gauging stations included in the basin of the rivers Rhône and Po and two stations in the Weser basin. Since the model computes grid-based runoff and aggregates results for the subcatchments between two gauging stations, the measured runoff of the upstream station is subtracted from the one of the downstream station. Data of the station Boretto are reduced by the values of the station Piacenza, data of the station Pontelagoscuro is reduced by the station data of Boretto for example. As a consequence, time series of the subcatchments can only be given for those years for which data exist of all upstream stations. It has to be recognized that measuring errors are added in this process.

Normally, discharges downstream should exceed discharges upstream due to a larger contributing area. But in dry and arid climates like in the Mediterranean region especially in summer months effluent conditions can turn into influent ones. The stream's surface is no

longer part of the groundwater table. Instead, water moves from the stream to the deeper groundwater. Additionally, water losses due to increased evaporation contribute to the fact that discharge amounts at a downstream station can fall below those upstream. This is the case at the stations in the lowland of the river Po with its predominantly unconsolidated rocks and once in the Rhône basin (see Table 4-17). Discharge values of the downstream subcatchment are set to zero in these cases.

Table 4-17: Cases of downstream runoff falling below those upstream.

River	***Station***	***Monthly discharge falling below that upstream***
Po	Boretto – Piacenza	May 1969
		May and August 1971
		June 1972
		June 1973
Po	Pontelagoscuro – Boretto	November 1968
Rhône	Beaucaire – la Mulatière	April 1970

Discharge data of gauging stations are given in m^3/s, but the model generally works with runoff data in the unit mm/month, which has the advantage that data are independent of the corresponding basin area. To ensure direct comparability between predicted and observed runoff, all measured station discharges are converted into the unit mm/month as well.

The last column of Table 4-16 contains the number of missing values within the time period specified in the previous column. Data are missing for the whole year of 1975 for the gauging stations at the French rivers Seine, Loire and Rhône (except for Chancy). Data of the river Drava are missing for 1974 and 1975, of the river Ebro for 1963, 1964 and 1975. The remaining are individual missing values. For further work these missing values have been replaced by the mean runoff of the corresponding month. For example the missing runoff value of February 1988 for the river Inn is substituted by the mean of all existing February runoff data of 1961-89.

It would have been desirable to get complete time series of 30 values for each month (1961-90). It has been tested to carry out a linear extrapolation into time periods before and after the period of available data (fifth column in Table 4-16). Taking the river Bug as an example, ‘observed‘ runoff of January 1988 was tried to be estimated by a regression function based on the time series of all January values of the period 1961-87. But this method had to be dismissed because of the following reasons:

- The resulting R squares were extremely small, since observed discharge varied strongly within the given time series.
- Linear trends sometimes fell that strongly, that negative observed discharge was estimated for the end of the 80s – which is senseless.

Since the input data temperature and precipitation are only available as monthly long-term means of the period 1961-90, model results represent long-term means of runoff for the same 30-year period. Long-term means of observed runoff data are derived as the arith-

metic mean of the given time series. This is methodically doubtful, as the 12 time series – one for each month – have different lengths and span different subperiods within the time interval of 1961-90. If for example runoff in the 80s was significantly higher than in the 70s, but the available time series only span a subperiod of 1961-79, the arithmetic mean of the subperiod's values falls below the correct long-term mean of the 30-year period. But it is beyond the scope of this work to analyse long-term structures or to find recurrence probabilities of peaks in order to give more suitable estimates of mean observed runoff.

Spatial fit of natural catchments to the grid cells

Figure 4-4 shows the deviation of catchment sizes of modelled from real (GRDC data) catchments. The catchment size in the model is the sum of areas of 0.5° grid cells. Greatest differences occur for Boretto and Pontelagoscuro, two stations of the Italian river Po whose subbasins border on each other. The modelled subbasin of the station Boretto consists of 8 grid cells whose sum of areas exceeds the real catchment size by 31.33 %. The area of the 5 grid cells of the Pontelagoscuro basin is 26.76 % smaller than the real catchment size. The modelled watersheds of the rivers Mosel, Kenijoki, the alpine part of the river Rhône (station Chancy), Mures and the upstream part of the river Weser (station Vlotho) fall below the natural catchment size 10-20 %. The watershed of the river Inn is too big by a little over 10 %. The remaining 23 basin sizes deviate less than 10 %. Of course, this is not a proof of the best fit, since positive and negative deviations can offset each other and the shapes of modelled and real watersheds can differ nonetheless.

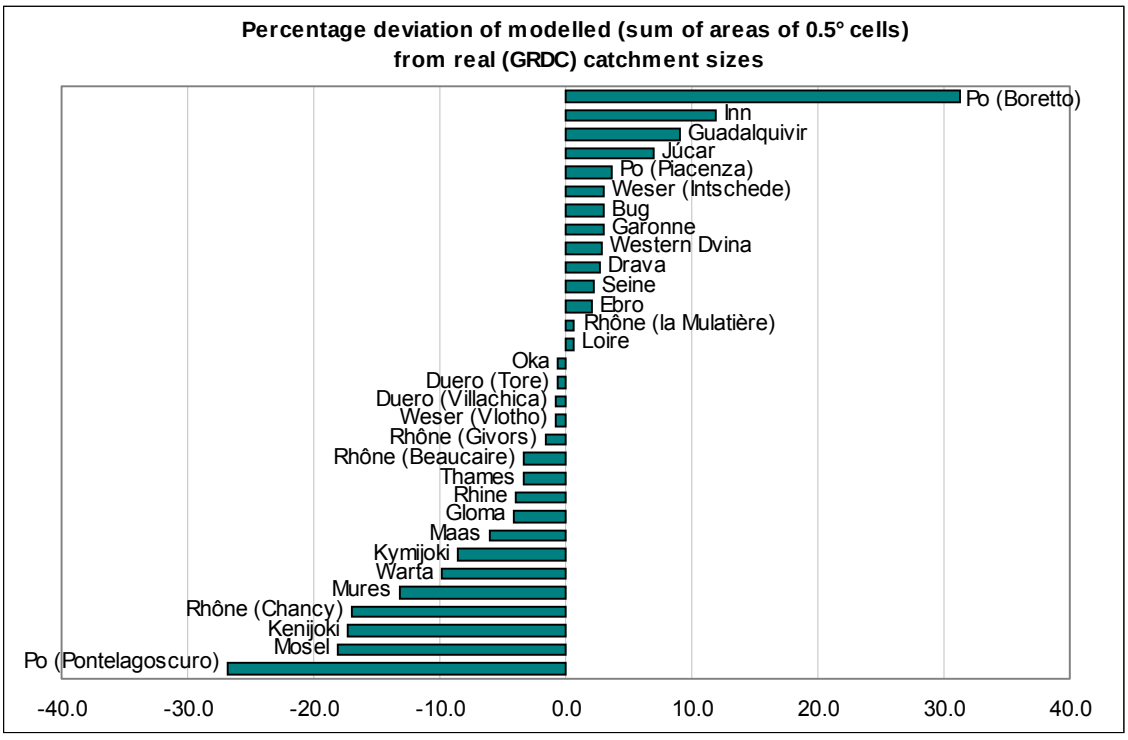

Figure 4-4: Percentage deviation of modelled (sum of areas of 0.5° cells) from real catchment sizes.

5 APPLICATION AND VALIDATION FOR EUROPE

5.1 Calibration of model parameters

5.1.1 Strategy during the calibration process

If the model had been started for all possible combinations of the 13 model parameters as introduced in chapter 3.2, several ten thousands of model runs would have had to be carried out. Since the sensitivity analysis has revealed that the model shows different sensitivities to the calibration parameters, the "strategy of stratified calibration" has been developed. This strategy can reduce the number of model runs enormously.

Two calibrations are carried out separately: one for the limit temperature of -2°C and another for the limit temperature of -1°C. The model is most sensitive to the calibration parameters of the snow melt module. Residuals are highest when snow melt peaks of the model do not cover those measured. So with the limit temperature set, in a second step all melting percentages are adjusted with the remaining parameters kept constant. First, the best fit for the lowland elevation class (≤ 500 m) is found. Afterwards, the snow melt for mountainous regions (> 500 m – ≤ 1600 m) and the High Mountains (> 1600 m) is adapted.

Once having found the best fit of those nine calibration parameters, the model efficiency shows a much higher sensitivity to the calibration parameter of the base flow module than to those of the surface runoff module. Thus, on this third level of calibration, the best fit of the recession constant is sought with fixed values for the limit temperature and the melting percentages. As a forth step, the two slope factors controlling surface runoff are adjusted.

This procedure results in two sets of parameters producing highest model efficiencies – one for each limit temperature. In the very last step, among these two sets that one is chosen that produces the higher area-weighted model efficiency.

This described procedure is performed on two levels:

a) The area-weighted mean of the ME values of all test catchments (except for the Kymijoki and Júcar basin, see later on) is determined ($\overline{ME}_{all}$). The combination of model parameters producing a maximum $\overline{ME}_{all}$ is then sought.

b) The test catchments are grouped into 5 classes of runoff regime types according to Table 5-1. Area-weighted means of ME values are determined separately for all 5 classes of catchments ($\overline{ME}_{class1}$ to $\overline{ME}_{class5}$). For each runoff regime class one optimal combination of model parameters is searched.

Table 5-1: Classification of runoff regime types (The Kymijoki and Júcar basins are not assigned because ME is extremely negative there. The Po subbasin between Piacenza and Boretto does not match to any of these classes due to its complex runoff regime.)

class	***description of the runoff regime***	***accompanying catchments***
1	Nival, nivo-pluvial, High Mountains (Alps and Carpathians)	Rhône to Chancy, Rhône between la Mulatière / Givors and Beaucaire, Rhine to Rheinfelden, Inn to Passau-Ingolstadt, Po to Piacenza, Drava to Donij Miholjac, Mures to Arad
2	nival, nivo-pluvial, lowland of Northern and Eastern Europe	Oka to Kaluga, Western Dvina to Daugavpils, Bug to Wyszkov, Kenijoki, Gloma to Langnes
3	pluvial, pluvio-nival, low mountain ranges	Loire to Blois, Garonne to Mas-D'agenais, Rhône between Chancy and la Mulatière / Givors, Mosel to Cochem, Maas to Borghaven, Weser to Vlotho
4	pluvial, pluvio-nival, lowland	Thames to Teddington, Seine to Paris, Weser between Vlotho and Intschede, Warta to Gorzov, Po between Boretto and Pontelagoscuro
5	pluvial, low amount of annual runoff	Duero to Tore / Villachica, Ebro to Zaragoza, Guadalquivir to Alcala del Rio

5.1.2 Exclusion of the Kymijoki and Júcar basins

Among the remaining 12 catchments where model efficiencies never exceeded 0.0 there are two outliers: the catchments of Kymijoki in Finland and Júcar in Spain. Model efficiencies varied in the range of -150 and -400 for them.

The runoff curves at both corresponding gauging stations, at the Finnish Anjala and the Spanish Masia de Pompo do not show any characteristic peaks but run almost straight. In the Kymijoki basin this is caused by the vast areas of lakes in Southern Finland with their immense retention effect. Due to them the long-term mean of observed monthly runoff at Anjala only varies between 19.0 mm in September and 25.0 mm in May. Since the model in its current version does generally not yet consider this retention effect, it falsely produces a steep snow melt runoff peak with a mean monthly runoff of 100 mm in April (similar to those in the basins of Western Dvina and Oka) and a second much smaller surface runoff peak in October and November (see Figure 5-1). But in reality both runoff maxima are stored and evened out in the Finnish lakes reacting with changing water levels.

In contrast to the Kymijoki basin where the straight runoff curve has a natural reason, the straight runoff curve at Masia de Pompo in the Júcar basin is evoked anthropogenically. Two reservoirs with capacities of 1112 million m³ and 860 million m³ control runoff at the upstream part of the river Júcar south of the Sierra de Cuenca. A third reservoir with a capacity of 412 million m³ is located only a few kilometres before the gauging station at Masia de Pompo. As a consequence, mean measured runoff only varies between 5.0 mm

(September) and 6.5 mm (May). The model falsely produces a surface runoff maximum in spring and another in autumn similar to those of the other three Spanish test catchments (see Figure 5-1). Although differences between modelled and measured runoff are lower than in the Kymijoki catchment, model efficiencies for the Júcar basin are still worse because the variance of measured runoff data is especially small here (see equation (2.1)). For these reasons Kymijoki and Júcar were excluded from the further calibration process.

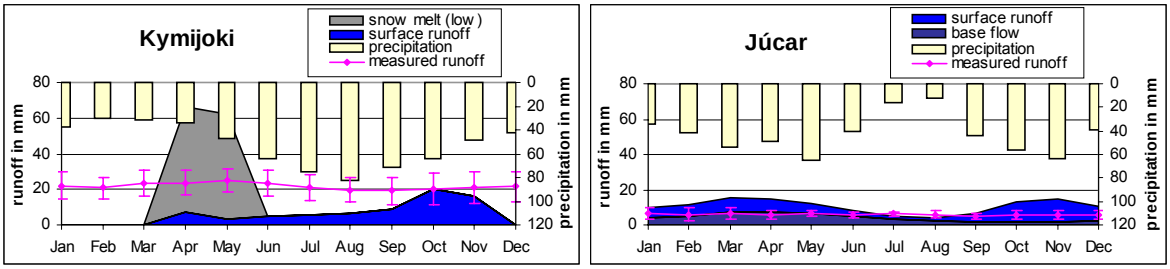

Figure 5-1: Observed and modelled runoff at the Kymijoki and Júcar test catchments.

5.1.3 Calibration results

Table 5-2 summarizes the resulting optimal combinations of model parameters for all remaining 27 test catchments and for each of the runoff regime classes. The median of all ME values is positive since for 16 of 27 test catchments the variance of the residuals is lower than the variance of observed data. Nevertheless, the area-weighted mean $\overline{ME}_{all}$ never becomes positive because the distribution of ME values has a negative skew.

Although model runs have been carried out for the limit temperature of -1°C as well, the model generally worked more efficiently with a limit temperature of -2°C. The Spanish catchments united in runoff regime class 5 are completely insensitive to both all nine melting percentages and the limit temperature because long-term means of mean monthly temperatures are positive during the whole year. As a consequence, a snow cover never accumulates or melts. Runoff regime classes 2 and 4 mainly consist of lowland basins that do not contain any grid cell with elevations higher than 1600 m nor with a slope steepness of more than 10°, so that they are insensitive to high1, high2, high3 and slope_fac2.

The melting percentages for the intermediate (500-1600 m) and high elevation classes (> 1600 m) are equal for almost all model runs of Table 5-2. So snow melt in low and high mountain ranges behave in a similar fashion while snow melt in the lowland differs strongly. One of two exceptions is the Gloma basin where the snow cover of the intermediate elevation class melts much faster than elsewhere. The second exception are the Po subbasins. The snow cover of the southern exposed slopes of the Italian alpine mountains melts faster since the process of melting is not only dependent on air temperatures but also on the intensity and daily duration of solar radiation.

Table 5-2: Optimal combinations of model parameters for all test catchments (except for the Kymijoki and Júcar basins) and for each runoff regime class. Dashes indicate that the test catchments are insensitive to this model parameter.

maximum area-weighted ME	***number of test catchments with ME > 0.0***	***limit temperature***	***melting percentages for the 1st, 2nd and ≥ 3rd month of snow melt***									***daily recession constant***	***slope_fac1***	***slope_fac2***
			elevation ≤ 500 m			*500 m < elevation ≤ 1600 m*			*elevation > 1600 m*					
			low1	***low2***	***low3***	***mid1***	***mid2***	***mid3***	***high1***	***high2***	***high3***			
$\overline{ME}_{all}$ = -0.216	16 of 27	-2.0	0.4	1.0	0.0	0.0	0.2	0.3	0.0	0.2	0.3	0.99	1.0	2.0
$\overline{ME}_{class1}$ = -0.651	3 of 7	-2.0	0.4	1.0	0.0	0.0	0.2	0.3	0.0	0.2	0.3	0.99	1.7	2.0
$\overline{ME}_{class2}$ = 0.155	4 of 5	-2.0	0.4	1.0	0.0	0.0	0.5	1.0	–	–	–	0.99	1.7	–
$\overline{ME}_{class3}$ = 0.334	5 of 6	-2.0	0.3	1.0	0.0	0.0	0.2	0.3	0.0	0.2	0.3	0.97	1.1	2.0
$\overline{ME}_{class4}$ = -0.402	3 of 5	-2.0	0.3	1.0	0.0	0.0	0.2	0.3	–	–	–	0.99	1.0	–
$\overline{ME}_{class5}$ = -0.348	2 of 3	–	–	–	–	–	–	–	–	–	–	0.99	1.0	–

slope_fac1 factor for determining runoff factors, if 2° < slope ≤ 10°
slope_fac2 factor for determining runoff factors, if slope > 10°

The calibration results of the daily recession constant k and the two slope factors have to be regarded with caution for two reasons. First, a recession constant of 0.99 for most of the catchments is simply unlikely, since the k-values of the hydrograph analyses spread within the interval of 0.91-0.98. This is a ground for the supposition, that retentional effects of great lakes, marshes and managed reservoirs which are all not considered in the model are partly evened out by this high recession constant. Model efficiencies would be much worse if the recession constant was not used as a calibration parameter but determined realistically on the basis of hydrogeological and soil characteristics. Second, for all catchments with elevations of more than 500 m the daily recession constant and the slope factors influence each other. A smaller k producing a steeper base flow curve can reduce or increase the slope factors depending on the climatological parameters.

5.2 Model results on the grid level

Figure 5-2 shows the IIASA mean monthly precipitation field used as model input. Figure 5-3 to Figure 5-12 summarize model predictions that have been yielded with the parameters maximizing $\overline{ME}_{all}$ (see Table 5-2). Since measured runoff data are not available on the grid level, all these results can generally just be evaluated qualitatively.

Figure 5-3 and Figure 5-4 visualize model results for potential and actual evapotranspiration (ET_p and ET_a) – each as monthly means in the course of the year. ET_p in Europe is minimum in January with values of 0-40 mm and maximum in July with predominantly 100-250 mm. Since Thornthwaite approximates ET_p to be zero, if the air temperature falls

below 0°C, in vast areas of Northern and Eastern Europe ET_p and ET_a is predicted to be zero during the winter months from November to March. The broadest expansion is reached in January when the model computes zero evaporation for Iceland, all of Scandinavia, the Balkans, the complete regions of the Black, Caspian and Aral Sea and Anatolia.

Absolute differences between January and July extremes are lowest in the British Irelands and the French and Spanish Atlantic coast, indicating a relatively mild and moderate climate. The range of ET_p amounts is highest in Lapland, in the deserts between the Caspian and Aral Sea and in the Syrian valley of the rivers Euphrates and Tigris. During the winter months from December to March Portugal shows highest ET_p of Europe ranging between 20 and 60 mm, whereas maximum evaporation of more than 200 mm is reached in the region of Euphrates and Tigris and around the Caspian Sea during the summer season of June to August.

Figure 5-5 and Figure 5-6 show the results of further map calculations carried out with the GIS Arc/Info. Figure 5-5 shows the deficit of evapotranspiration for July computed as:

$$\frac{ET_p - ET_a}{ET_p} \cdot 100\,\%$$

In winter ET_p and ET_a do not differ very much (compare Figure 5-3, Figure 5-4). In July, however, the model predicts ET_a to fall more than 90 % below ET_p south of 40° N (that is the south parts of the Iberian Peninsula, Kalabria, Sicily, Sardinia, Greece and Turkey) and north and east of the Caspian Sea in the Caspian Depression, in Kazakhstan and in the Karakum desert in Turkmenistan (see Figure 5-5). The deficit of evaporation is less than 10 % in the High Mountains of the Alps and the Carpathians.

Figure 5-6 gives an overview of the absolute difference between precipitation (P) and ET_p separating dry and wet regions throughout the year. This information is of special interest because the model only allows infiltration of water into the soil if P exceeds ET_p. In most areas in Europe P exceeds ET_p from October to April, whereas P falls below ET_p from May to September. In the winter season precipitation surplus is maximum at the west coasts of Norway, Scotland and Portugal, the Turkish Taurus and Pontic Mountains and in the Western Caucasus. In the summer season precipitation deficit is highest in Spain, southern Italy, Turkey and the region around the Caspian Sea. In several mountainous regions a precipitation surplus is kept during the whole year due to high amounts of P and low estimates for ET_p, which are in turn the impact of low temperatures. When interpreting Figure 5-6 it has to be kept in mind that infiltration cannot take place if P falls as snow. In the model P is assumed to fall as snow if the air temperature falls below the limit temperature, which was set equal to -2°C in the current model run. So the model neither computes infiltration nor percolation in Northern and Eastern Europe, although P is greater than ET_p there in the winter season.

The maps of Figure 5-7 to Figure 5-12 visualize model predictions for the snow storage and for the three runoff components surface runoff, snow melt runoff and base flow as well as for the total runoff – each as monthly means in their course of the year again.

The module controlling snow depth generates a vast snow cover in Northern and Eastern Europe during winter and spring months from November to April (see Figure 5-7). Its greatest expansion is reached in February when the snow cover stretches over all of Scandinavia and the Russian continent to the Black and the Caspian Sea in the south and to the Baltic ridge and the Carpathians in the west. In comparison to the time of greatest expansion, the steepest snow depth is delayed one month. The latter is produced in March in the northern Ural Mountains.

All year round the model computes regional snow covers in the Scandinavian Mountains, the Alps, the Dinaric Alps, the Pontic and the Caucasian Mountains and in Iceland. In contrast to the soil storage, which is forced to keep constant on the annual level, the amount of snow accumulation and snow melt is not necessarily balanced on the annual level. Affected test catchments, showing a greater snow storage at the end of the year than at the beginning, are the Gloma and all alpine basins.

In correspondence with the snow storage module, the snow melt module generates a belt of snow melt from the Baltic ridge to the Black and Caspian Sea in March, followed by the Russian and Scandinavian lowlands where the snow cover melts in April and May (see Figure 5-8). In Lapland, the Kola Peninsula and at the coast of the Barents Sea the snow does not melt before June. The snow coverage and the glaciers in the mentioned mountains melt totally or only partly during the summer months from June to September.

The surface runoff module computes highest amounts of surface runoff for the west sides of the continents and the mountains (see Figure 5-9). Reasons lie, on the one hand, with the westerlies that provide huge amounts of rainfall to the west sides of the continents and low mountain ranges and equally huge amounts of snowfall to the west sides of higher mountains. On the other hand, the introduction of relief-dependent runoff factors leads to an additional increase of surface runoff in mountainous regions. Surface runoff is zero in Northern and Eastern Europe during the winter months from November to March because precipitation is assumed to fall exclusively as snow.

Setting model results of the soil water storage in relation to the water holding capacity (WHC) of the soil, leads to the observation that from December to April soils in Central, South and South-East Europe are nearly saturated with water (see Figure 5-10). From June to September saturated soils can only be found in High Mountains. Low mountain ranges show a medium relative water content and lowland regions a very low one. The reason for this pattern might lie with the fact that in higher elevations temperature is lower so that the snow melts later. In vast areas of the Central Russian Plateau, the Volga Plateau and the

Caspian Depression as well as Kazakhstan and Turkmenistan the relative water content of the soil is lower than 10 % in these summer months (see Figure 5-10).

The results of the base flow module do not seem to be very meaningful, because the only parameter controlling base flow, the daily recession constant, is invariant both spatially and temporally. It is neither changed in dependence on hydrogeology nor seasonally nor in the course of months. Therefore, the estimates are rather a result of a combination of

a) precipitation data and

b) the water holding capacity (WHC).

to a): The higher the amount of rainfall, the higher the soil water content and the higher the amount of percolating water. Highest amounts of base flow are therefore generated for the west sides of the Dinaric Alps and the Caucasian and Scandinavian Mountains as well as for the west sides of the European continent, especially of the Iberian Peninsula and the British Irelands (see Figure 5-11).

to b): WHC controls when and how much soil water can percolate to recharge the groundwater storage. In regions with high water holding capacities and/or low amounts of precipitation falling as rain the soil water storage seldom or never exceeds its WHC so that the groundwater storage cannot be filled up. As a consequence, it only drains and runs dry. This is the case in Eastern and Northern Europe with the exception of the west coast of Norway (see Figure 5-11). The same effect can be recognized in the Turkish Highland of Anatolia and the Spanish Plateau of Castile for similar reasons.

The fact that the resulting base flow pattern only varies marginally in the course of the year is caused by the high recession constant of 0.99 assuming groundwater storages with very flat depletion curves.

Regarding total runoff (see Figure 5-12) as the sum of the patterns of the three runoff components, it is clearly noticeable that in Northern and Eastern Europe runoff equals zero during the winter months because of the snow cover. In April and May snow melt runoff is predominant and in the summer months a low amount of surface runoff remains. In Central and south-west Europe the pattern of the three runoff components, each showing runoff maxima at the west sides of the continents and the mountains, is only reinforced.

➔ Qualitatively, these results of the mapped variables seem to make sense, at least their variation in the course of the year and their general spatial patterns. How far these grid results, aggregated onto the test catchment level, can approximate measured data, shall be investigated in the following chapter.

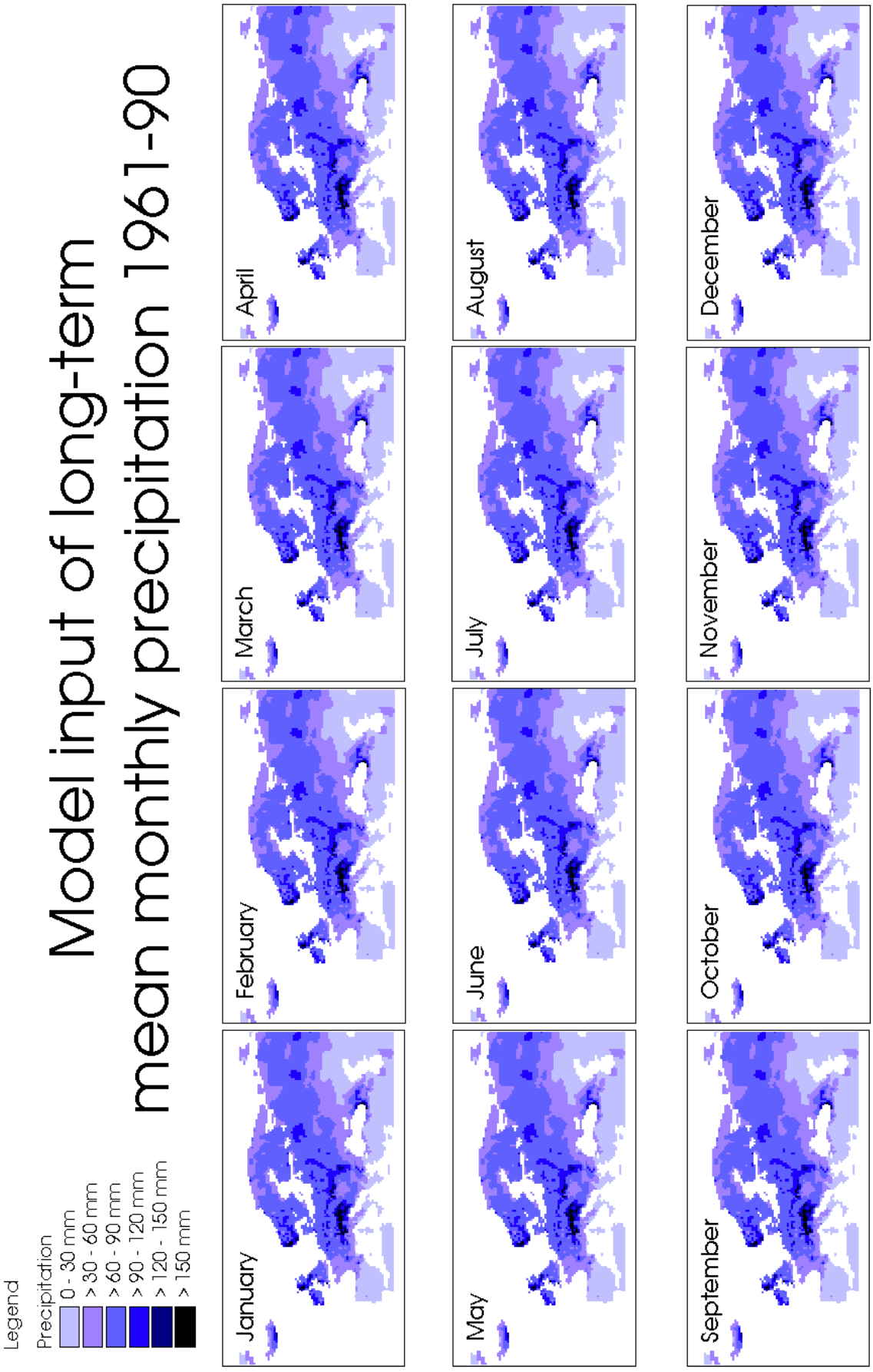

Figure 5-2: Model input of long-term mean monthly precipitation (1961-90) according to IIASA.

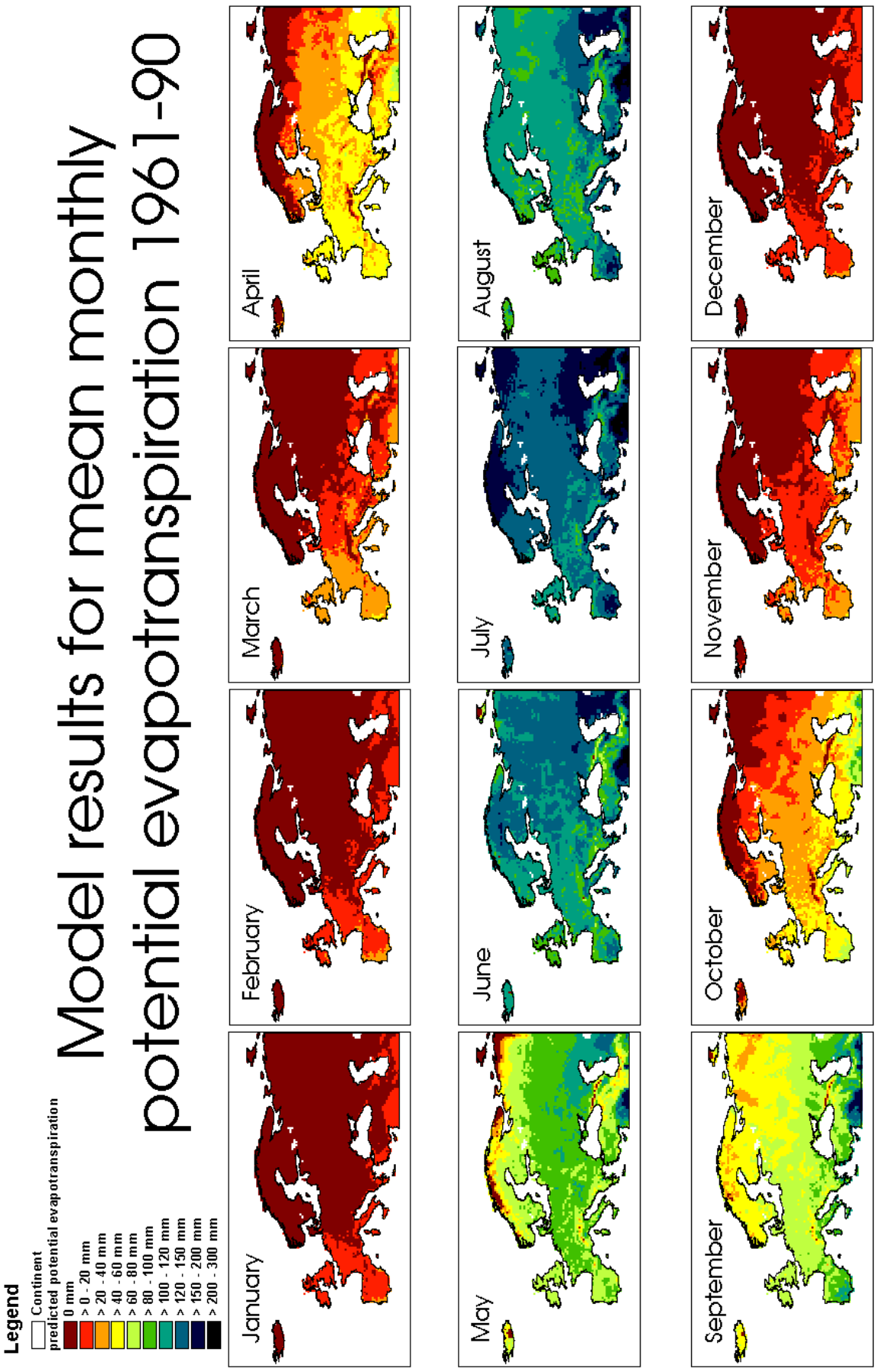

Figure 5-3: Model results of mean monthly potential evapotranspiration (1961-90).

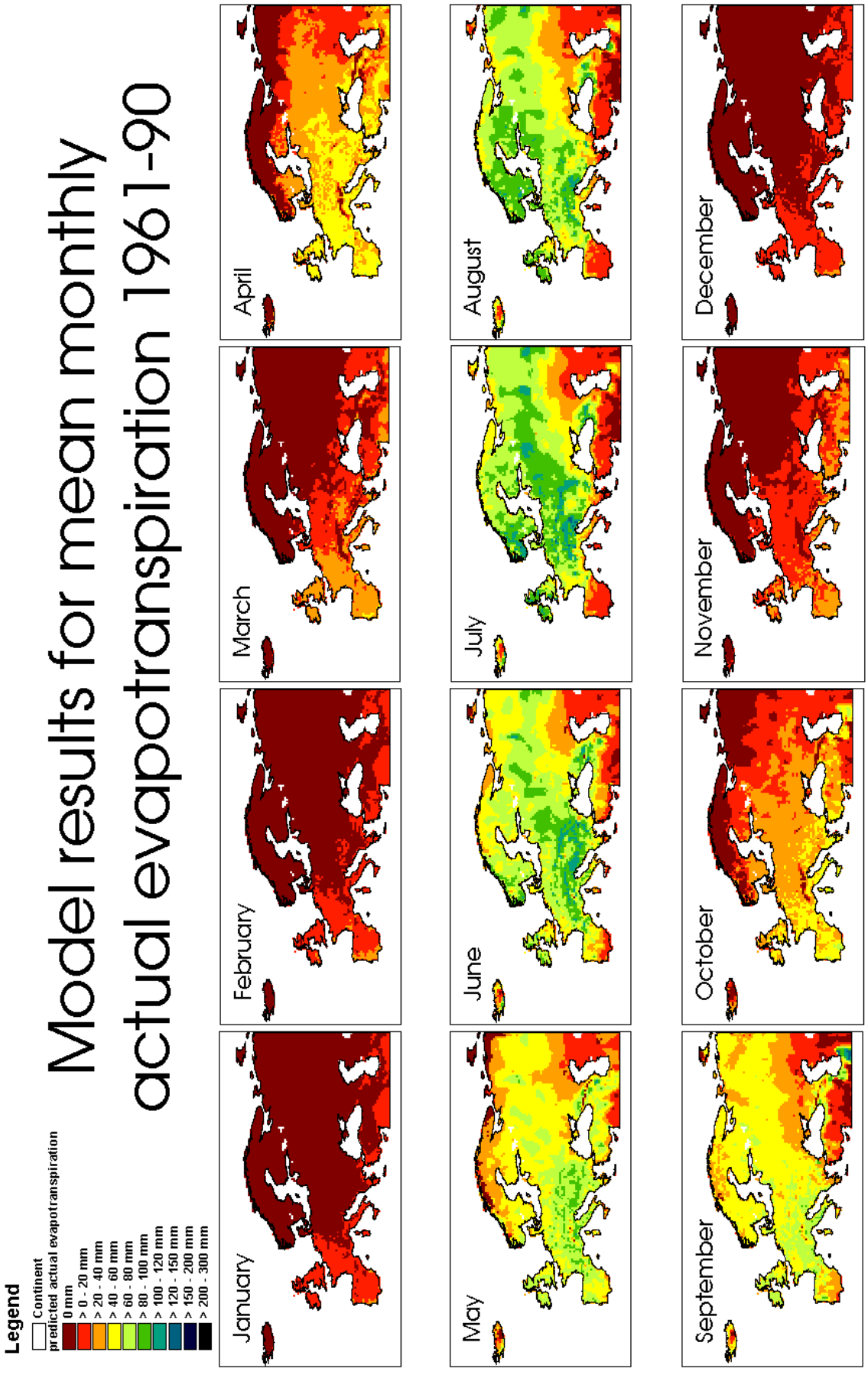

Figure 5-4: Model results of mean monthly actual evapotranspiration (1961-90).

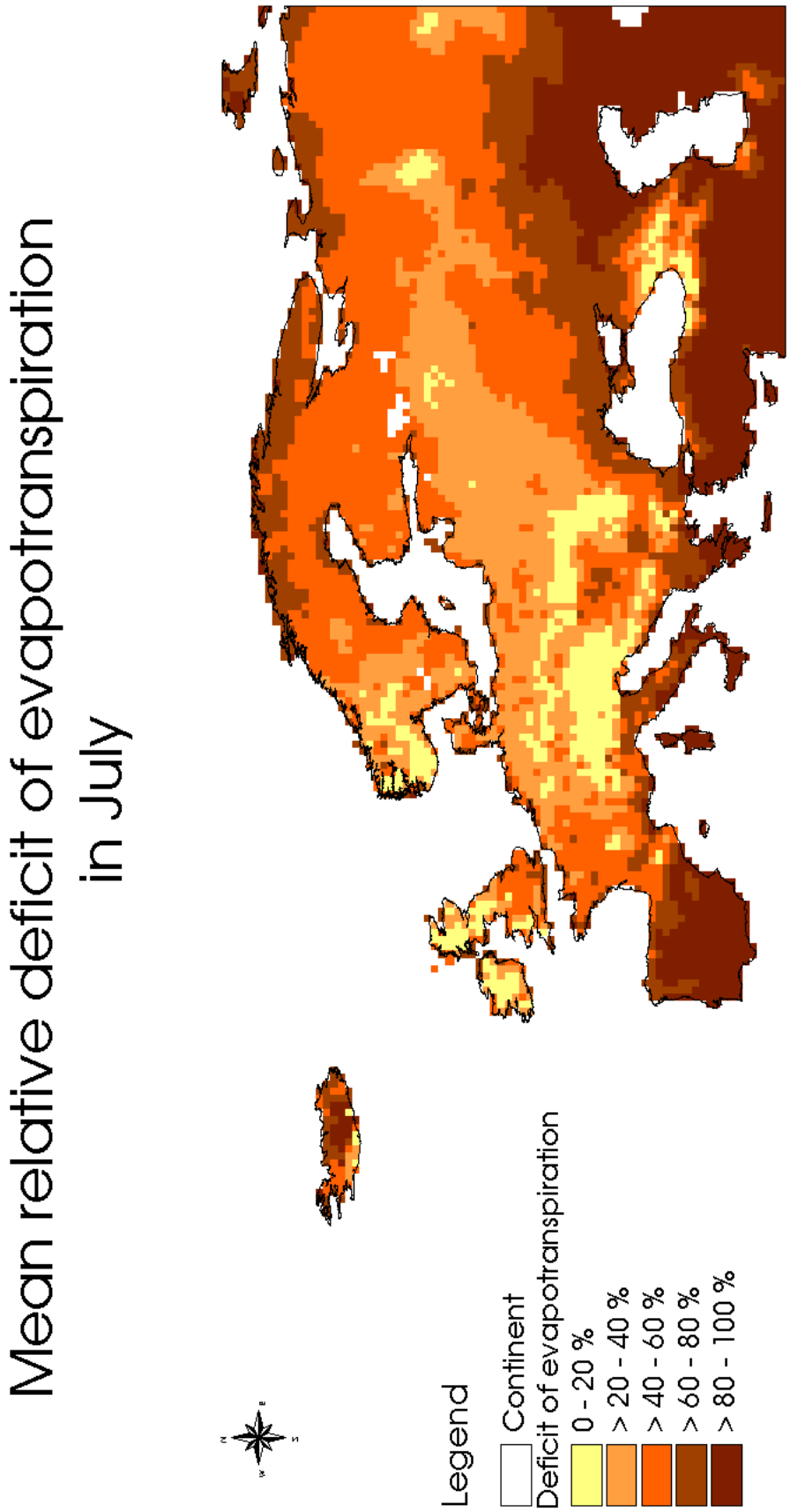

Figure 5-5: Mean relative deficit of evapotranspiration for July (in mm per month).

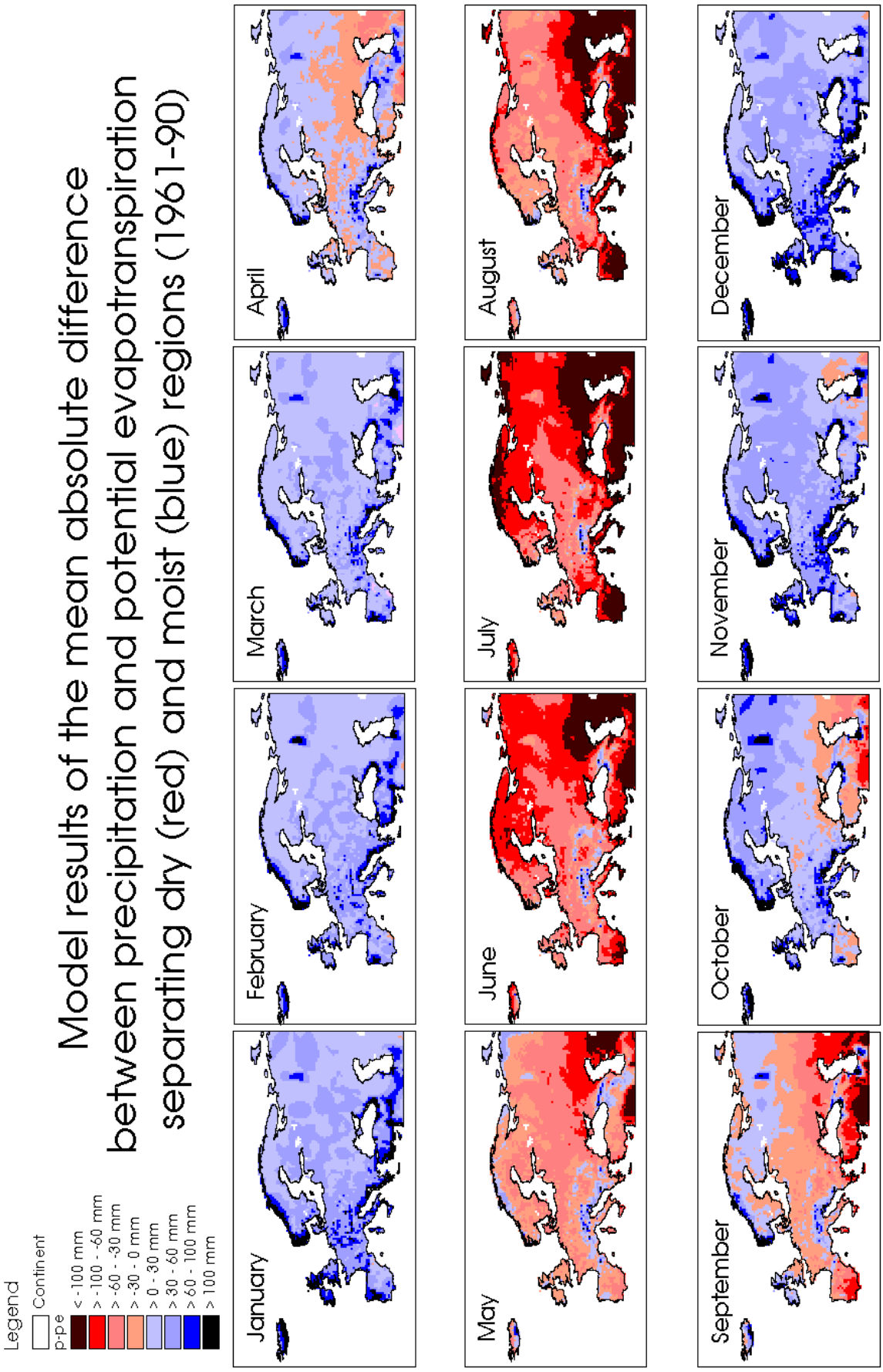

Figure 5-6: Mean absolute difference between precipitation and potential evapotranspiration (in mm per month) separating dry and moist regions in the course of the year.

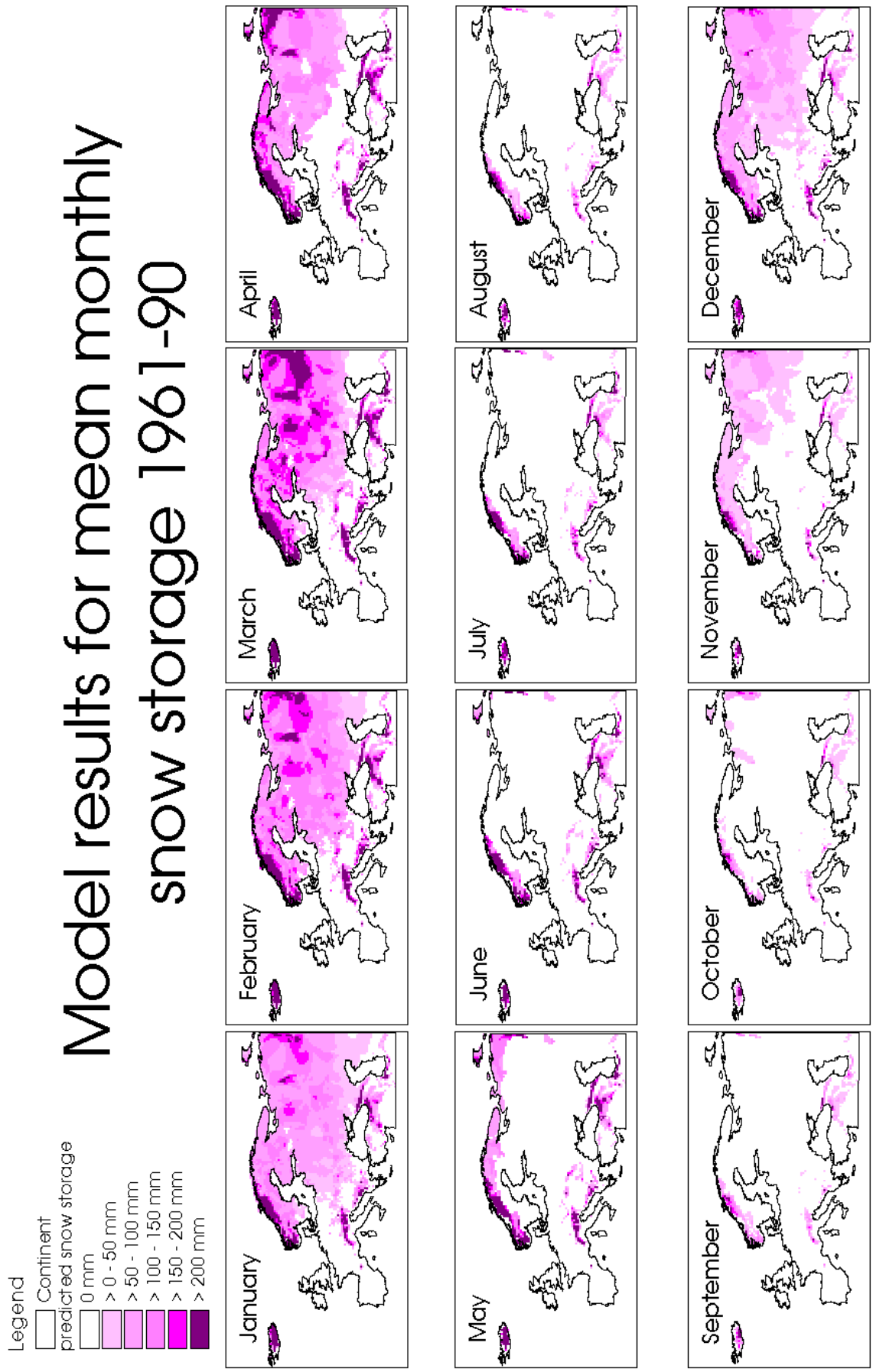

Figure 5-7: Model results of mean monthly snow storage (1961-90).

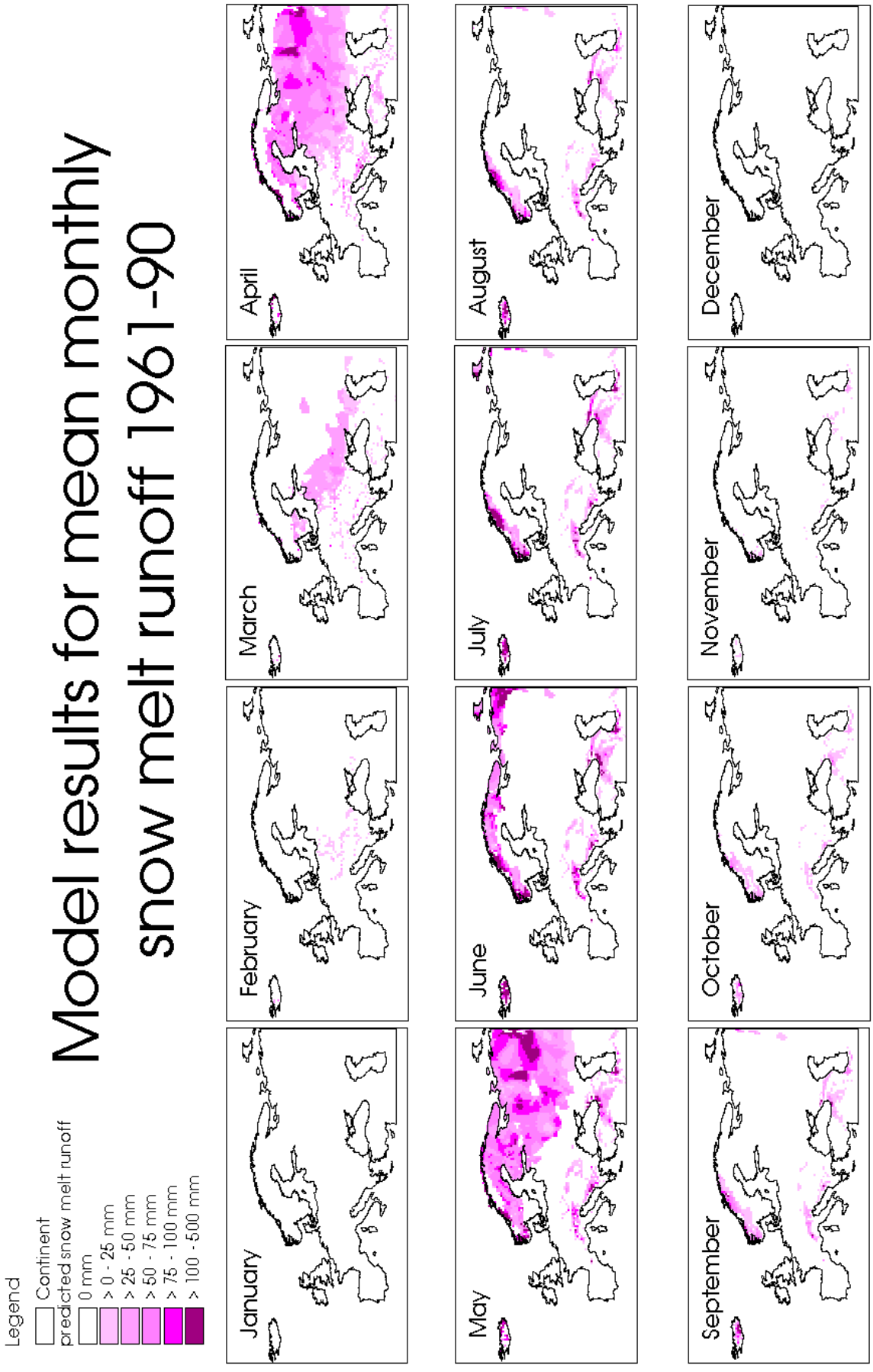

Figure 5-8: Model results of mean monthly snow melt runoff (1961-90).

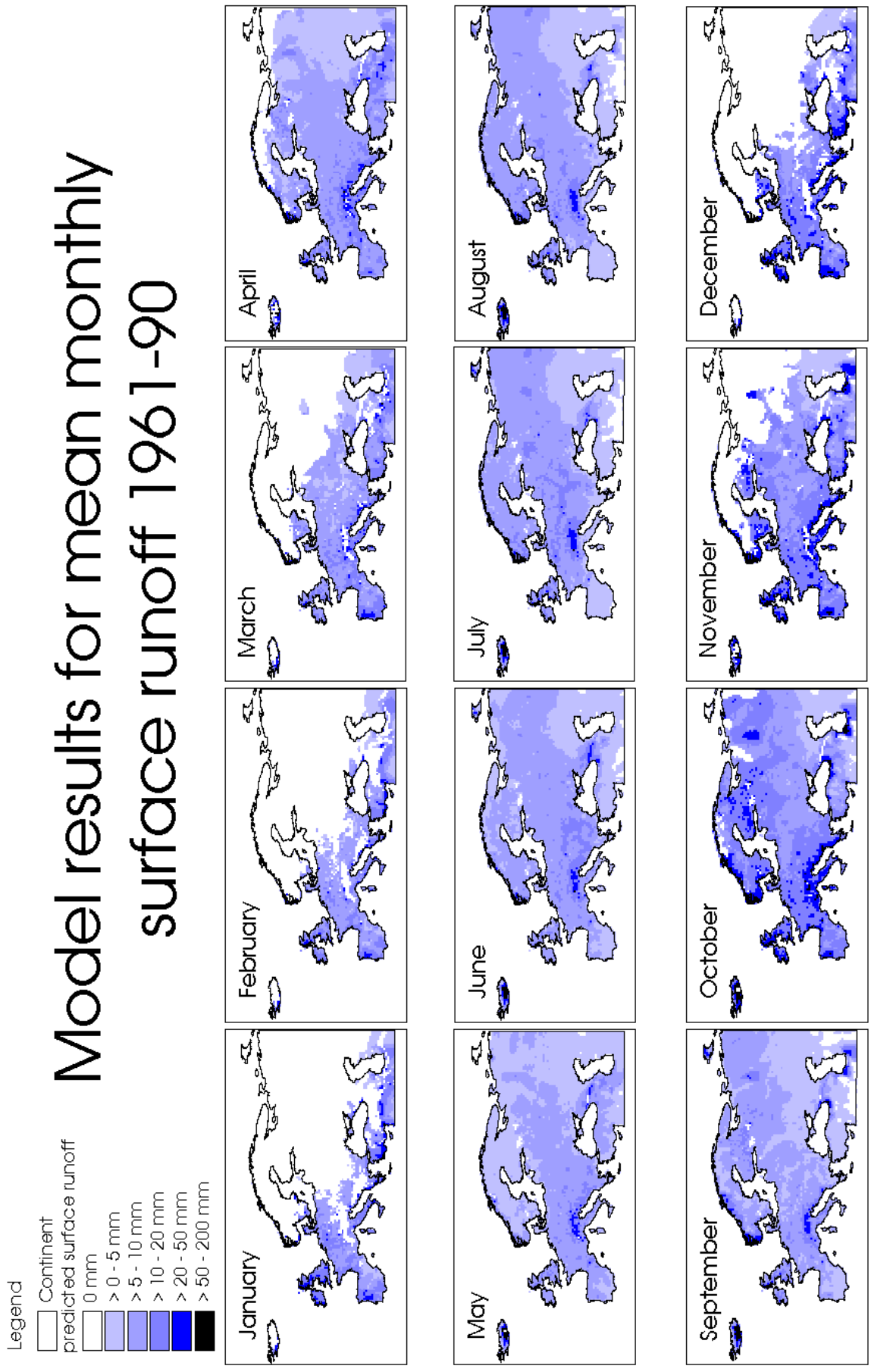

Figure 5-9: Model results of mean monthly surface runoff (1961-90).

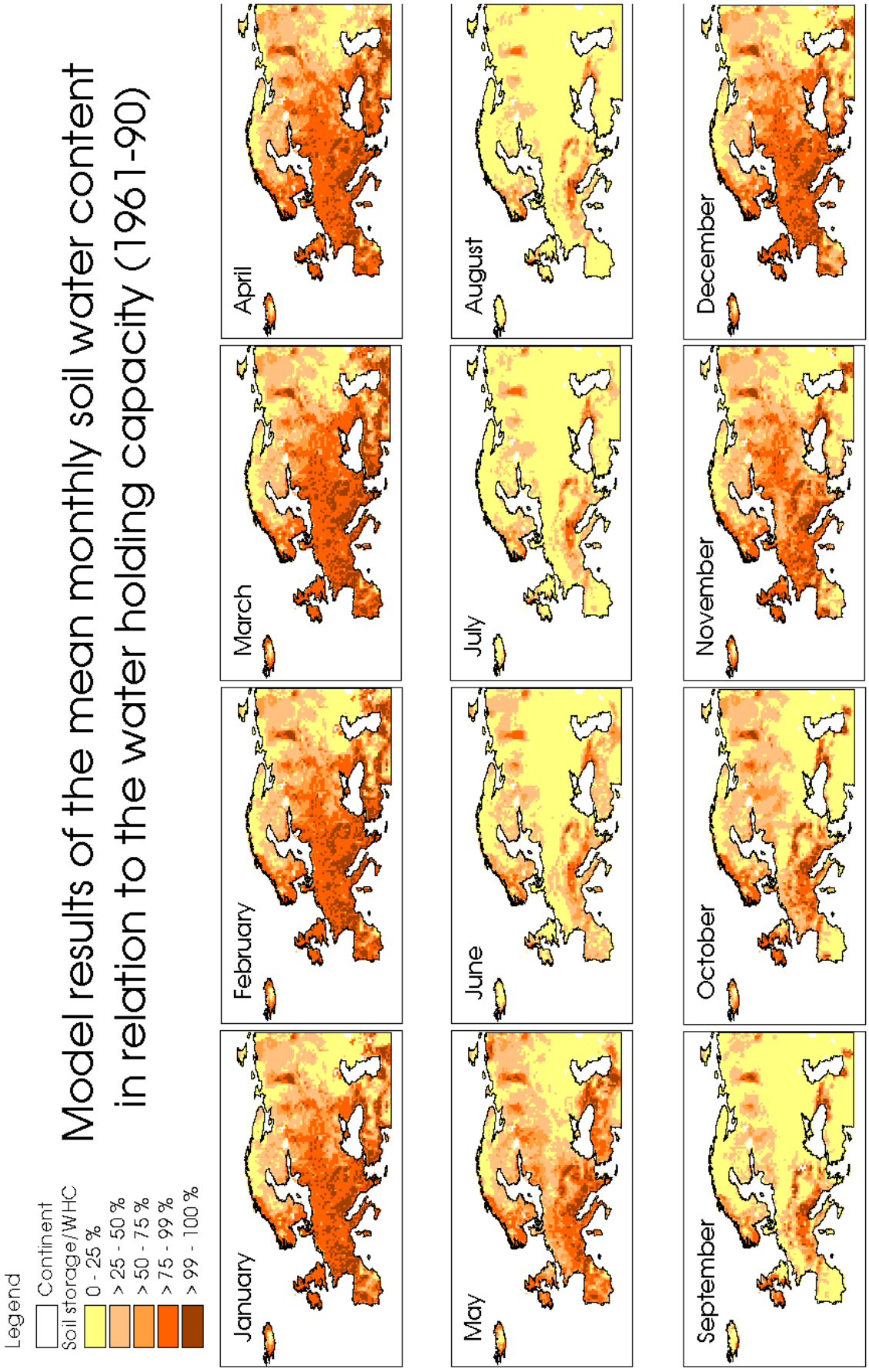

Figure 5-10: Soil water storage in relation to the corresponding water holding capacity WHC (monthly means 1961-90 in %).

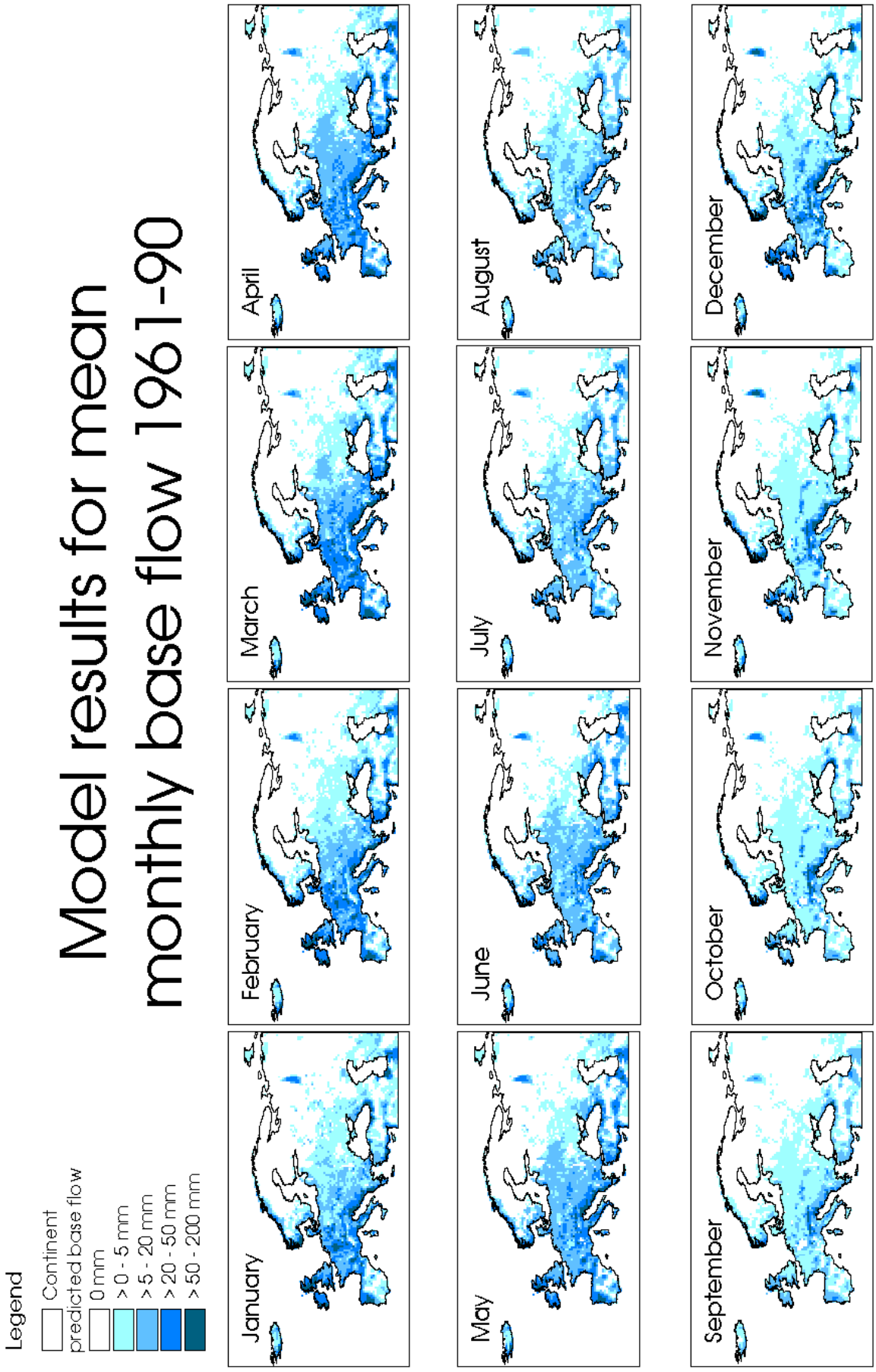

Figure 5-11: Model results of mean monthly base flow (1961-90).

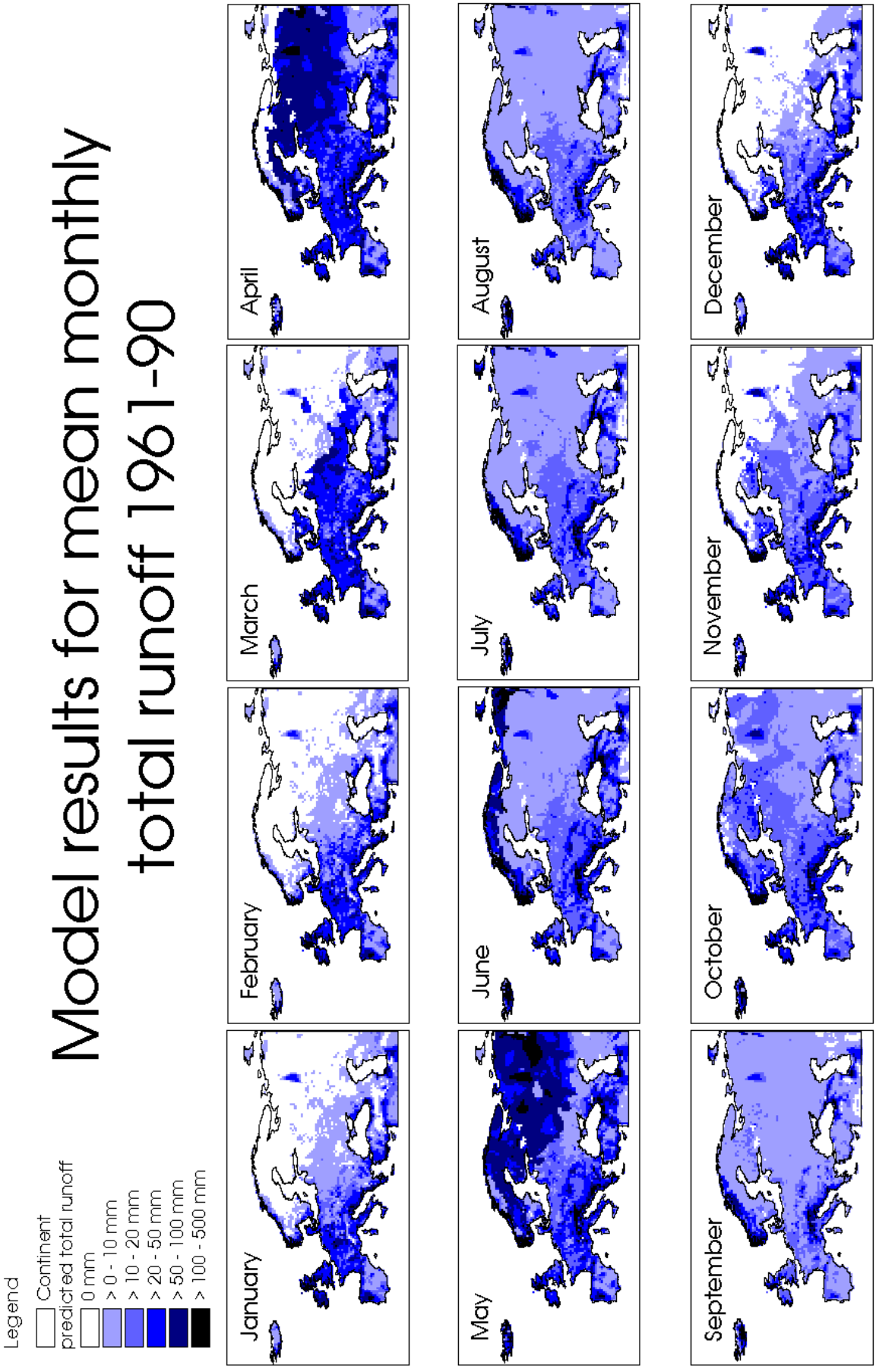

Figure 5-12: Model results of mean monthly total runoff (1961-90).

5.3 Validation of the model on the catchment level

5.3.1 Model efficiency for each European test catchment

The histogram in Figure 5-14 gives an overview of the model efficiencies of all European test catchments, excluding the Kymijoki and Júcar basins. First it shows ME values of the model run with a maximum $\overline{ME}_{all}$, second those for all five model runs with a maximum area-weighted ME within each runoff regime class and third maximum ME values of each individual basin found during the calibration process. The model has not been optimized for each individual basin separately, so still better ME values might be possible for some basins. The runoff curves of the alpine parts of Rhône and Rhine, of the Gloma basin and of the lowland part of the Weser basin could better be approximated with a limit temperature of -1°C than of -2°C.

Differences between model predictions and observations are highest (ME < -1.0) in the nival and nivo-pluvial alpine basins of the rivers Rhône and Inn, in the complex regimes of all three investigated subbasins of the river Po, in the nival lowland regime of the river Bug, in the pluvio-nival regime of the upstream part of the river Weser basin as well as the Warta basin and in the Mediterranean pluvial regime of the Guadalquivir basin. The model works best (ME > 0.5) for the catchments of the rivers Drava, Mures, Oka, Western Dvina, Mosel, Rhône between Chancy and la Mulatière/Givors, Garonne and Thames.

5.3.2 Model efficiency for each month

For each model run model efficiencies are not only computed for each test catchment but also for each month. Figure 5-13 shows that ME is positive for all months in all described model runs. The model produces best results (ME > 0.6) in the summer months from June to September. With ME values between 0.2 and 0.4 the model works less well in January. Medium model efficiencies between 0.4 and 0.6 are reached from February to May and from October to December.

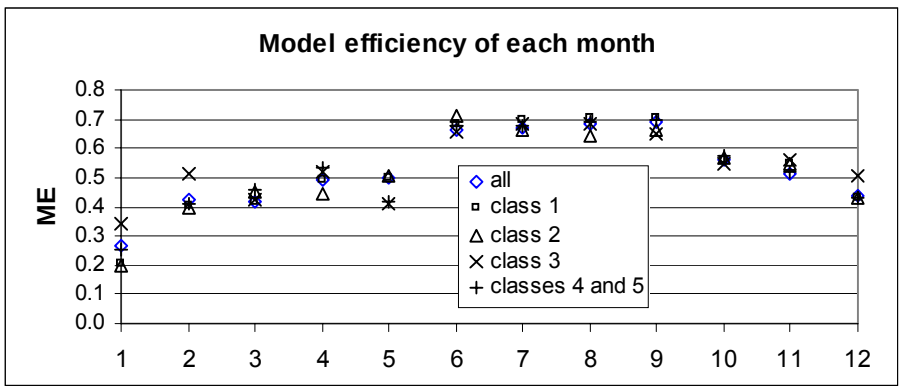

Figure 5-13: Model efficiencies of each month for all European test basins and each runoff regime class.

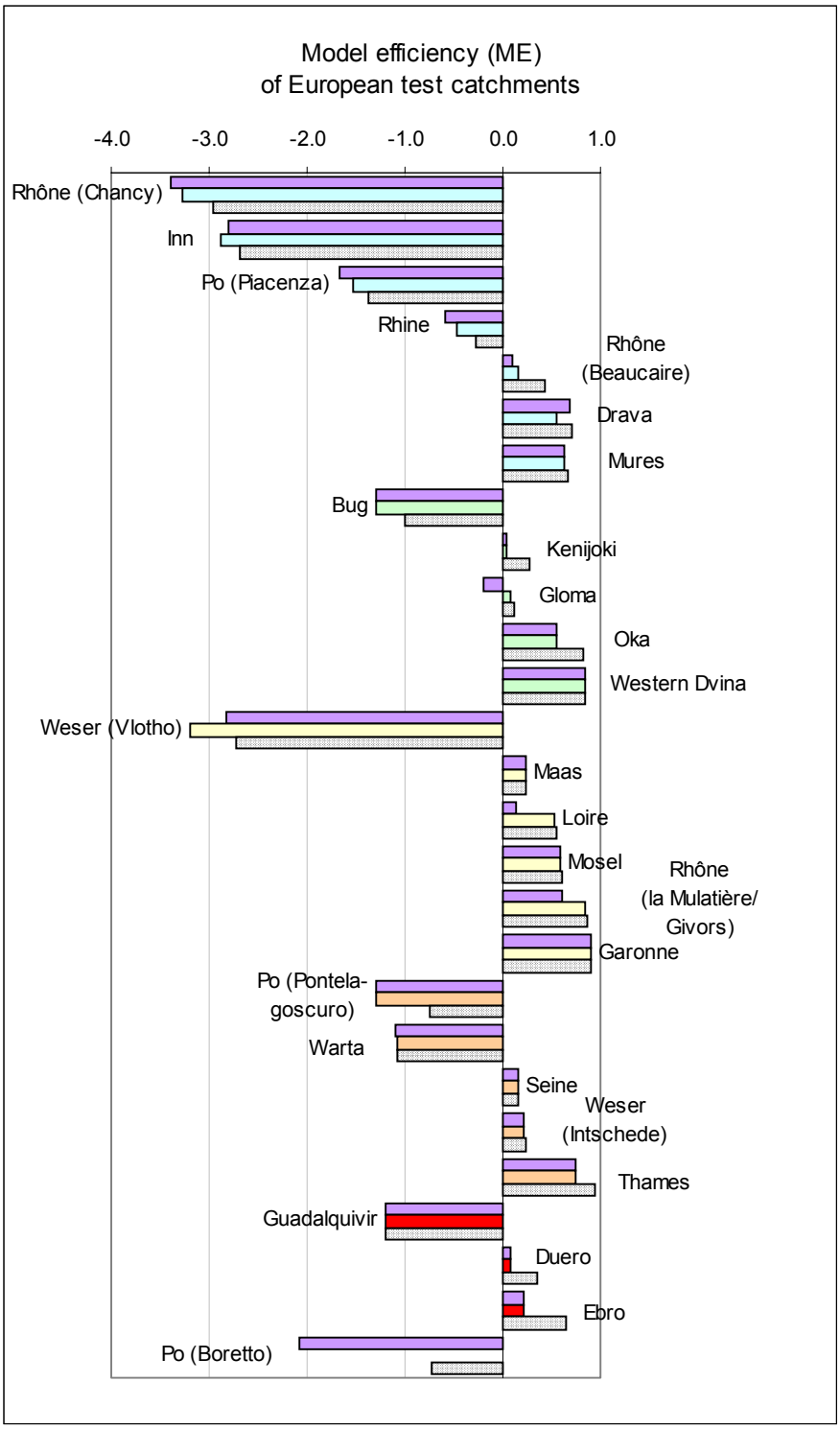

Figure 5-14: Overview of model efficiencies of all European test catchments (except for the Kymijoki and Júcar basins) for the model runs with the parameter combinations listed in Table 5-2. Violet – model run with maximum $\overline{ME}_{all}$; light blue – model run with maximum $\overline{ME}_{class1}$; light green – model run with maximum $\overline{ME}_{class2}$; yellow – model run with maximum $\overline{ME}_{class3}$; light orange – model run with maximum $\overline{ME}_{class4}$; red – model run with maximum $\overline{ME}_{class5}$; dotted white – best ME values of individual catchments found during the calibration process.

5.3.3 Over- and underestimation of the annual runoff

Annual sums of total modelled and observed runoff are compared in the map of Figure 5-15. Table 5-3 lists the corresponding absolute and relative differences. Two tendencies become plainly recognizable:

- On the one hand, total annual runoff is underestimated for the nival and nivo-pluvial regimes of the Alps, the Carpathians and Northern Europe. Observed runoff is more than 50 % higher than predicted in the model for the alpine parts of the river Rhône and for the Scandinavian river basins Kenijoki and Gloma. They are still more than 20 % higher for the alpine Rhine basin, for the upstream part of the Po catchment, for the Romanian Mures and the Finnish Kymijoki basin. In the Gloma and the alpine basins these deviations are partly explained by the changes in the snow storage. The amount of snow accumulated in winter months exceeds that melted during the summer months there (see Figure 5-7 and chapter 5.2).

  But since snow accumulation and snow melt compensate each other in the Carpathians and in Northern and Eastern Europe apart from the Scandinavian Mountains, there must be further reasons for the underestimation of total annual runoff in snowy regions. Possible explanations are an overestimation of potential evapotranspiration or a too low measured precipitation depth. The former is less probable, because in these cold snowy regions the model approximates evapotranspiration to be zero anyway, at least as long as the air temperature keeps below 0°C. However, it is a well-known problem, that precipitation falling as snow is not collected very well in common rain gauges due to snowdrift [RICHTER 1995]. Snowfall data provided by common measuring devices have been systematically too small up to now. So the big differences between measured and modelled data can at least partly be put down to these measuring errors.

  It is quite striking that differences between modelled and measured runoff are highest in the Western Alps – especially in the upstream part of the Rhône basin to the station at Chancy –, and decrease in eastern direction. This observation might be explained by the zone of westerlies causing higher amounts of orographical precipitation and snowfall at the west side of the Alps. The absolute measuring error might consequently be higher there as well.

- On the other hand, the model overestimates total annual runoff in the Mediterranean region. In the Spanish test catchments of the rivers Júcar and Guadalquivir model results exceed measured data by more than 70 %. Runoff in the Duero basin has been more than 35 % higher than the model has predicted. As precipitation can actually not be measured too high, this observation indicates that potential evapotranspiration is strongly underestimated by the model in these regions. This conclusion agrees with the

findings of MINTZ & SERAFINI (1992: 19) who pointed out that in dry regions the Thornthwaite calculation is always smaller than estimates of other formulas. The Thornthwaite formula only takes the air temperature as an input, but disregards relative humidity. Calibration of this formula has been done for a certain interval of relative humidity. Comparing a dry and a humid region with the same air temperature, potential evapotranspiration is higher in the dry region due to a higher vapour pressure gradient.

Best correspondence of modelled and measured total annual runoff is achieved for the northern Weser, Mosel, Garonne and the Po river basin between Piacenza and Boretto. Model results differ less than 3 % from measured results for these basins.

Table 5-3: Deviation of modelled from measured total annual runoff in %.

River basin	***Total annual runoff [mm]***		***Percent deviation [%]***
	modelled	***measured***	
Gloma	224.9	514.63	-56.3
Rhône (Chancy)	477.9	1046.53	-54.3
Kenijoki	162.2	342.70	-52.7
Po (Piacenza)	493.1	765.43	-35.6
Ebro	200.9	277.49	-27.6
Loire	231.1	314.53	-26.5
Kymijoki	192.5	260.31	-26.0
Rhine	708.7	940.84	-24.7
Mures	175.4	225.45	-22.2
Po (Pontelagoscuro)	389.1	486.20	-20.0
Oka	133.4	158.78	-16.0
Rhône (la Mulatière/Givors)	494.2	545.59	-9.4
Western Dvina	181.7	190.87	-4.8
Rhône (Beaucaire)	446.7	460.86	-3.1
Weser (Intschede)	243.3	248.96	-2.3
Mosel	384.6	388.76	-1.1
Garonne	404.0	404.42	-0.1
Po (Boretto)	619.9	616.46	0.6
Drava	490.8	475.84	3.1
Thames	266.0	257.62	3.3
Inn	869.5	729.69	19.2
Maas	419.2	350.84	19.5
Warta	175.3	137.97	27.1
Bug	172.2	134.81	27.7
Duero	132.1	96.12	37.4
Weser (Vlotho)	440.2	304.95	44.4
Seine	272.5	187.91	45.0
Júcar	125.7	71.99	74.6
Guadalquivir	157.2	83.56	88.1

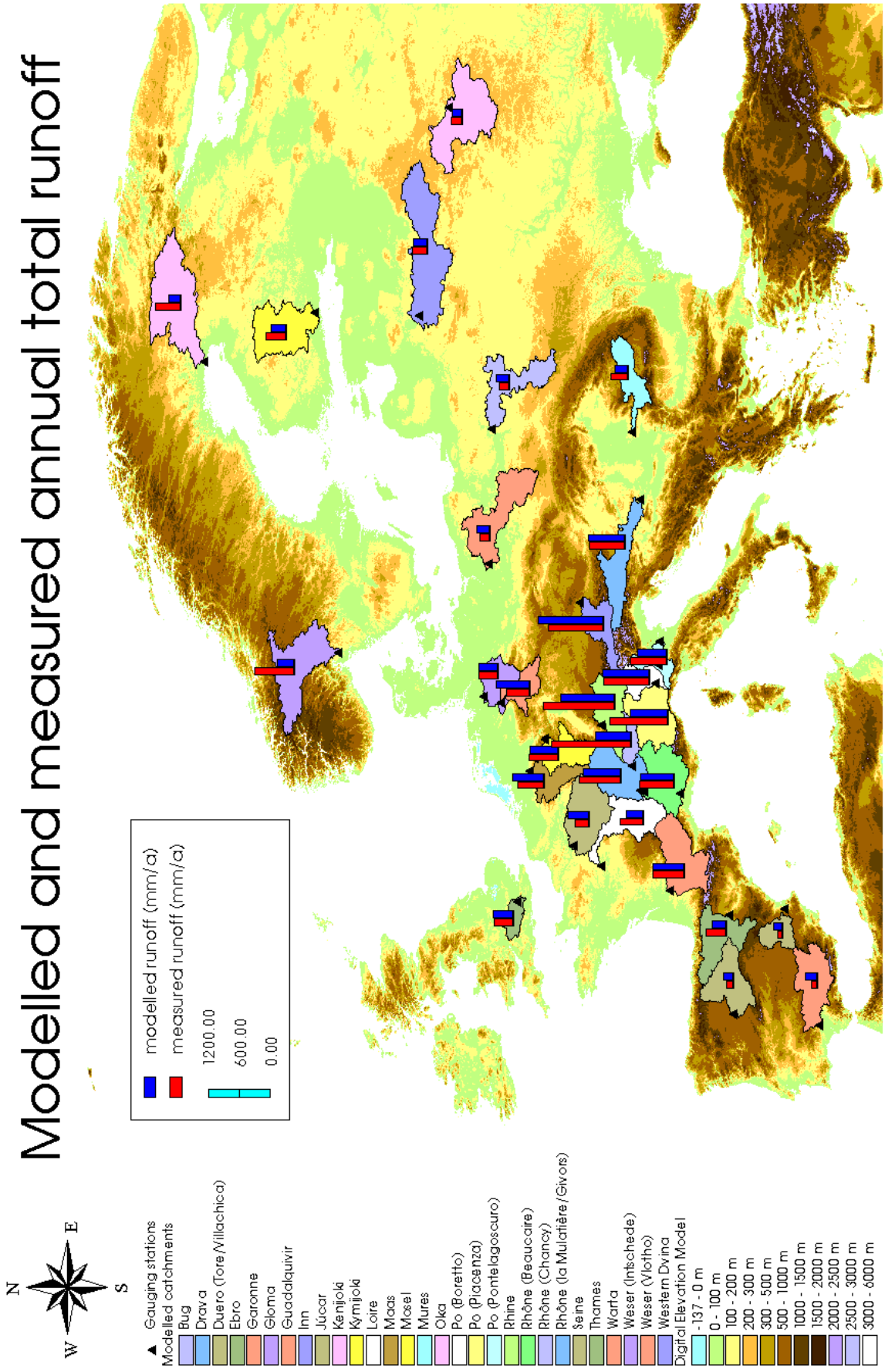

Figure 5-15: Comparison of modelled and measured annual total runoff for all European test catchments.

5.3.4 Residuals on the monthly level

5.3.4.1 Discussion of the residuals

REFSGAARD & STORM (1996) define four sources of uncertainty in hydrological modelling:

- random or systematic errors in input data like precipitation and temperature,
- random or systematic errors in measured runoff data,
- errors due to non-optimal values of model parameters and
- errors lying with a non-optimal model structure.

Differences between measured and modelled runoff can additionally be caused by anthropogenic influences on the natural runoff regime like reservoir and channel management. Totals of residuals are always the result of the combination of all mentioned sources of errors. Unfortunately, it is impossible to split residuals exactly into the four categories of errors or to give their percentages. Reasons are diverse:

- Neither the errors of the input data like precipitation and temperature nor those of the measured runoff data are known.
- Although it is obvious that a macro-scale model like the one used can only roughly approximate the much more complicated and interdepending processes of the natural water cycle, it cannot be quantified how far away from optimal the model structure is.
- It has to be emphasized that during the calibration process all types of errors can partly compensate each other, because they may have different signs.
- The first, the second and the forth error can partly be compensated by the model parameters during the calibration process.

For these reasons it has to be kept in mind that it is generally impossible to explain the residuals exactly. Only most likely explanations can be given when having a closer look at the residuals in each runoff regime type.

Figure 5-16 to show the results of those model runs for which the area-weighted model efficiency of all test catchments within a runoff regime class ($\overline{ME}_{class\,1}$ to $\overline{ME}_{class\,5}$) could be maximized[8].

[8] It has to be remembered that the figures do not necessarily mirror the best possible model result for each individual catchment. On the contrary, there are basins for which a much better adjustment to observed data can be reached with other combinations of model parameters. So it has to be remembered that the aim here was not to find those optimal parameters for each individual watershed but to optimize the model for each runoff regime class.

Runoff regime class 1:

The area-weighted model efficiency for this runoff regime class with $\overline{\overline{ME}}_{class\,1}$ = -0.651 is the lowest one of all five regime classes. Among the seven test catchments of the Alps and the Carpathians with a nival or nivo-pluvial runoff regime there are only three for which model efficiencies can become positive. These are the catchments of the rivers Mures and Drava and the most downstream part of the Rhône basin between la Mulatière/Givors and Beaucaire. For the remaining four catchments of the upper Alps, the alpine parts of the Rhine, Rhône, Po and Inn, no parameter combination could be found that could produce positive model efficiencies. The model is generally not suitable for these basins (see Figure 5-16). There are three main reasons for the residuals in these four basins:

a) unjustified changes in the snow storage,

b) too low an input data of precipitation and

c) the retention effect of big lakes and reservoirs in the Alps. In contrast to these four basins with a negative model efficiency, the Mures, Drava and southern Rhône basins do not contain such big lakes.

a) Unjustified changes in the snow storage

According to the model simulations, the amount of snow accumulation in winter is higher than the amount of snow melt in summer, at least in the High Mountains. The comparison of modelled and measured total annual runoff (see chapter 5.3.3) revealed that the corresponding simulated change of the snow storage is not justified. In reality, snow accumulation and snow melt are much more balanced on the annual level. Thus, either the simulated amount of snow accumulation is too high or/and the model results for snow melt are too small.

Concerning modelled snow accumulation, it has to be stressed that the calibrated limit temperature of -2°C already causes a relatively low amount of snow accumulation during the winter months. A still lower limit temperature of for example -3°C brings about that snow melt begins much too early in the year. So a reduction of snow accumulation does not make sense within the given model structure.

The total amount of simulated snow melt can easily be enlarged by setting higher melting percentages. Setting the third melting percentage to 1.0 would force a complete compensation between snow accumulation and snow melt. But this would produce a much too steep and pointed snow melt curve. Besides the snow melt in High Mountains generally lasts longer than three months. Setting a higher melting percentage for the first month of snow melt yields a snow melt curve that rises too early in spring. So these two extreme solutions can be excluded. Setting higher melting percentages for the further months – say high2 =

0.4 and high3 = 0.8 – enlarges the amount of snow melt and reduces the annual increase in the snow storage. One problem concerned with this solution is that the resulting computed snow melt curve is still much steeper than the measured one then. But the most important conclusion is that the part of the area under the measured total runoff curve, that is visually interpreted as summer snow melt, is much lower than the simulated snow melt then. In other words, the total amount of snow melt in reality seems to be lower than the simulated amount of snow accumulation.

This observation evokes three conjectures about processes taking place in reality which are not considered in the model structure. First precipitation in winter might not completely fall as snow, at least in spring and autumn months, but to a certain percentage as rain, so that the accumulation of snow is smaller and surface runoff and base flow are enlarged in winter (although it is not quite clear if or how the water can infiltrate and percolate when a snow cover blocks the soil surface). Second the amount of water infiltrating into the soil during snow melt might be immensely higher than 30 mm. This could partly explain the strongly underestimated base flow in winter. Third lakes and reservoirs may retain a certain amount of snow melt in summer (see below, *Retention effect of big lakes and reservoirs*).

b) Too low input data of precipitation

As already remarked in chapter 5.3.1 the input variable precipitation seems to be too low for the catchments of the alpine Rhine, Rhône and Po river resulting in an underestimation of the snow cover depth in winter and an underestimation of snow melt in summer (see Figure 5-16). For unknown reasons this effect cannot be observed in the Inn basin, since the annual amount of modelled runoff exceeds the annual amount of measured runoff.

c) Retention effect of big lakes and reservoirs

The retention effect of lakes and reservoirs might partly explain the underestimation of total runoff especially in the winter months for all four test catchments with the negative model efficiency (see Figure 5-16). There are four big lakes within the alpine Rhine basin that can store snow melt runoff in summer and release it in the winter months. The biggest lake and probably the one with the highest retention effect is the Bodensee. Within the subbasin of the river Aare, flowing into the Rhine downstream of the Bodensee, there are the Lake Neuchâtel of the river Orbe, the Vierwaldstädter See of the river Reuss and the Zürichsee of the river Limmat, which are all tributaries of the river Aare. Additionally there are several reservoirs in the glacier regions of the Aare Massif in the east part of the Bernese Alps. Within the basin of the river Inn the Chiemsee might be partly responsible for the overestimation of total runoff in the summer months. In the alpine part of the Rhône basin to the gauging station at Chancy the Lake of Geneva together with a set of reservoirs

in the Bernese Alps north of the main river and in the Alpes Pennines south of it might contribute to the underestimation of total runoff in the winter season.

A similar situation can be found in the upstream Po basin. The contribution of the river Ticino, the main tributary of the river Po to the gauging station in Piacenza, is controlled by the Lago Maggiore reservoir which has a capacity of 900 million m³. The Lago Maggiore can partly store snow melt from the Adula group and the Ticino Alps. But this can only partly explain the fact that measured runoff shows a minimum in the driest months July and August. In addition, the melting percentages must probably be set higher for High Mountains with predominantly southern slope expositions because solar radiation accelerates snow melt there in comparison to slopes with northern exposition.

In order to find the reason for the fact that absolute residuals are by far highest in the Rhône basin to Chancy, Figure 5-17 will be helpful. The amount of precipitation exceeds potential evaporation during the whole year in the Rhine, Inn and Drava basins, so that infiltration and percolation of water can take place if the temperatures make us assume that precipitation falls as rain (March to November). In contrast, potential evaporation exceeds precipitation in both Rhône subbasins and the Po subbasin to Piacenza from June to August preventing water from infiltration and percolation in the model's actual structure. In the Mures basin this situation is given with a delay of one month from July to September. Including the restrictions caused by low temperatures for the basins of the rivers Mures, Po to Piacenza and Rhône to Beaucaire 7-8 months remain for filling the soil's and the groundwater storage. But in the Rhône subbasin down to Chancy only four months remain: April and May in spring and September and October in autumn (see Figure 5-17). For this reason the groundwater recharge is too small to produce higher amounts of base flow in the model. It is not completely clear, whether the measured runoff, which is about three times as high in the winter season (see Figure 5-16), can be explained by a combination of too low precipitation data and an immense retention effect of the Lake of Geneva only, or whether there are additional reasons lying with the model structure.

Concerning the surface runoff module one aspect is plainly visible in this runoff regime class. Estimates of surface runoff are too high in direction in October. If the runoff factor was lower for that month, a higher amount of rainfall could infiltrate and recharge the groundwater storage, so that base flow would be higher in January and February, when the sum of all three runoff components is usually too small. Up to now, the proportion of surface runoff in the lowland has been set to 15 % from January to April, 10 % from May to September and 20 % from October to December. Due to a slope factor of 2.0 the proportion of surface runoff rises up to 40 % in the High Mountains. Since this slope factor has generally been confirmed during the calibration process, it seems more suitable to avoid a sudden doubling of the surface runoff proportion from September to October.

Instead the transition to high runoff factors should be performed with at least one intermediate step.

The recession constants determining the spread of base flow in the course of the year cannot be evaluated because the measured runoff curves in this regime class are composed of too many different overlapping runoff components.

Runoff regime class 2:

This runoff regime class shows that the model can work in nival or nivo-pluvial regimes as well, for the maximum area-weighted model efficiency $\overline{ME}_{class\,2}$ is positive here and individual ME values are positive for four of five included test catchments (see Table 5-2 and Figure 5-14).

Snow melt peaks – lying in May for the Scandinavian watersheds Kenijoki and Gloma and in April for the Russian watersheds Western Dvina and Oka and the Polish-Ukrainian watershed Bug – are hit for all mentioned basins except for the latter (see Figure 5-18). For the Bug basin the model computes the highest amount of snow melt already for March. The absolute amount of annual snow melt is approximately correct as well – except for the Bug basin again, for which the absolute amount of snow melt is overestimated.

But it is noticeable that the model parameter low1, the lowland melting percentage of the first month, is by far the most sensitive parameter in this runoff regime class. In the Scandinavian watersheds residuals can be minimized for low1 = 0.1 (Gloma) or low1 = 0.2 (Kenijoki), whereas in the Russian watersheds best approximations of measured runoff were reached for low1 = 0.5 (Western Dvina) or low1 = 0.6 (Oka). In the actual model run low1 was set to 0.4. For this reason the predicted snow melt runoff curve has a bulge on the left side for the Kenijoki basin and one on the right side for Western Dvina and Oka basins, producing broader but lower peaks in comparison to those observed.

Despite of this fact the Bug basin is the only one within this runoff regime class for which the model is inefficient. Main reasons are the overestimated amount of snow melt and an underestimation of total runoff from December to February. In the model in January and February precipitation is assumed to fall as snow and is completely accumulated as a snow cover. This indicates that the structure of the model is actually too simple only distinguishing between 100 % rainfall and 100 % snowfall. The Bug basin seems to be a quite good example for the fact that in months with a mean temperature around the melting temperature of water precipitation falls partly as rain and partly as snow. If this was implemented in the model, total runoff in January and February would be higher and the total amount of snow melt lower.

The Gloma basin is the only one within this runoff regime class that is influenced by snow melt from the elevation class of 500-1600 m. So the three corresponding melting

percentages are optimized especially for the Gloma catchment. In comparison to the catchments of runoff class 1, especially the Drava and Mures basins, residuals are minimized here for much higher values. Obviously, in the Eastern Alps and the Carpathians the snow melts more slowly (mid1 = 0.0; mid2 = 0.3; mid3 = 0.3) in this elevation class than in the Scandinavian Mountains (mid1 = 0.0; mid2 = 0.5; mid3 = 1.0).

The second runoff component that shall be discussed for this runoff regime is the base flow. In six months of the year the air temperature lies below the limit temperature of -2°C (November to April). During this half-year neither infiltration nor percolation of water occur in the model. According to the computations of the model, the groundwater storage of the Scandinavian and Russian basins is drained completely (Kenijoki, Gloma, Oka) or almost completely (Western Dvina) during that time. The velocity of depletion is controlled by the daily recession constant k in the model: the higher k, the more slowly the depletion and vice versa. The daily recession constant for the Kenijoki basin was fix during the calibration process since it has been determined with the help of hydrograph analysis before (k = 0.9546). The recession constant of the other basins was 0.99 in the actual model run, already producing an extremely slow storage depletion.

Assuming that it is true that the total annual amount of runoff is too low due to systematic measuring errors in the input data precipitation, higher amounts of precipitation in the winter months could not lead to an increased amount of base flow. Instead this would only increase the amount of snow melt runoff in spring.

The most probable explanation for these residuals lies in the retention effect of the lakes in the Gloma and the Kenijoki basin. The greatest lake within the Gloma basin is the Mjösa in the Gudbrandsdal valley. The river Lagen which flows through this valley is a chief tributary of the river Gloma. Lagen and its tributaries rise in the Jotunheimen and the Dovre Fjell, two High Mountain ranges with an altitude of 2000-2500 m. So the Mjösa is filled in spring with large amounts of snow melt from these High Mountains and provides the Gloma river with a relatively constant outflow of about 15-20 mm per month during the rest of the year. The greatest lakes in the Kenijoki basin lie in the upstream part of the basin and are a bit smaller than the one in the Gloma basin. So they should have a smaller retention effect. But the eastern part of the Kenijoki basin is dominated by vast marshes which have an additional retention effect. So the main reasons of the summer and autumn residuals in the Gloma and Kenijoki basin do not necessarily lie with the base flow module but, instead, residuals seem to be caused by an insufficient or missing consideration of lakes and marshes in the model structure.

This hypothesis is encouraged when regarding the two investigated Russian catchments. There is almost no difference between measured and modelled runoff in the Oka and

Western Dvina basins during the summer and autumn months and there are neither great lakes nor marshes in the area[9].

Runoff regime class 3:

Among the six test catchments of the low mountain ranges with a pluvial or pluvio-nival runoff regime (see Figure 5-20) there are five for which the model efficiency is positive. In general this is the runoff regime class with the highest area-weighted model efficiency ($\overline{\overline{ME}}_{class\,3}$ = 0.334).

The only catchment for which the residual variance exceeds the variance of observed runoff is the southern part of the Weser basin down to the gauging station at Vlotho. Residuals are highest in March and April here because the model computes snow melt runoff from the low mountain ranges of the Thüringer Wald, the Rhön and the Rothaargebirge (see Figure 5-20). At least the amount of snow melt of the Rothaargebirge, reaching the Weser through the rivers Eder and Diemel, is partly retained in the Eder and Diemel reservoirs.

In contrast to the situation in the upstream part of the Weser, the summer snow melt component of the Alps seems to be predicted quite well in the Garonne basin (see Figure 5-20).

All remaining residuals seem to be caused by the base flow component. The daily recession constant k has been determined by hydrograph analysis for the Mosel, Maas, Garonne and the upstream part of the Weser basins (see Table 4-10), whereas the recession constants of the rivers Loire and Rhône between Chancy and la Mulatière/Givors have been determined by calibration resulting in k = 0.97. The values of k for the Mosel, Maas and upper Weser basins seem to be too low, since base flow is overestimated in the winter months and underestimated in the summer months. Higher recession constants leading to a smoother base flow curve could further improve model results for these three basins.

Runoff regime class 3 is the one with the highest absolute amount of groundwater runoff. On the one hand, these regions are not dominated by snowfall and a snow storage like in runoff regime classes 1 and 2. So water can infiltrate and percolate during the whole year. On the other hand, the total amount of rainfall is higher in the low mountain ranges than in the lowland of runoff regime class 4 or in the rainless Mediterranean region of runoff regime class 5.

[9] The basin of the river Pripjet, a tributary of the river Dnieper, in Belarus is strongly dominated by marches. In a region like this the model would probably fail completely.

Runoff regime class 4:

This runoff regime class is characterized by pluvial or pluvio-nival runoff regimes in which at least the Thames, Seine, northern Weser and Warta basins almost exclusively consist of lowland regions. The most downstream one of the three studied Po basins (station Pontelagoscuro) actually is a mixture of runoff regime classes 1, 4 and 5 for it partly consists of high mountain ranges of the Adamello mountain group in the Southern Alps (class 1), and the precipitation curve shows two peaks, one in April/May and one in October/November with quite dry summer months in between which is typical for the Mediterranean region (class 5). But since it is mainly stamped by the plains of the river Po and since the total amount of precipitation is still much higher than in the Spanish test catchments, it has been assigned to regime class 4 (see Figure 5-22).

For the model run, producing a maximum area-weighted model efficiency $\overline{ME}_{class\,4}$, individual ME values are positive for the Thames, Seine and lower Weser catchment and negative for the Po and Warta basin. The model computes small amounts of snow melt for the two latter basins, that are not mirrored in the measured runoff curve.

The recession constant of the downstream part of the Weser basin has been determined by hydrograph analysis to be k = 0.9689. But similar to the situation in the upstream part of the Weser catchment and the watersheds of the rivers Mosel and Maas, this recession constant turns out to be too small because model estimates are too high in winter and too low in summer (see Figure 5-22). A second possible explanation for the residuals might be that a certain amount of precipitation falling in the Harz Mountains is stored in the seven reservoirs of the Western Harz in winter and released additionally in summer.

For the other four catchments of this runoff regime class calibration yielded an optimal recession constant of 0.99. For the British Thames catchment this k-value produces too straight a base flow curve (see Figure 5-22). Residuals could be further reduced here for k = 0.98 resulting in a model efficiency of 0.939 then, which is the highest ME value that has been reached for an individual catchment during the whole calibration process.

The model computes a snow melt runoff of the alpine mountains in the summer months and surface runoff mirrors the two precipitation peaks in spring and autumn. But in contrast to the model predictions, measured runoff keeps relatively constant at 45 mm per month from September to April in the long-term mean. Only in the summer months when precipitation is low and temperatures are high, observed runoff falls to 20 mm in July. A possible explanation for these differences between modelled and measured data might lie with the Lago di Garda and the smaller Lago d'Iseo, two lakes that can store alpine snow melt runoff so that a snow melt runoff maximum cannot be observed any more at the gauging station at Pontelagoscuro.

Runoff regime class 5:

Among these purely pluvial Mediterranean runoff regimes ME values for the Duero and Ebro basins are positive, but for the Guadalquivir catchment ME values remained negative for all tested parameter combinations. Underestimation of evapotranspiration by the Thornthwaite formula leads to a light overestimation of total runoff in the Duero catchment and a very strong one for the Guadalquivir basin in the south of Spain (see). Model predictions in the Guadalquivir basin mirror the two peaks of precipitation in March and December whereas measured runoff does not. Rainfalls in spring might partly be stored in the reservoirs of the northern tributaries in the Sierra Morena or the southern tributaries in the Sierras Béticas.

In the Ebro basin measured runoff data spread extremely in the winter months. In January the arithmetic mean of all January runoff amounts is 46.3 mm for the period of 1961-84 with a standard deviation of 56.1 mm. However, the median is as low as 29.6 mm indicating a distribution with a strongly positive skew. This is caused by two extreme runoff amounts in January 1961 (257.6 mm) and January 1962 (130.6 mm). Excluding these outliers the arithmetic mean is only 29.9 mm which is very close to the median. The situation is similar for other winter months. The dotted line in shows the curve of measured runoff when disregarding the two years of winter floods, 1961 and 1962, resulting in much lower residuals.

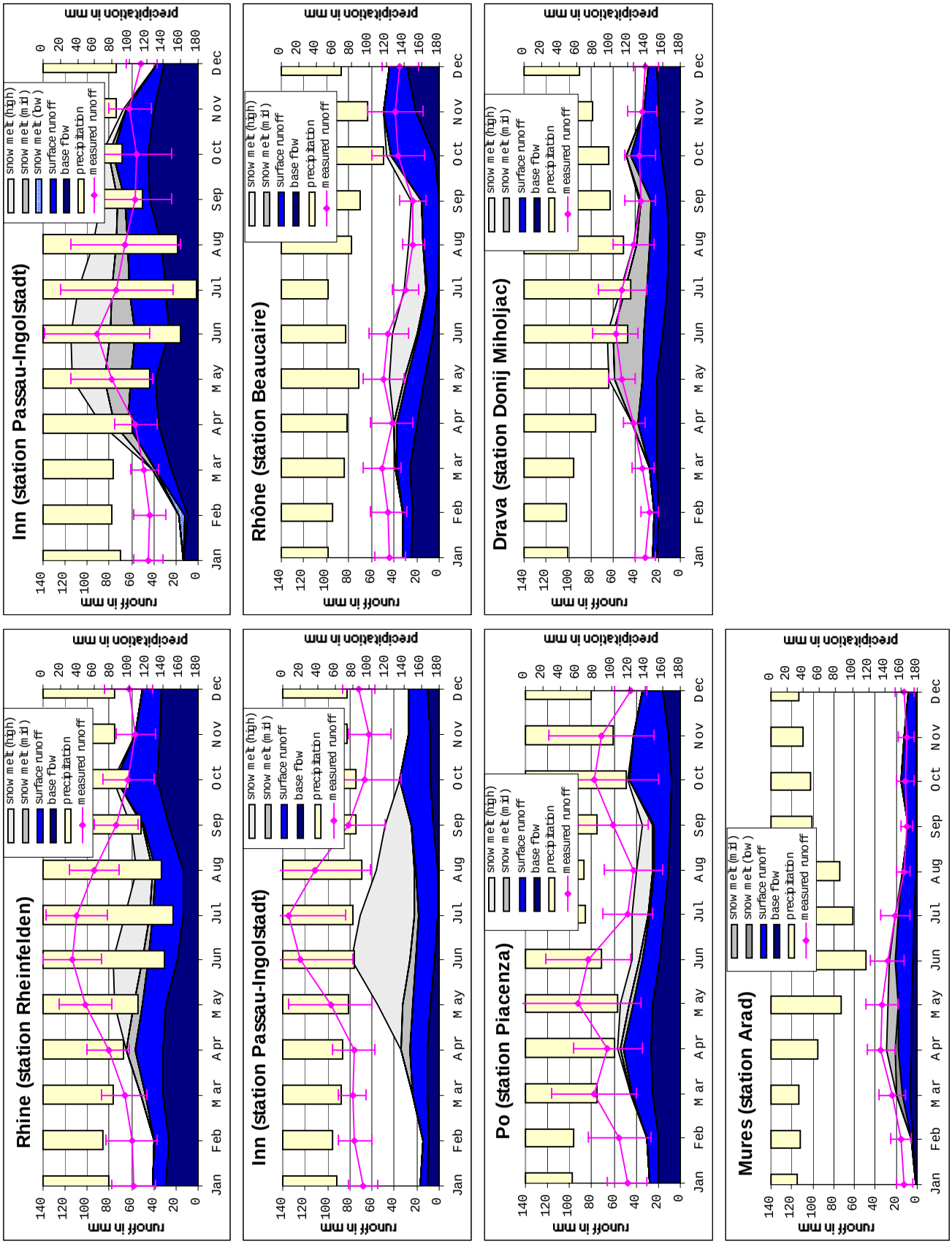

Figure 5-16: Observed and predicted runoff of the test catchments within runoff regime class 1 (monthly means 1961-90).

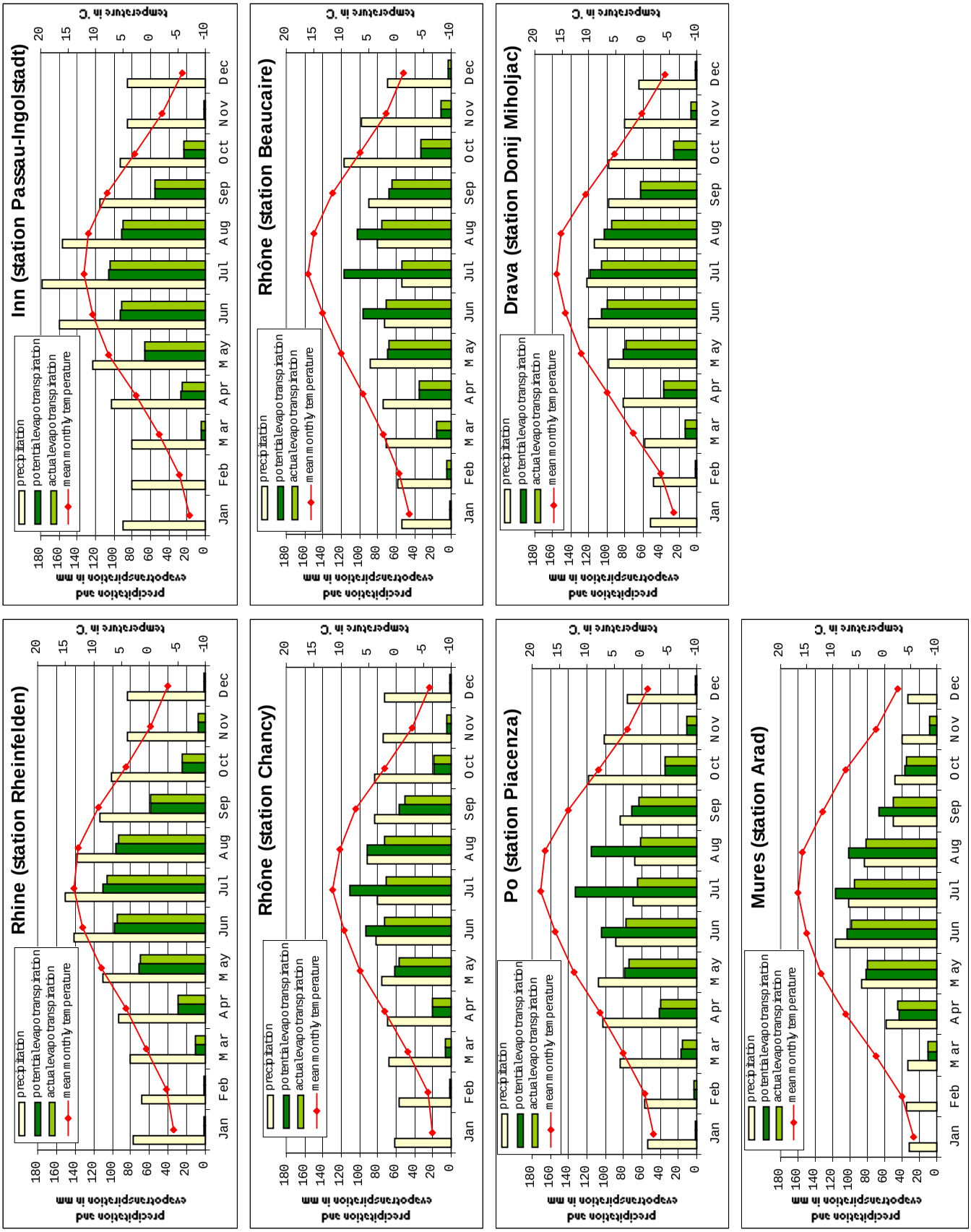

Figure 5-17: Temperature and precipitation as input data and potential and actual evapotranspiration as model results of the test catchments within runoff regime class 1 (monthly means 1961-90).

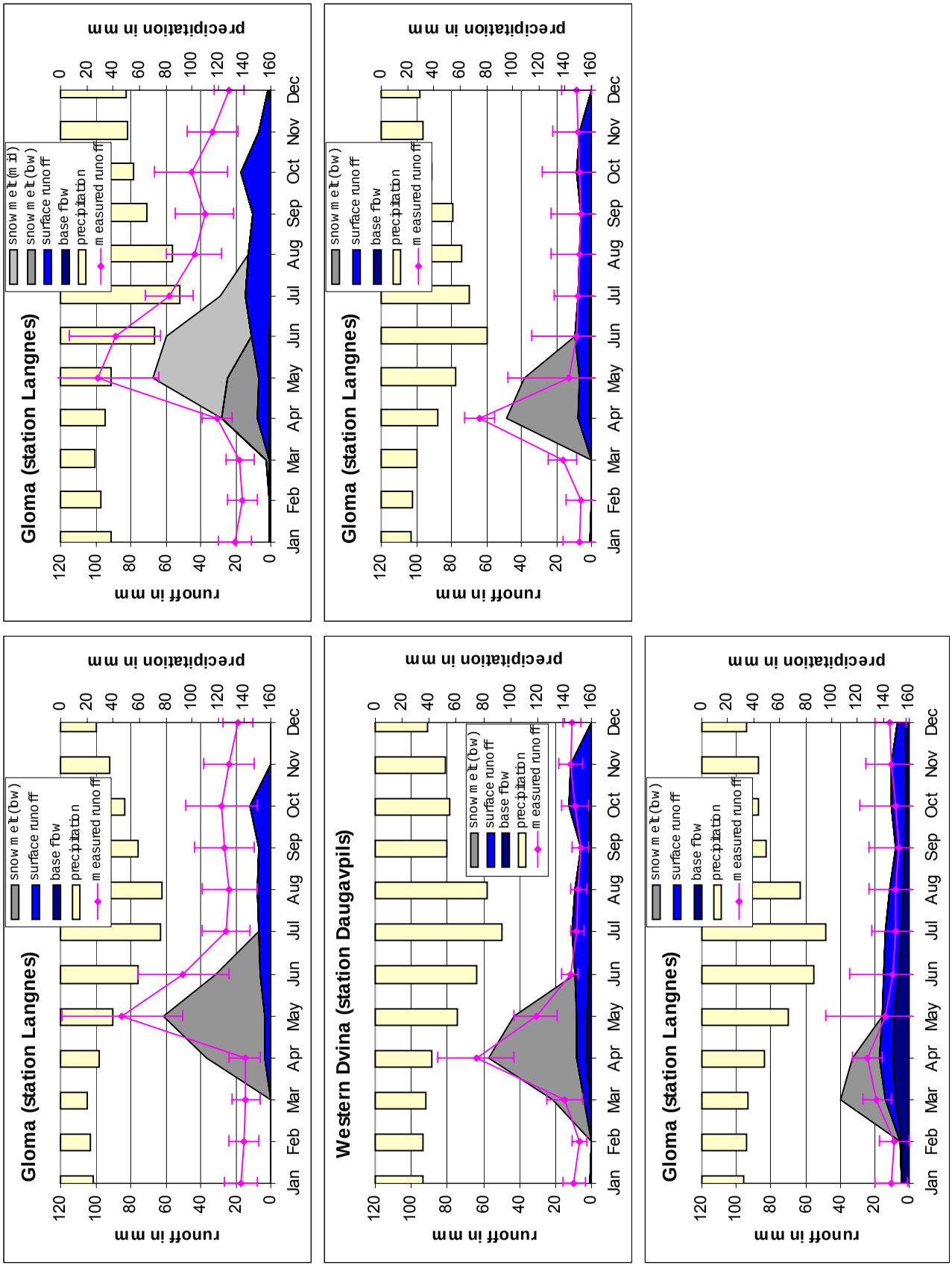

Figure 5-18: Observed and predicted runoff of the test catchments within runoff regime class 2 (monthly means 1961-90).

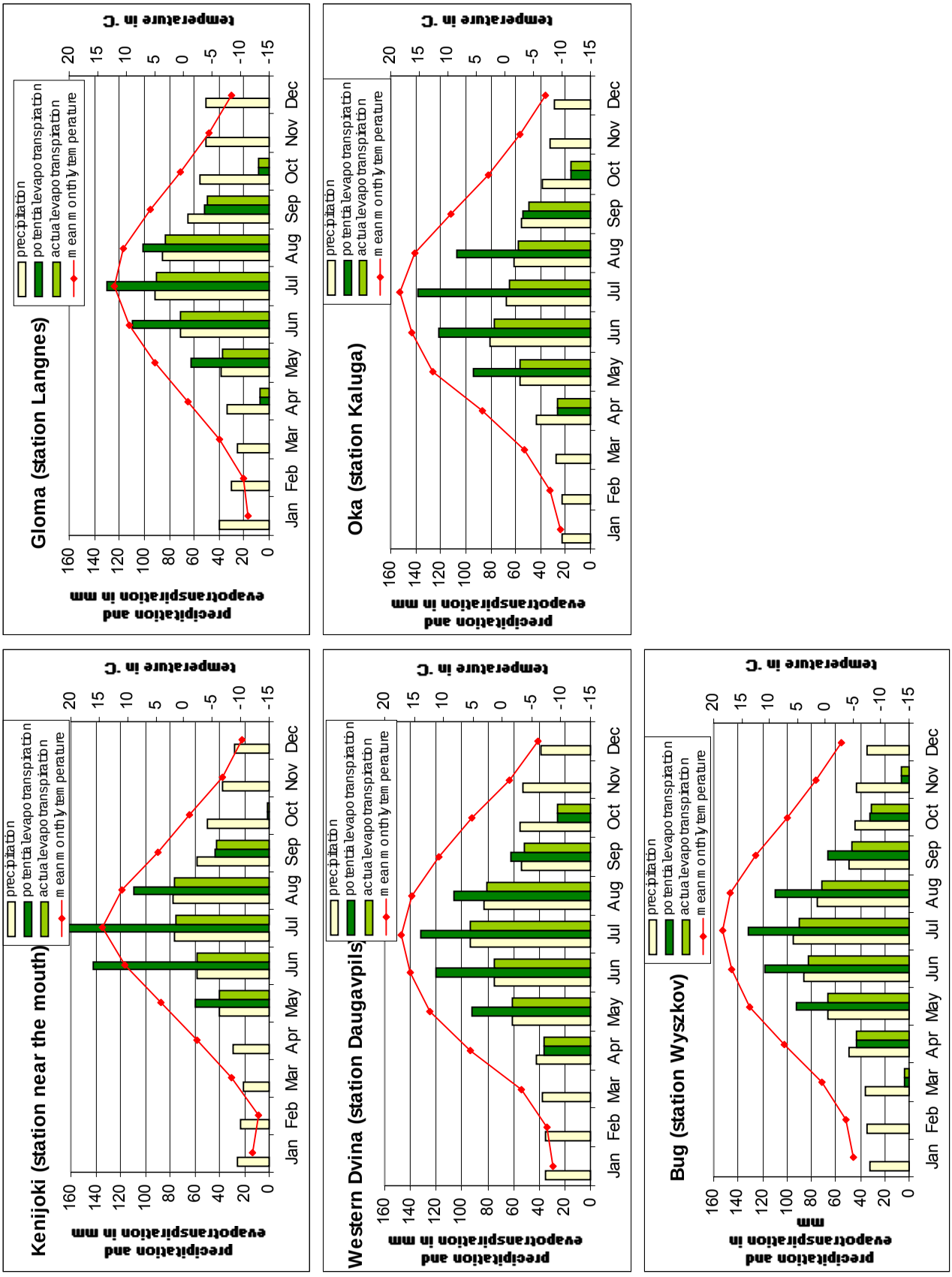

Figure 5-19: Temperature and precipitation as input data and potential and actual evapotranspiration as model results of the test catchments within runoff regime class 2 (monthly means 1961-90).

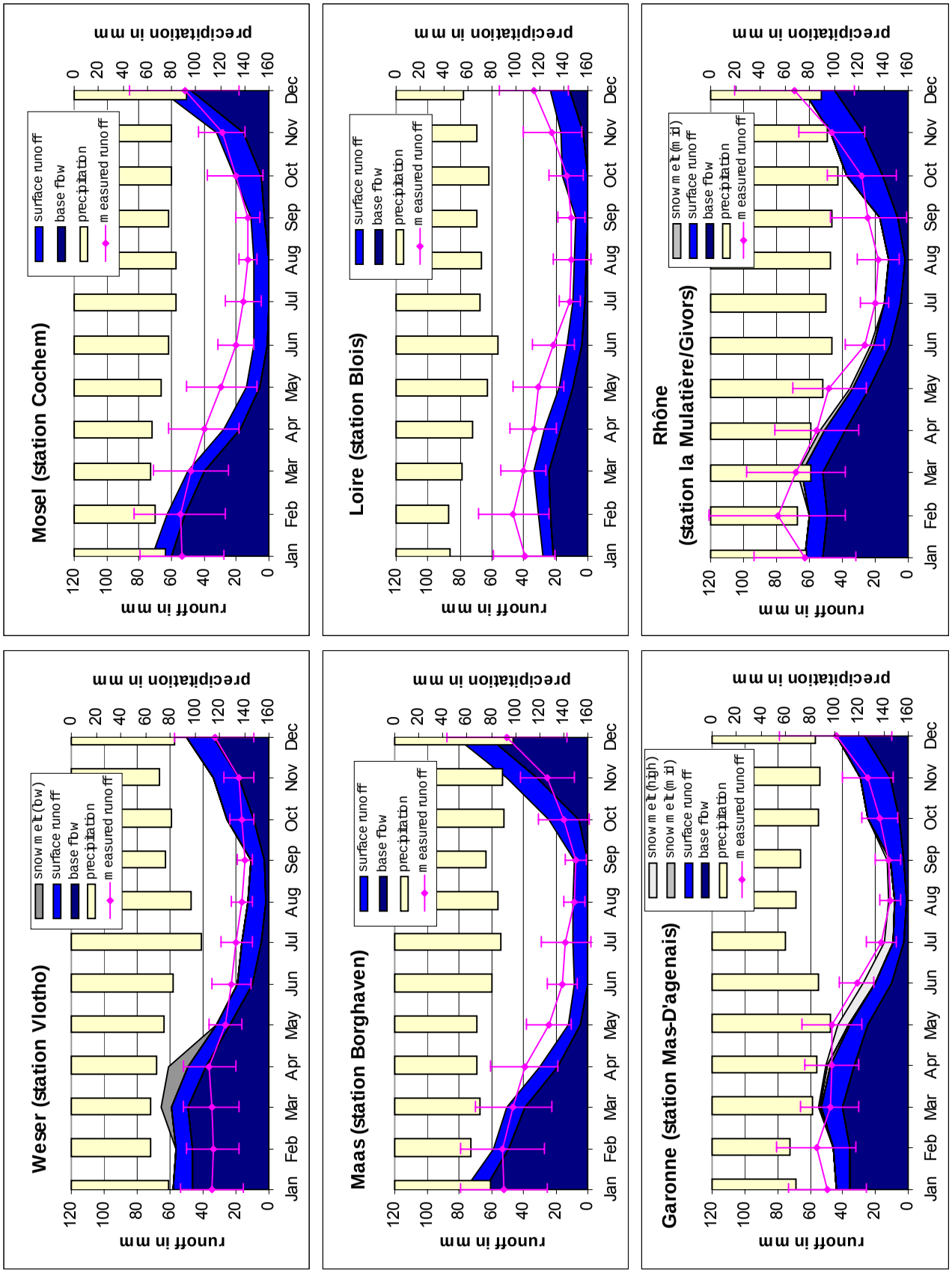

Figure 5-20: Observed and predicted runoff of the test catchments within runoff regime class 3 (monthly means 1961-90).

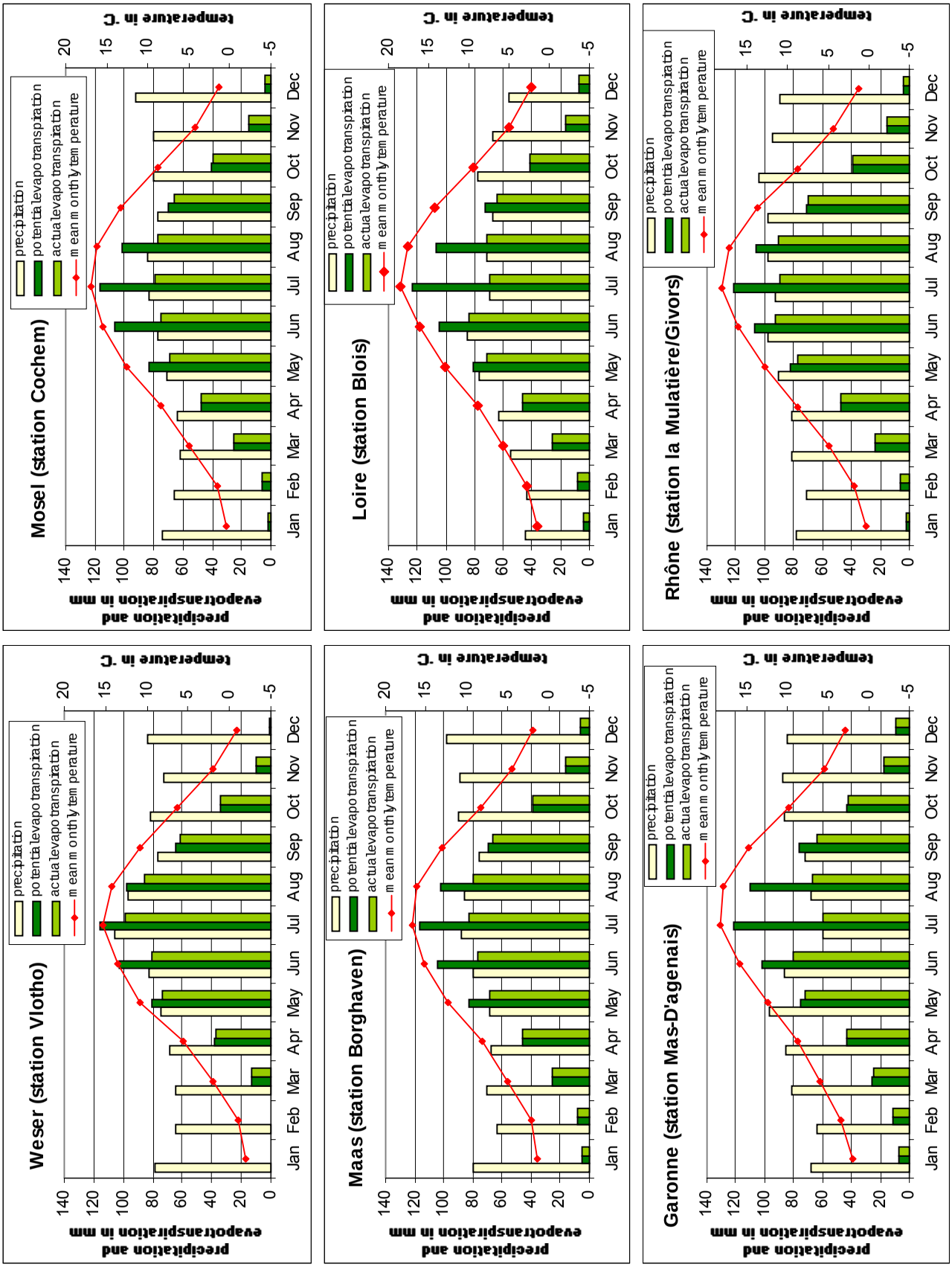

Figure 5-21: Temperature and precipitation as input data and potential and actual evapotranspiration as model results of the test catchments within runoff regime class 3 (monthly means 1961-90).

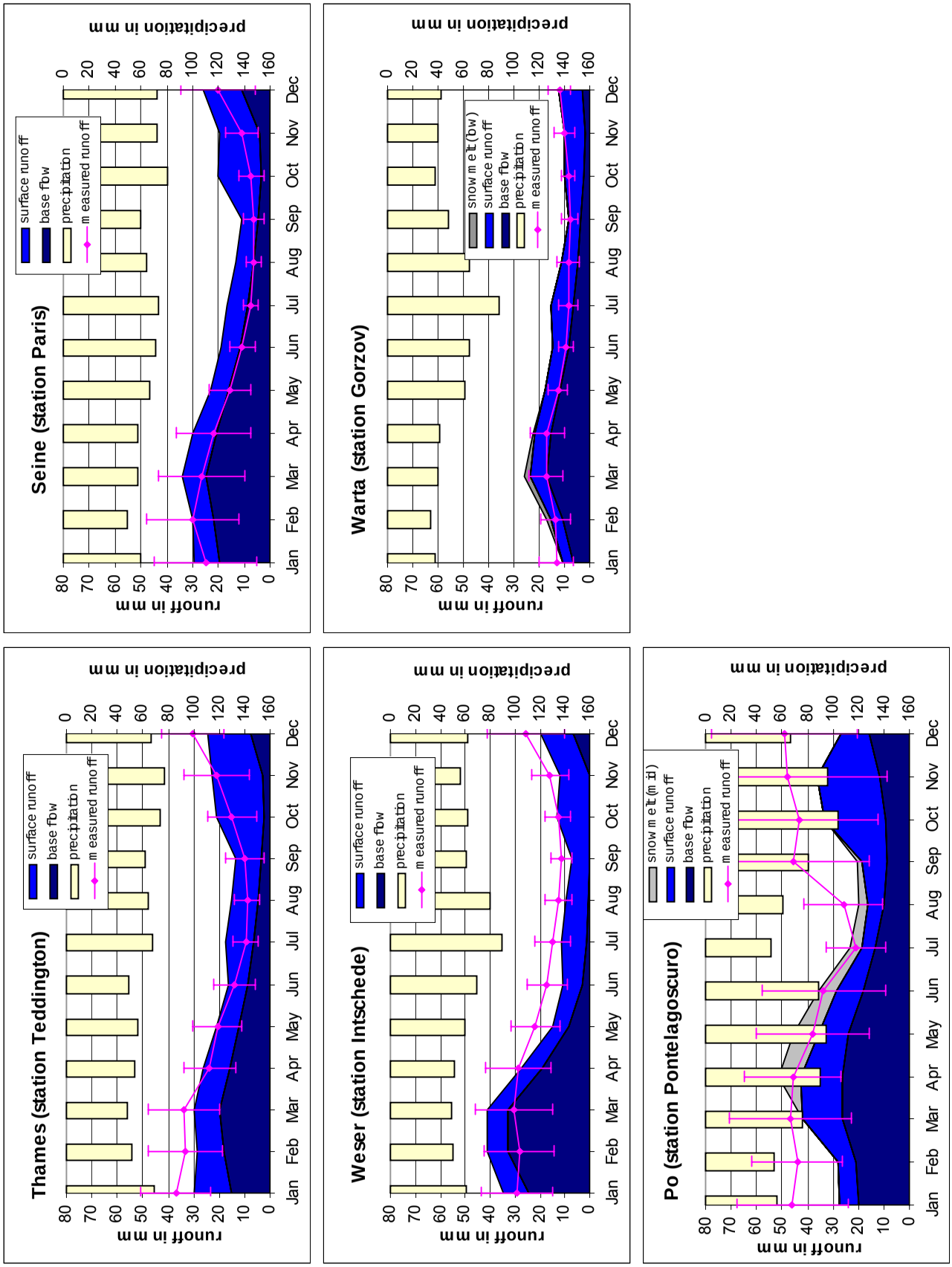

Figure 5-22: Observed and predicted runoff of the test catchments within runoff regime class 4 (monthly means 1961-90).

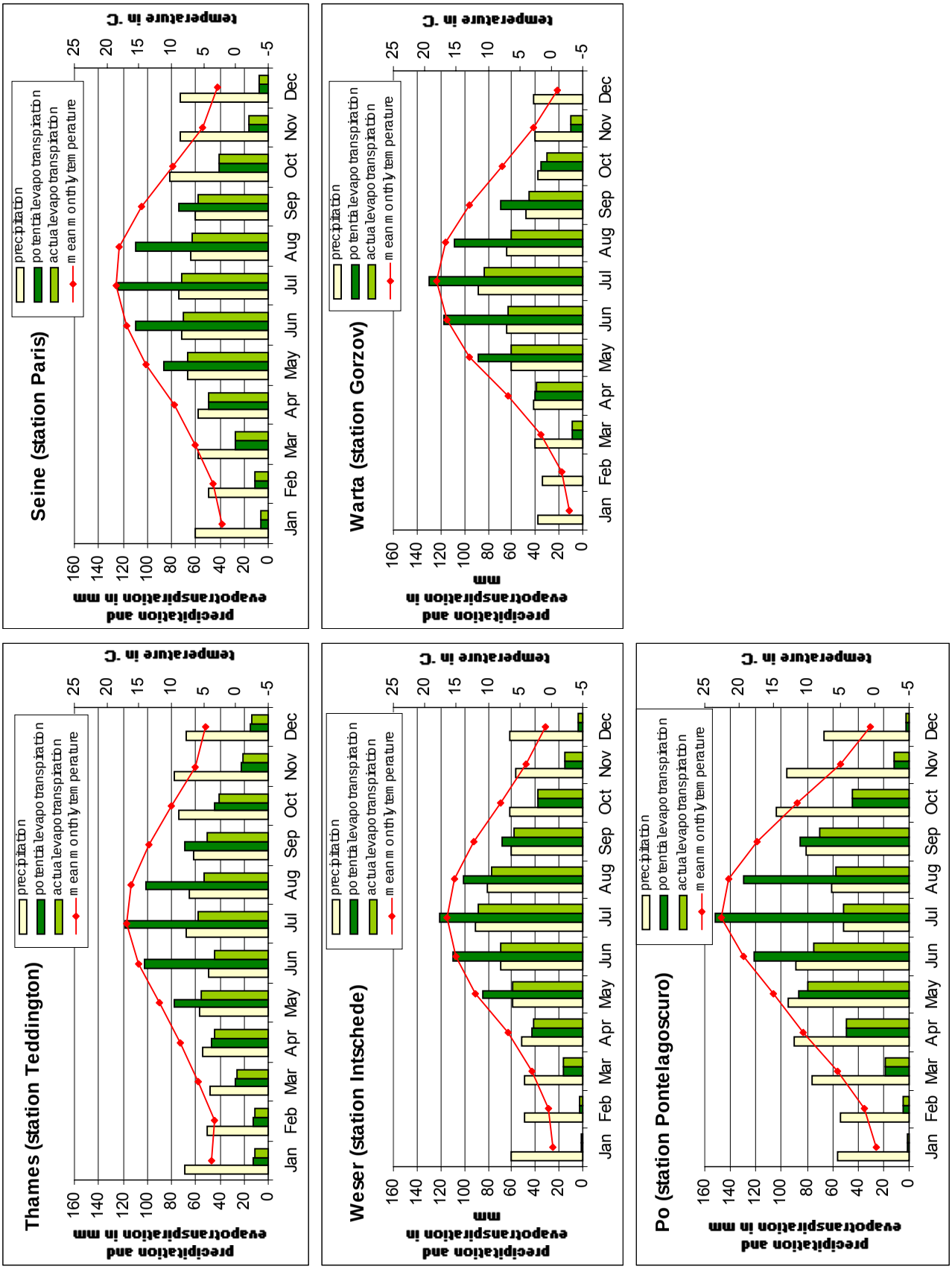

Figure 5-23: Temperature and precipitation as input data and potential and actual evapotranspiration as model results of the test catchments within runoff regime class 4 (monthly means 1961-90).

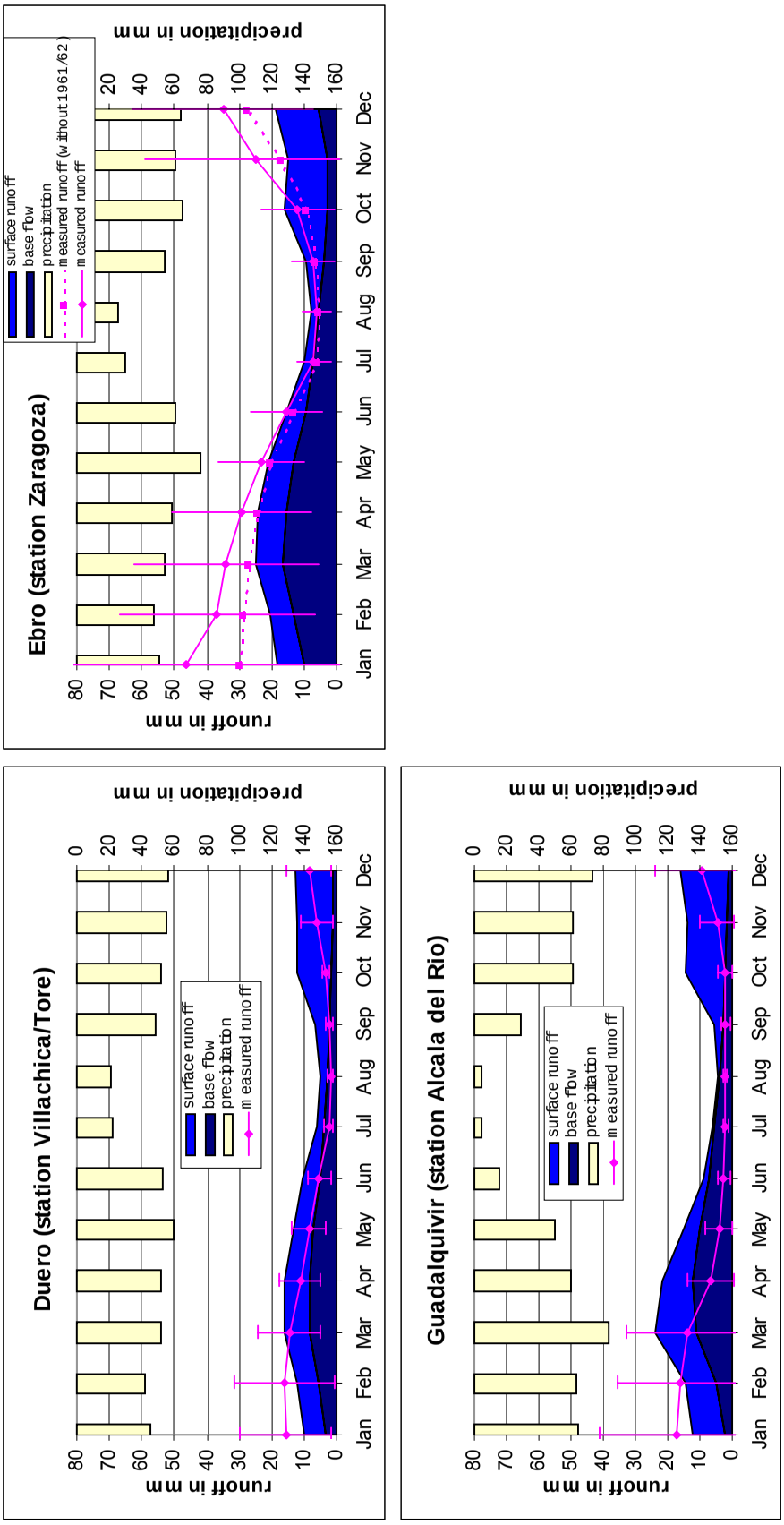

Figure 5-24: Observed and predicted runoff of the test catchments within runoff regime class 5 (monthly means 1961-90).

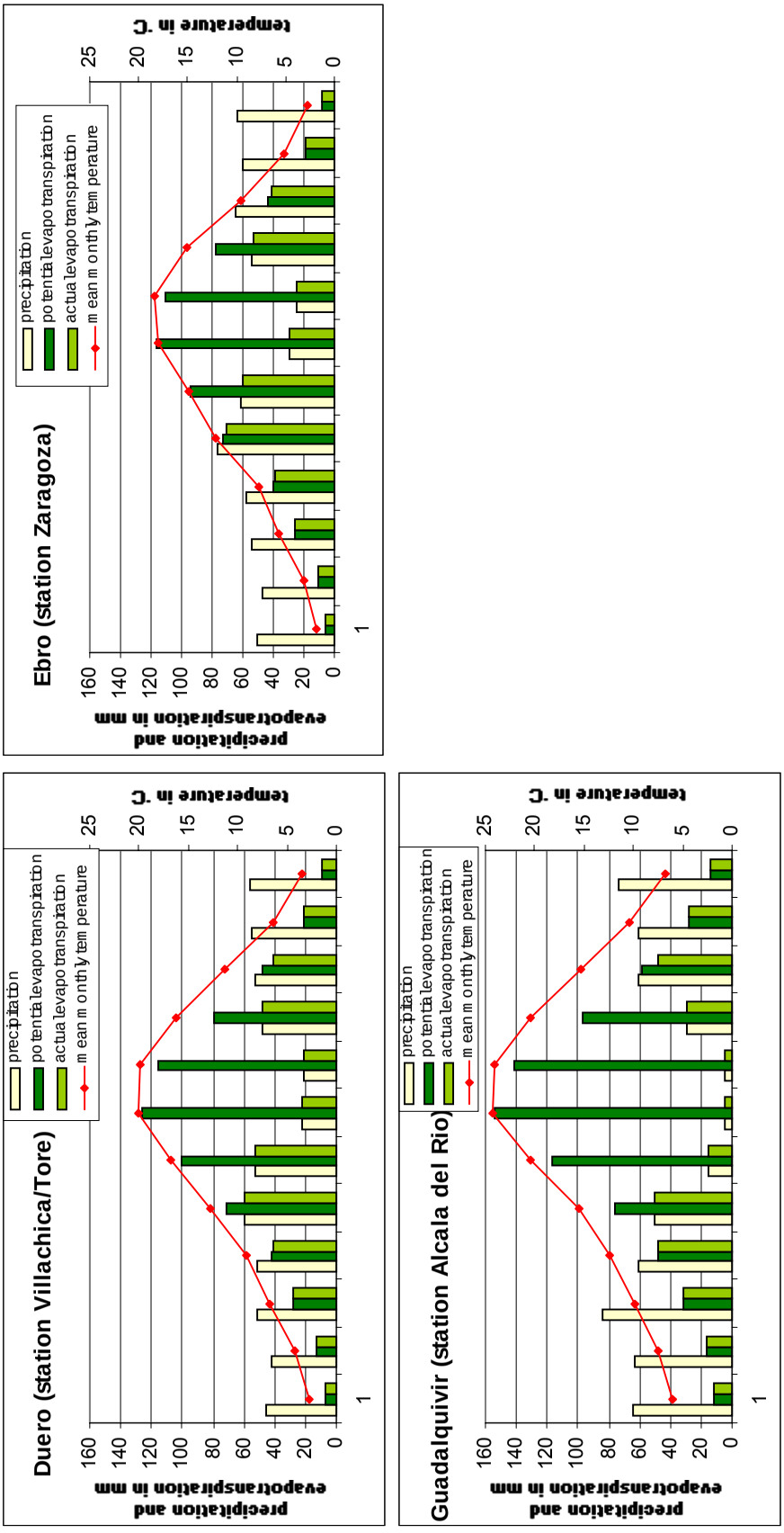

Figure 5-25: Temperature and precipitation as input data and potential and actual evapotranspiration as model results of the test catchments within runoff regime class 5 (monthly means 1961-90).

5.3.5 Significance for all European catchments

5.3.5.1 Analysis of model efficiencies concerning normal distribution

The distribution of the model efficiencies of the individual test catchments is described by Table 5-4 and Figure 5-26. It is characterized by a strong negative skewness of -1.158. This is best visualized by the boxplot (Figure 5-26a) framing the second and third quartile and plotting the median of the distribution. In contrast to the area-weighted mean the median is positive and by far closer to the maximum value than to the minimum value. The histogram of Figure 5-26b makes clearly visible that the distribution of ME values is much steeper than the normal curve, indicating a leptokurtic distribution. In fact the kurtosis is computed to be equal 0.636. The distribution of the transformed variable e^{ME} shows a much lower absolute skewness of only 0.163, and median and mean are lying closely together. But the kurtosis of -1.120 indicates a strongly platykurtic distribution. In contrast, the skewness and kurtosis of a normal distribution are zero by definition. Nevertheless, the boxplot as well as the histogram on the right side of Figure 5-26 clearly visualize that the distribution of e^{ME} can much better be approximated by a normal distribution than the distribution of the original ME values.

Table 5-4: Statistical parameters describing the distribution of the model efficiencies of all test catchments except for the Kymijoki and Júcar basins. The analysis is carried out for the model run resulting in a maximum $\overline{ME}_{all}$ (see Table 5-2).

		ME	e^{ME}
N	Valid	952947	952947
	Missing	0	0
Mean		-.216210	1.1518
Median		.141637	1.1522
Std. Deviation		1.022158	.7395
Variance		1.044807	.5469
Skewness		-1.158	.163
Std. Error of Skewness		.003	.003
Kurtosis		.636	-1.120
Std. Error of Kurtosis		.005	.005
Range		4.2967	2.43
Minimum		-3.3962	.03
Maximum		.9005	2.46

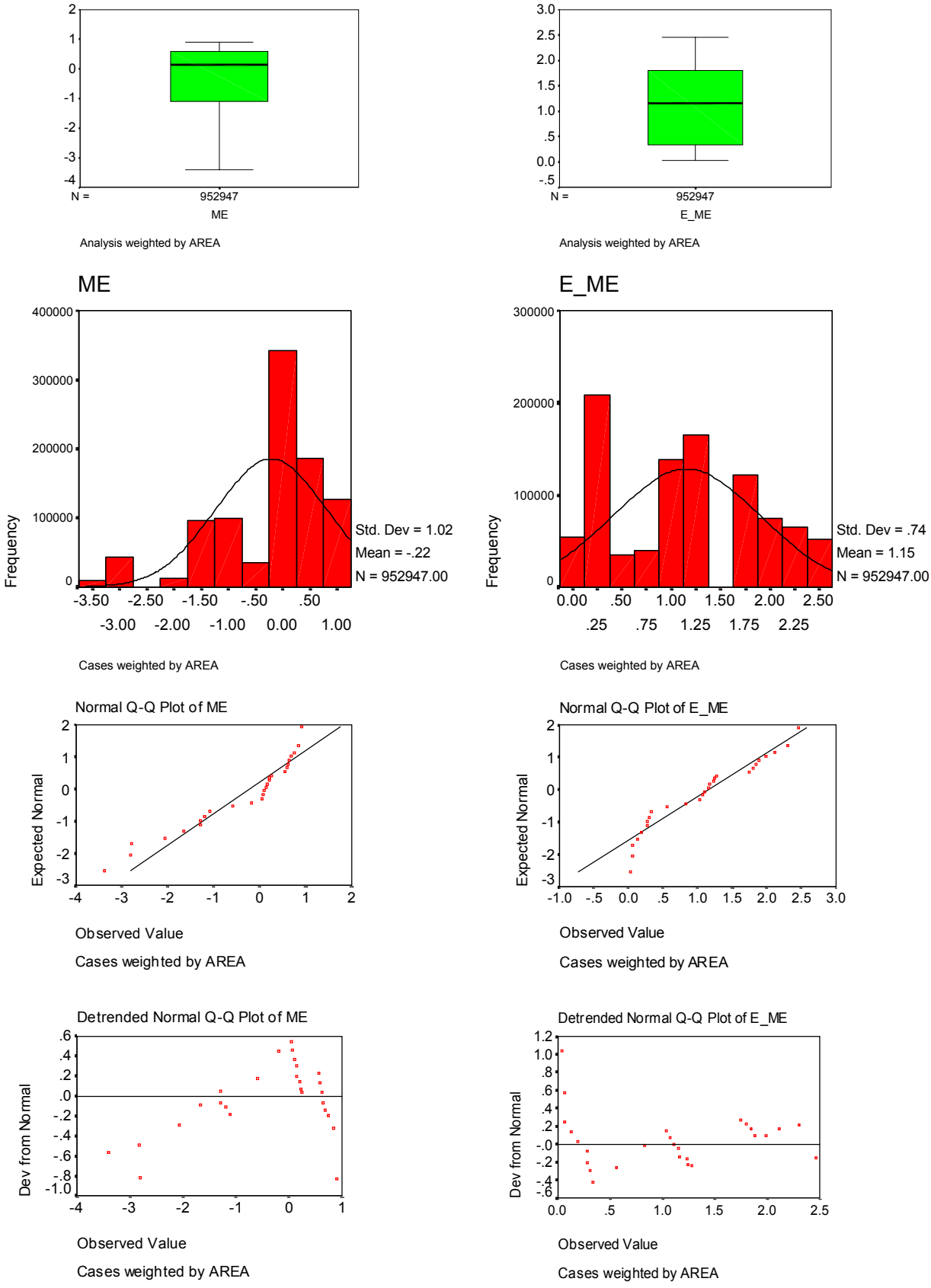

Figure 5-26: Explorative analysis of model efficiencies of all test catchments except for the Kymijoki and Júcar basins. Left: variable ME, right: variable e^{ME}. a) Boxplot, b) Histogram with normal curve, c) Normal Q-Q-Plot, d) Detrended normal Q-Q-Plot. The analysis is carried out for the model run resulting in a maximum $\overline{ME}_{all}$ (see Table 5-2).

A precondition for the T-Test of significance is that the tested variable, here the model efficiency, shows a normal distribution. In contrast to the theoretical normal distribution which is unlimited on both sides, the model efficiency can only take values within the interval $]-\infty;+1.0]$. So first it has to be tested whether the given distribution of ME, or e^{ME} respectively, is significantly different from a normal distribution. This is done with the help of the Kolmogorov-Smirnov-Test (see Table 5-5). The corresponding null hypothesis says that the empirical distribution does not significantly differ from a normal distribution. Both tests result in a significance of 0.000, indicating that this hypothesis must clearly be rejected for both ME and e^{ME}. The probability of falsely accepting the alternative hypothesis is nearly zero. So most certainly, neither the original nor the transformed values are a sample of a normally distributed population[10]. Assumptions for the implementation of a statistical T-Test are not met.

Table 5-5: Results of the Kolmogorov-Smirnov tests of normal distribution with Lilliefors significance correction for the original ME-values and the transformation e^{ME}.

	Kolmogorov-Smirnov		
	Statistic	df	Sig.
ME	.242	952947	.000
e^{ME}	.142	952947	.000

5.3.5.2 Statistical median test

A parameter free statistical one sample's median test [RINNE 1997: 554-556] has been carried through, in order to test if the area-weighted median of the model efficiencies, which is +0.142, exceeds the test value x = 0.0 significantly (one-tailed test). There are 16 basins with a positive ME covering 615.116 km² ($\approx 62 \cdot 10^4$ km²) altogether and 11 basins with a negative ME covering 337.831 km² ($\approx 34 \cdot 10^4$ km²) altogether. The total area covered by all those 27 test catchments is $\approx 96 \cdot 10^4$ km².

H_0: The median does not exceed 0.0 significantly.

H_A: The median exceeds 0.0 significantly.

Z is binomially distributed with n and p = 0.5. On the significance level $\alpha = 0.05$ the null hypothesis has to be rejected, if z is an element of the rejection region K_α with:

$$K_\alpha = \{0; \ldots; k_{n;\alpha}\} \tag{5.1}$$

The threshold value $k_{n;\alpha}$ of the rejection region must fulfil the following inequation:

[10] For a critical discussion of tests in which the more interesting case is the retainment of the null hypothesis like in the Kolmogorov-Smirnov-Test of normal distribution see JANSSEN & LAATZ (1994: 205-206).

$$\sum_{i=0}^{k_{n;\alpha}} \binom{n}{i} \cdot 0.5^n \leq \alpha < \sum_{i=0}^{k_{n;\alpha}+1} \binom{n}{i} \cdot 0.5^n \qquad (5.2)$$

→ *Case A: no area-weighting of the basins*

If Z is the number of test catchments with a negative ME, then n = 27. Table 5-6 shows some results of the binomial distribution function with n = 27 and p = 0.5.

Table 5-6: Distribution function of the discrete binomial distribution with n = 27 and p = 0.5.

$k_{n;\alpha}$	$P(Z \leq k_{n;\alpha}) = \sum_{i=0}^{k_{n;\alpha}} \binom{n}{i} \cdot 0.5^n$ [:= empirical significance level α*]
7	0.00958
8	0.02612
9	0.06104
10	0.12389
11	0.22103

→ For $\alpha = 0.05$, inequation (5.2) becomes true for $k_{27;\,0.05} = 8$: $0.02612 \leq 0.05 < 0.06104$

→ According to equation (5.1), H_0 is retained, since $z = 11 \notin K_{0.05} = \{0;\ldots;8\}$.

The median does not exceed 0.0 at the 5 %-level of significance. At maximum 8 basins are allowed to result in a negative ME (at least 19 catchments must have a positive ME respectively) in order to yield a significant result on the 5 %-level. Alternative argumentation on the basis of the empirical significance level α*: With 11 negative ME_i values the empirical significance level lies with 22.1 %. As this is equal to the probability of falsely rejecting H_0, H_0 is retained.

The problem concerned with this result is that the 16 test catchments with a positive ME are greater on average than the 11 test catchments with a negative ME, so that they should weight stronger. But when area-weighting the basins some arithmetical problems arise instead, as will be seen in the following case B.

→ *Case B: area-weighting of the basins*

If Z is the number of 10^4 km² areas with a negative ME, then n = 96. Table 5-7 shows some results of the binomial distribution function with n = 96 and p = 0.5.

Table 5-7: Distribution function of the discrete binomial distribution with n = 96 and p = 0.5.

$k_{n;\alpha}$	$P(Z \le k_{n;\alpha}) = \sum_{i=0}^{k_{n;\alpha}} \binom{n}{i} \cdot 0.5^n$ [:= empirical significance level α*]
34	0.00279
35	0.00517
36	0.00922
37	0.01577
38	0.02596
39	0.04110
40	0.06267

→ For $\alpha = 0.05$, inequation (5.2) becomes true for k96; 0.05 = 39:0.04110 ≤ 0.05 < 0.06267

→ According to equation (5.1), H0 has to be rejected, since $z = 34 \in K_{0.05} = \{0;...;39\}$.

The median exceeds 0.0 at the 5 %-level of significance. Even at the 0.5 %-level this is still significant, since the empirical significance level for $k_{n;\alpha} = 34$ is lower than 0.005.

This result has to be regarded with severe caution, since the relation of the threshold value $k_{n;\alpha}$ to n differs for different sample sizes[11]. If 10^5 km² areas had been taken as weighting basis for example, the rejection region for n = 10 would have been $K_{0.05} = \{0;1\}$, leading to a retention of the null hypothesis again, as z = 3 then.

Result:

Although for more than 50 % of the sample test catchments a positive ME could be yielded, the median could not be proven to be positive among the population of all European catchments. This is partly caused by the fact that the basins with a positive ME cover a greater area than those with a negative ME, but the possibilities of performing the median test in an area-weighted manner are restricted. In addition, High Mountain basins, where ME was worst, are numerically over-represented in the sample.

[11] Compare these examples: For a sample size of n = 10 the rejection region $K_{0.05} = \{0;1\}$; n = 50 results in $K_{0.05} = \{0;18\}$; n = 100 results in $K_{0.05} = \{0;41\}$. The probability of not more than 1 flood in 10 years is higher than the probability of not more than 10 floods in 100 years.

6 SUMMARY

With the objective of providing raster-based runoff for coupled ocean-atmospheric General Circulation Models the water balance model WABIMON, based on the approach of THORNTHWAITE & MATHER (1957), is applied, improved, calibrated and validated for Greater Europe. The model works in a monthly time step and on a horizontal resolution of 0.5° longitude and 0.5° latitude. Input data sets of precipitation and temperature are given as long-term monthly means of the period 1961-90. GIS-based information are required on mean elevation, slope steepness, water holding capacity of the soil, and the recession constant. The model computes potential and actual evapotranspiration as well as total runoff, consisting of the components of base flow, surface and snow melt runoff. The modules computing snow cover accumulation, snow melt, surface runoff and the soil water balance are extended within the frame of this study.

For model validation measured catchment-based runoff of 29 European test catchments is used. The evaluation of the model quality occurs with the help of the Sutton-Rathcliffe coefficient (model efficiency, ME), which is defined within the interval $]-\infty;+1]$. For positive values of this parameter the residual variance is lower than the variance of all observed data, so that the model can be said to work effectively.

The ME of the Finnish Kymijoki basin and the Spanish Júcar basin were so negative due to the retention effect of the Finnish plain of lakes and reservoir management respectively that they had to be excluded from further model calibration. The area-weighted arithmetic mean of the individual ME is still negative although for 16 of the remaining 27 European test catchments a positive ME is reached. The positive median does not exceed zero significantly. This hypothesis had to be retained on the 5 %-level in a parameter free median test. This is partly caused by the fact that the basins with a positive ME cover a greater area than those with a negative ME, but the possibilities of performing the median test in an area-weighted manner are restricted. In addition, High Mountain basins, where the ME was worst, are numerically over-represented in the sample. Most important reasons for high residuals are too low a precipitation input data due to measurement errors in snowy regions, reservoir management, the retention effect of lakes and marshes and the underestimation of potential evapotranspiration in the Mediterranean by the very simple Thornthwaite formula. In High Mountains the annual water balance is not always outweighed since the model structure does not guarantee that the snow cover accumulated during the winter months melts completely in summer.

The model produces most satisfactory results for maritime regions with pluvial runoff regimes, pluvio-nival regimes of low mountains, and the vast areas of nival lowland regimes. WABIMON is quite reliable there concerning the general temporal and spatial distribution of runoff. But the model results should not be interpreted on the individual grid level as the model has not been proven to provide satisfactory accuracy there yet.

Before using WABIMON model results as input for GCMs, the model structure should further be improved and validated. If the gridded runoff fields are still used as GCM input, it has to be considered that runoff is underestimated in the High Mountains, overestimated in the southern Mediterranean and that the data set is completely unreliable in regions of great lakes, marshes and managed reservoirs.

7 OUTLOOK

In order to minimize residuals, reliable precipitation input data are most effective. There is a set of possible model expansions which could not be employed is this study either due to lack of data availability and/or because their employment would have been too time-consuming for this diploma thesis. Further improvements of the model structure can be distinguished in three categories of importance:

Most important extensions:

- Improvement of the computation of potential evapotranspiration by employing more precise formulas if data on wind speed, air humidity, radiation and on the height and density of the vegetation cover are available (see Appendix B).
- Creating separate modules computing the water balance of lakes and marshes.
- Consideration of anthropogenic reservoir management (water withdrawal and supply).
- Additional consideration of the monthly minimum and maximum and/or the standard deviation of temperature and precipitation for an improvement of the surface runoff, snow accumulation and snow melt modules.
- Modification of the snow melt module in order to guarantee that the accumulated wintry snow cover melts completely during summer months. Techniques for runoff prediction from glaciated areas can be found in YOUNG (1985, 1993). For an intercomparison of models simulating snow melt runoff see WMO (1986).

Medium important extensions:

- Coupling a routing model [LOHMANN ET AL 1996].
- Derivation of the recession constant for each individual grid cell from hydrogeological and soil properties. First, this is more precise than the current determination for whole catchments since aggregation effects are dropped. Second, the recession constant no longer has to be calibrated in those catchments where daily runoff data are not available for hydrograph analysis.
- Further differentiation of the runoff factors concerning a) precipitation intensity and b) land use proportions within a grid cell, c) the degree of soil water saturation. The latter is also introduced in the VIC-2L model [LOHMANN ET AL 1998], in the VIC model [LIANG ET AL 1994, WOOD ET AL 1992], in the Xinanjiang model [ZHAO 1992] and in the HBV-2 model [BERGSTRÖM & FORSMAN 1973].
- Reaching a more precise determination of the soil water holding capacity by considering that the available field capacity is not only dependent on soil texture but also on the soil type, for example by using pedotransfer functions [BATJES ET AL 1996].

Less important extensions:

- Surface runoff separation into real surface runoff and interflow.
- Soil water percolation in fact depends on the actual hydraulic conductivity [MEIN & LARSON 1971, BROOKS & COREY 1964], not simply on the question whether the soil water holding capacity is exceeded. Estimates of all seven required Green-Ampt and Brooks-Corey parameters can be found for each USDA soil texture class in RAWLS ET AL (1982: 1318). Alternatively, the hydraulic conductivity K can be computed in dependence on the texture separates and the soil water content by the regression equation given by SAXTON ET AL (1986: 1036).
- Estimation of groundwater recharge from hydrogeology with the help of lithofacies units [GABRIEL & ZIEGLER 1989]. Unfortunately, this concept is restricted to solid rocks.
- Base flow separation into quick and slow components [SCHWARZE ET AL 1991, 1989].
- Separated consideration of interception if the degree of soil cover and the leaf area index are available.
- Differentiation of snow melt and ice melt as done by BRAUN ET AL (1993).
- Inclusion of evaporation from the snow cover [RACHNER 1987, BENGTSSON 1980].
- Consideration of evaporation in sealed areas [DVWK 1996] due to the increased temperatures in urban heat islands and due to the increased Bowen ratio (relation of sensible to latent heat).

For further model applications on the European scale test catchments in the south-east of Europe, especially in Turkey, the countries of Euphrates and Tigris and the region around the Caspian Sea should be introduced. These regions are particularly important because runoff decreases are expected to reach a maximum there in future.

REFERENCES

AGUNG, B. I., CODERY, I. (1995): Estimation of recharge and runoff volumes from ungauged catchments in eastern Australia. *Hydrological Sciences Journal* **40** (4).

ALLEN, R. G., SMITH, M., PERRIER, A., PEREIRA, L. S. (1994): An update for definition of reference evapotranspiration. *ICID Bulletin* (2) **43**: 1-34.

ARBEITSGEMEINSCHAFT BODENKUNDE (HRSG.) (1971): Bodenkundliche Kartieranleitung. Richtlinien zur Herstellung der Bodenkarte 1: 25 000. Stuttgart: Schweizerbart.

BACKHAUS, K., ERICHSON, B., PLINKE, W., WEIBER, R. (1996): Multivariate Analysemethoden. Eine anwendungsorientierte Einführung. Berlin u.a.: Springer.

BATJES, N. H. (1996): Development of a world data set of soil water retention properties using pedotransfer rules. *Geoderma* **71**: 31-52.

BAUMGARTNER, A., LIEBSCHER, H.-J. (1990): Lehrbuch der Hydrologie. Berlin, Stuttgart: Gebrüder Borntraeger.

BECKER, A., DIEKKRÜGER, B., KLEEBERG, H.-B., MAUSER, W., PESCHKE, G., SCHWARZE, R., SCHULTZ, G. A., STREIT, U. (1999): Regionalisierung in der Hydrologie. Ergebnisse eines DFG-Schwerpunktprogramms (1992-1998), in press.

BENGTSSON, L. (1980): Evaporation from a snow cover. Review and Discussion of Measurements. *Nordic Hydrology* **11**: 221-234.

BERGSTRÖM, S., FORSMAN, A. (1973): Development of a conceptual deterministic rainfall-runoff model. *Nordic Hydrology* **4**: 147-170.

BEVEN, K. (1989): Changing ideas in hydrology – The case of physically-based models. *Journal of Hydrology* **105**: 157-172.

BOUSSINESQ, J. (1904): Recherches théoriques sur l'écoulement des nappes d'éau infiltrées dans le sol et sur debit des sources. *Journal Mathématique pures appl.*: 5-78.

BROOKS, R. H., COREY, A. T. (1964): Hydraulic properties of porous media. *Hydrological Papers* **3**. Colorado State University, Ft. Collins.

BUNDESMINISTER FÜR UMWELT, NATURSCHUTZ UND REAKTORSICHERHEIT (HRSG.) (1995): Entwicklung eines mathematischen Modells zur Untersuchung des Einflusses von Klima- und Landnutzungsänderungen auf den Hoch- und Niedrigwasserabfluß im Einzugsgebiet der Mosel sowie zur Echtzeitvorhersage unter Verwendung von Fernerkundungstechniken. Forschungsbericht Wasser 102 01 304. Abschlußbericht Oktober 1995.

CANADALL, J., JACKSON, R. B., EHLINGER, J. R., MOONEY, H. A., SALA, O. E., SCHULZE, E.-D. (1996): Maximum rooting depth of vegetation types at the global scale. *Oecologia* **108**: 583-595.

CHANG, J.-H. (1959): An evaluation of the 1948 Thornthwaite classification. *Annals of the Association of American Geographers* **49**: 24-30.

DARDANELLI, J. L., BACHMEIER, O. A., SERENO, R., GIL, R. (1997): Rooting depth and soil water extraction patterns of different crops in a silty loam Haplustoll. *Field Crops Research* **54**: 29-38.

DEMUTH, S. (1993): Untersuchungen zum Niedrigwasser in West-Europa (Investigation of low water in Western Europe). *Freiburger Schriften zur Hydrologie* **1**. Freiburg im Breisgau.

DEMUTH, S., HAGEMANN, I. (1994a): Case study of regionalising base flow in SW Germany applying a hydrogeological index. Flow Regimes from Experimental and Network Data (FREND). Vol. II. Hydrogeological Data. Institute of Hydrology, Wallingford.

DEMUTH, S., HAGEMANN, I. (1994b): Estimation of flow parameters applying hydrological area information. *IAHS Publication No.* **221**: 151-157.

DEYHLE, C. (1995): Die Lysimeteranlage Koblenz-Niederwerth – Aufbau, Meßwertverarbeitung und erste Ergebnisse zur Verdunstungsbestimmung. *Deutsche Gewässerkundliche Mitteilungen* **39**: 49-57.

DUNNE, K. A., MILLY, P. C. D. (1994): Sensitivity of the Global Water Cycle to the water holding capacity of land. *Journal of Climate* **7**: 506-526.

DUNNE, K. A., WILLMOTT, C. J. (1996): Global distribution of plant-extractable water capacity of soil. *International Journal of Climatology* **16**: 841-859.

DVWK (HRSG.) (1996): Ermittlung der Verdunstung von Land- und Wasserflächen. *Merkblätter zur Wasserwirtschaft* **238**. Bonn.

DVWK (HRSG.) (1982): Bodenkundliche Grunduntersuchungen im Felde zur Ermittlung von Kennwerten meliorationsbedürftiger Standorte. Teil II: Ermittlung von Standortkennwerten mit Hilfe der Grundansprache der Böden. *DVWK-Regeln zur Wasserwirtschaft* **116**.

DVWK (HRSG.) (1980): Bodenkundliche Grunduntersuchungen im Felde zur Ermittlung von Kennwerten meliorationsbedürftiger Standorte. Teil I: Grundansprache der Böden. *DVWK-Regeln zur Wasserwirtschaft* **115**.

ESRI (1994): Cell-based Modeling with GRID. Handbook to Arc/Info Version 7. Environmental Systems Research Institute, Inc. Redlands. USA.

FEDERAL INSTITUTE OF HYDROLOGY (1997): Übertragung von gemessenen Abflußwerten auf Gitterpunkte. BfG-1062. Koblenz.

FEDERER, C. A., VÖRÖSMARTY, C. J., FEKETE, B. (1996): Intercomparison of methods for calculating potential evaporation in regional and global water balance models. *Water Resources Research* **32**: 2315-2321.

FERGUSON, B. K. (1996): Estimation of Direct Runoff in the Thornthwaite Water Balance. *Professional Geographer* **48** (3): 263-271.

FRANCHINI, M., PACCIANI, M. (1991): Comparative analysis of several conceptual rainfall-runoff models. *Journal of Hydrology* **122**: 161-219.

GABRIEL, B., ZIEGLER, G. (1989): Lithofacieskonzept – ein neues Konzept zur Berechnung der Grundwasserneubildung in Abhängigkeit von Einzugsgebietseigenschaften. (The lithofacies unit – A new concept for the calculation of groundwater recharge in hard rock areas) *Wasserwirtschaft – Wassertechnik* **33**: 163-165.

GOTTSCHALK, L., KRASOVSKAIA, I. (1998): Grid estimation of runoff data. Report of the WCP-Water Project B.3: Development of Grid-related Estimates of Hydrological Variables. WMO/TD-No. 870.

GUSTARD, A., BULLOCK, A., DIXON, J. M. (1992): Low flow estimation in the United Kingdom. Report 108. Institute of Hydrology. Wallingford. UK.

HÖLTING, B. (1996): Hydrogeologie. Einführung in die Allgemeine und Angewandte Hydrogeologie. Stuttgart: Enke.

HORTON, R. E. (1933): The role of infiltration in the hydrologic cycle. *American Geographical Union Transactions* **14**: 446-460.

INSTITUTE OF HYDROLOGY (1980): Low flow studies report. Institute of Hydrology, Wallingford, UK.

JANSSEN, J., LAATZ, W. (1994): Statistische Datenanalyse mit SPSS für Windows. Springer-Verlag. Berlin, Heidelberg, New York, Tokyo.

KELLER, R. (1961): Gewässer und Wasserhaushalt des Festlandes. Eine Einführung in die Hydrogeographie. Berlin: Haude & Spener.

KILLE, K. (1970): Das Verfahren MoMNQ, ein Beitrag zur Berechnung der mittleren langjährigen Grundwasserneubildung mit Hilfe der monatlichen Niedrigwasserabflüsse. *Zeitschrift der Deutschen Geologischen Gesellschaft, Sonderheft Hydrogeologie Hydrogeochemie*: 89-95.

KLEIDON, A., HEIMANN, M. (1998a): Optimised rooting depth and its impacts on the simulated climate of an Atmospheric General Circulation Model. *Geophysical Research Letters* **25**: 345-348.

KLEIDON, A., HEIMANN, M. (1998b): A method of determining rooting depth from a terrestrial biosphere model and its impacts on the global water and carbon cycle. *Global Change Biology* **4**: 275-286.

KRAHÉ, P., DAAMEN, K., MÜLDERS, R., WILKE, K. (1997): GIS-related baseflow simulation for water balance and precipitation-runoff modelling in the River Rhine basin. IAHS Scientific Assembly Rabat, Marokko, April 1997.

KRAHÉ, P., DAAMEN, K., PINNOW, J. (1996): Continental Water Balance Computation for Europe Preliminary Results. In: Second International Scientific Conference on the Global Energy and Water Cycle. Proprint Volume. Washington DC.

LEEMANS, R., CRAMER, W. P. (1990): The IIASA Database for Mean Monthly Values of Temperature, Precipitation and Cloudiness of a Global Terrestrial Grid. IIASA, Laxenburg, Austria. WP-90-41.

LIANG, X., LETTENMAIER, D. P., WOOD, E. F., BURGES, S. J. (1994): A simple hydrologically based model of land surface water and energy fluxes for general circulation models. *Journal of Geophysical Research* **99**: 14415-14428.

LOCKWOOD, J. G. (1995): Thornthwaite, C.W. 1948: An approach toward a rational classification of climate. Classics in physical geography revisited. *Progress in physical geography* **19:** 243-248.

LOHMANN, D., NOLTE-HOLUBE, R., RASCHKE, E. (1996): A large-scale horizontal routing model to be coupled to land surface parametrization schemes. *Tellus* **48A**: 708-721.

LOHMANN, D., RASCHKE, E., NIJSSEN, B., LETTENMAIER, D. P. (1998): Regional scale hydrology: I. Formulation of the VIC-2L model coupled to a routing model. *Journal of Hydrological Sciences* **43**: 131-141.

LOUIE, P. Y., PUGSLEY, W. I. (1981): Application of near realtime water budgets in monitoring climate-related events. Proceedings of the Fifth Annual climate diagnostic workshop, University of Washington, Seattle, 22.-24. October 1980, National Oceanic and Atmospheric Administration, US Department of Commerce: 158-166.

MAILLET, E. (1905): Mécanique et physique du globe. Essais d'hydraulique souterraine et fluviale. Paris.

MARK, D. M. (1988): Network Models in Geomorphology. Modelling in Geomorphological Systems. Chichester: Wiley.

MEIN, R. G., LARSON, C. L. (1971): Modeling the infiltration component of the rainfall-runoff process. *Bulletin* **43**. Minneapolis: Water Resources Center, University of Minneapolis.

MILLY, P. C. D., DUNNE, K. A. (1994): Sensitivity of the Global Water Cycle to the Water-Holding Capacity of land. *Journal of Climate* **7**: 506-526.

MINTZ, Y., SERAFINI, Y. V. (1992): A global monthly climatology of soil moisture and water balance. *Climate Dynamics* **8**: 13-27.

MOLNAR, L. (1990): Hydrology of Montainous Areas. *IAHS Publication No.* **190**.

MONTEITH, J. L. (1973): Principles of Environmental Physics. New York: Elsevier.

NASH, J. E., SUTCLIFFE, J. V. (1970): River flow forecasting through conceptual models: Part I – A discussion of principles. *Journal of Hydrology* **10**: 282-290.

NATERMANN, E. (1951): Die Linie des langfristigen Grundwassers (A^uL) und die Trockenwetterabflußlinie (TWL). Die Wasserwirtschaft. Sonderheft. Vorträge September 1950: 12-14.

NIEDERSÄCHSISCHES LANDESAMT FÜR BODENFORSCHUNG (HRSG.) (1992): Dokumentation zur Methodenbank des Fachinformationssystems Bodenkunde (FIS Boden). *Technische Bereichte zum NIBIS* **3**. Hannover.

NOVICKÝ, O., KASPÁREK, L., KOLÁROVÁ, S. (1993): Hydrological design data estimation techniques. Report of the WCP-Water Project C.5: Re-analysis of Hydrological Observations in Czechoslovakia. WMO/TD-No. 554.

PALMER, W. C. (1968): Keeping track of crop moisture conditions nationwide: the new moisture index. *Weatherwise* **21**: 156-161.

PALMER, W. C. (1965): Meteorological drought. *Research Papers* **45**. US Weather Bureau. US Department of Commerce. USA.

PENMAN, H. L. (1948): Natural evaporation from open water, bare soil and grass. *Proc R Soc* **193**: 120-145.

PEREIRA, L. S., KELLER, H. M. (1982): Recession characterization of small mountain basins, derivation of master recession curves and optimization of recession parameters. In: Hydrological Aspects of Alpine and High Mountain areas (Proceedings Exeter Symposium, July 1982). *IAHS Publication No.* **138**: 243-255.

PRESS, F., SIEVER, R. (1995): Allgemeine Geologie. Eine Einführung. Heidelberg: Spektrum.

RACHNER, M. (1987): Verdunstung von der Oberfläche der Schneedecke. Ergebnisse der an der Forschungsstation Harzgerode durchgeführten Messungen. *Zeitschrift für Meteorologie* **37**: 285-290.

RAWLS, W. J., BRAKENSIEK, D. L., SAXTON, K. E. (1982): Estimation of soil water properties. *Transactions of the American Society of Agricultural Engineers* **25**: 1316-1320.

REFSGAARD, J.C., STORM, B. (1996): Construction, calibration and validation of hydrological models. In: Abbott, M. A., Refsgaard, J. C. (eds) (1996): Distributed Hydrological Modelling. Dordrecht [a.o.]: Kluwer.

RICHTER, D. (1995): Ergebnisse methodischer Untersuchungen zur Korrektur des systematischen Meßfehlers des Hellmann-Niederschlagsmessers. *Berichte des DWD* **194**, Offenbach am Main.

RINNE, H. (1997): Taschenbuch der Statistik. Frankfurt am Main: Deutsch.

ROWELL, D. L. (1997): Bodenkunde. Untersuchungsmethoden und ihre Anwendungen. Berlin u.a.: Springer.

SAXTON, K. E., RAWLS, W. J., ROMBERGER, J. S., PAPENDICK, R. I. (1986): Estimating Generalized Soil-water Characteristics from Texture. *Soil Science Society of America Journal* **50**: 1031-1036.

SCHEFFER, F., SCHACHTSCHABEL, P. (1992): Lehrbuch der Bodenkunde. Stuttgart: Enke.

SCHRÖDTER, H. (1985): Verdunstung. Anwendungsorientierte Meßverfahren und Bestimmungsmethoden. Berlin u.a.: Springer.

SCHULTZ, G. A., HORNBOGEN, M., VITERBO, P., NOILHAN, J. (1995): Coupling large-scale hydrological and atmospheric models. *IAHS Special Publication No.* **3**.

SCHWARZE, R., GRÜNEWALD, U., BECKER, A., FRÖHLICH, W. (1989): Computer-aided analyses of flow recessions and coupled basin water balance investigations. *IAHS Publication No.* **187**: 75-83.

SCHWARZE, R., HERRMANN, A., MÜNCH, A., GRÜNEWALD, U., SCHÖNINGER, M. (1991): Rechnergestützte Analyse von Abflußkomponenten und Verweilzeiten in kleinen Einzugsgebieten. (Computer assisted analysis of runoff components and transit times in small catchments). *Acta hydrophysica* **35**: 143-184.

SEMMEL, A. (1983): Grundzüge der Bodengeographie. Stuttgart: Teubner.

SIEGERT, E., SCHRÖDTER, H. (1975): Erfahrungen mit dem Wasserbilanzschreiber nach Klausing. *Deutsche Gewässerkundliche Mitteilungen* **19**: 167-171.

SINGH, V. P. (1995): Computer Models of Watershed Hydrology. Colorado: Water Resources Publications.

THORNTHWAITE, C. W. (1948): An approach towards a rational classification of climate. *Geographical Revue* **38**.

THORNTHWAITE, C. W., HARE, F. K. (1965): The loss of water to the air. *Meteorological Monographics* **28**: 163-180.

THORNTHWAITE, C. W., MATHER, J. R. (1957): Instructions and tables for computing potential evaporation and the water balance. *Publications in Climatology* **10** (3).

THORNTHWAITE, C. W., MATHER, J. R. (1955): The water balance. *Publications in Climatology* **8** (1).

UHLIG, S. (1959): Wasserhaushaltsbetrachtungen nach Thornthwaite. *Zeitschrift für Acker- und Pflanzenbau* **109**: 384-407.

U.S. SOIL CONSERVATION SERVICE (1986): Urban Hydrology for small watersheds. *Technical Release No.* **55**. Washington DC.

U.S. SOIL CONSERVATION SERVICE (1972): National Engeneering Handbook, Section 4, Hydrology. Washington DC.

VÖRÖSMARTY, C. J., FEDERER, C. A., SCHLOSS, A. (1998): Potential evaporation functions compared on US watersheds: Possible implications for global-scale water balance and terrestrial ecosystem modeling. *Journal of Hydrology* **207**: 147-169.

VÖRÖSMARTY, C. J., MOORE, III B. (1991): Modelling basin-scale hydrology in support of physical climate and global biogeochemical studies: An example using the Zambesi river. *Surveys in Geophysics* **12**: 271-311.

VÖRÖSMARTY, C. J., MOORE III B., GRACE, A. L. (1989): Continental Scale Models of Water Balance and Fluvial Transport: An application to south America. *Global Biogeochemical Cycles* **3** (3): 241-265.

WEBB, R. S., ROSENZWEIG, C. E. (1993): Specifying land surface characteristics in general circulation models: soil profile data set and derived water-holding capacities. *Global Biogeochemical Cycles* **7**: 97-108.

WENDLING, U. (1995): Berechnung der Gras-Referenzverdunstung mit der FAO Penman-Monteith-Beziehung. *Wasserwirtschaft* **85**: 602-604.

WILHELM, F. (1993): Hydrogeographie. [= Das Geographische Seminar] Braunschweig: Westermann.

WILLMOT, C. J., ROWE, C. M., MINTZ, Y. (1985): Climatology of the terrestrial seasonal water cycle. *Journal of Climatology* **5**: 589-606.

WITTENBERG, H. (1997): Der nichtlineare Speicher als Alternative zur Beschreibung von Basisabfluß, Grundwasserspeicherung und Trockenwetterganglinie. *Wasserwirtschaft* **87**: 570-574.

WMO (1986): Intercomparison of Models of Snowmelt runoff. *Operational Hydrology Report No.* **23**.

WOOD, E. F., LETTENMAIER, D. P., ZARTARIAN, V. G. (1992): A Land-Surface Parameterization With Subgrid Variability for General Circulation Models. *Journal of Geophysical Research* **97**: 2717-2728.

WRIGHT, C. E. (1974): The influence of catchment characteristics upon low flows in South-East England. *Water Services* (7): 227-230.

WRIGHT, C. E. (1970): Catchment characteristics influencing low flow. *Water and Water Engineerings: 468-471.*

WUNDT, W. (1958): Die Kleinstwasserführung der Flüsse als Maß für die verfügbaren Wassermengen. In: Grahmann, R. (1958): Die Grundwasser der Bundesrepublik Deutschland und ihre Nutzung. *Forschungen zur deutschen Landeskunde* **104**: 47-54.

YOUNG, J. Y. (1993): Snow and Glacier Hydrology. *IAHS Publication No.* **218**.

YOUNG, J. Y. (1985): Techniques for prediction of runoff from glacierized areas. *IAHS Publication No.* **149**.

ZHAO, R.-J. (1992): The Xinanjiang model applied in China. *Journal of Hydrology* **135**: 371-381.

ZUBENOK, L. I. (1978): Potential and actual evaporation. World Water Balance and Water Research of the Earth. *Unesco Studies and Reports in Hydrology* **25**: 130-139.

ZUBENOK, L. I. (1965): World maps of evaporativity. *Soviet Hydrology*: 274-289. (English translation by Molansky, S. from *Tr. Glav. Geofiz. Obs.* **179**: 144-160).

LIST OF TABLES

LIST OF FIGURES

LIST OF ABBREVIATIONS

BfG	Federal Institute of Hydrology (Koblenz, Germany)
BMU	Bundesministerium für Umwelt, Naturschutz und Reaktorsicherheit
CFC	chlorofluorocarbon
CHR	International Commission for the Hydrology of the Rhine River
DKRZ	Deutsches Klimarechenzentrum (Hamburg, Germany)
DVWK	Deutscher Verband für Wasserwirtschaft und Kulturtechnik
DWD	German Weather Service (Offenbach, Germany)
FAO	Food and Agriculture Organization of the United Nations
GCM	General Circulation Models
GIS	Geographic Information System
GPCC	Global Precipitation Climatology Centre (Offenbach, Germany)
GRDC	Global Runoff Data Centre (Koblenz, Germany)
IAHS	International Association of Hydrological Sciences
ICID	International Commission of Irrigation and Drainage
ICSU	International Council of Scientific Union
IHP	International Hydrology Programme
IIASA	International Institut for Applied System Analysis (Laxenburg, Austria)
LSP	Land Surface Parameterizations
MPI	Max-Planck-Institut for Meteorology (Hamburg, Germany)
NOAA	National Oceanic and Atmosphere Administration
PIK	Potsdam Institute for Climate Impact Research (Potsdam, Germany)
UNEP	United Nations Environment Programme
USDA	United States Department of Agriculture
USGS	United States Geological Survey
WCP – Water	World Climate Programme – Water
WCRP	World Climate Research Programme
WMO	World Meteorological Organization (Geneva, Switzerland)

APPENDIX A: Flowcharts of the program modules

Module 1:
Potential evapotranspiration

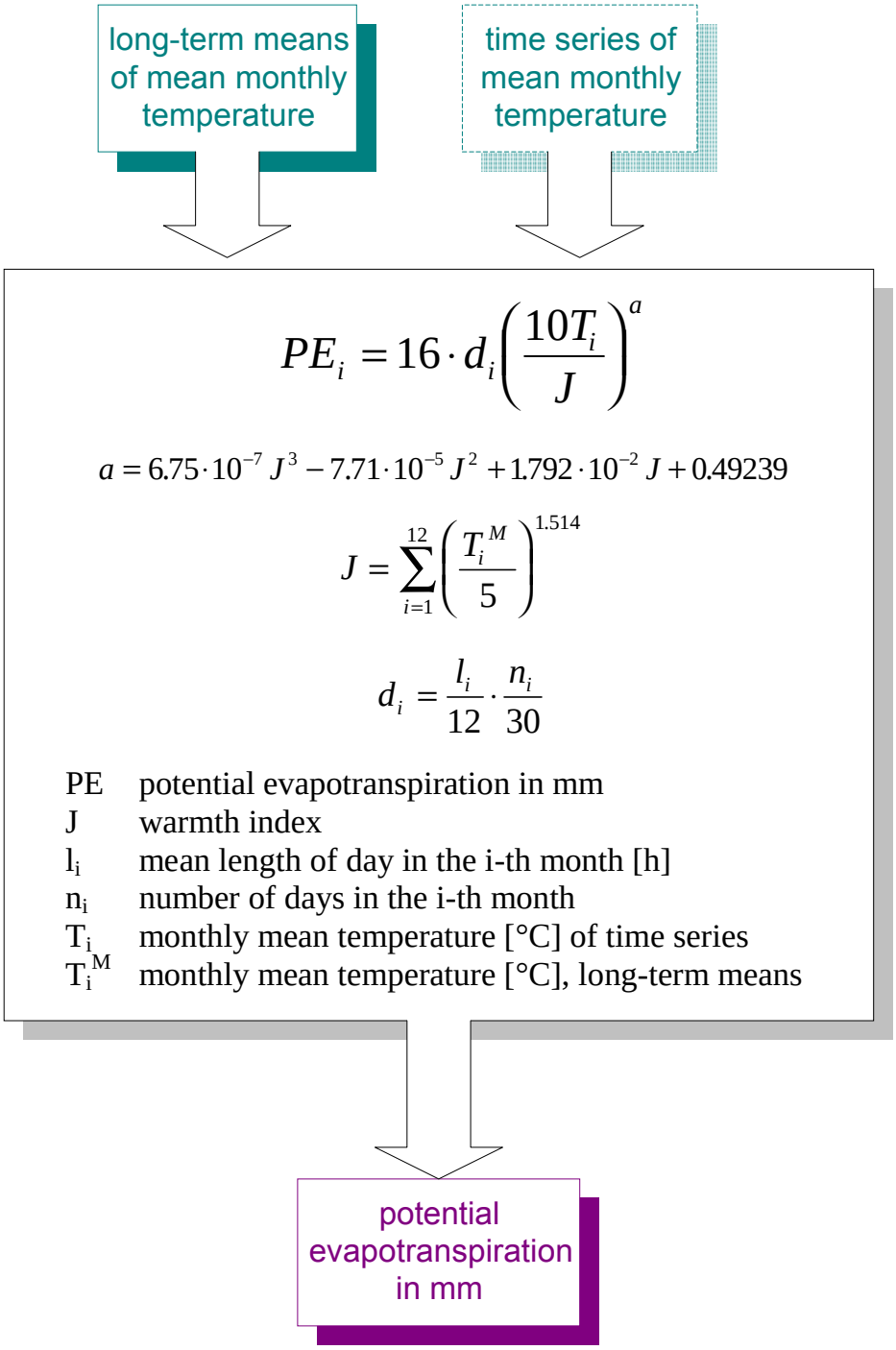

Module 3: Surface runoff

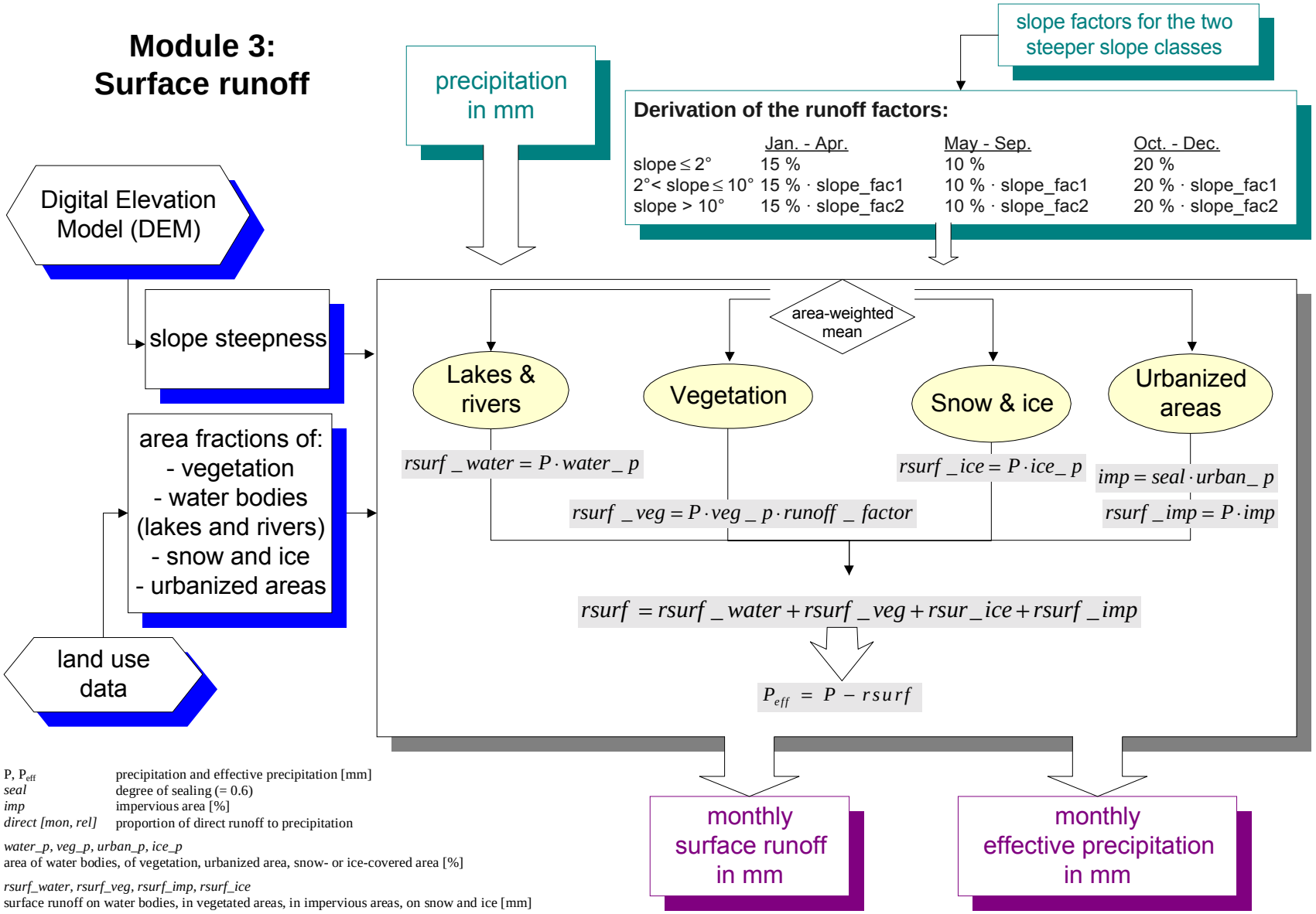

P, P_{eff}	precipitation and effective precipitation [mm]
seal	degree of sealing (= 0.6)
imp	impervious area [%]
direct [mon, rel]	proportion of direct runoff to precipitation

water_p, veg_p, urban_p, ice_p
area of water bodies, of vegetation, urbanized area, snow- or ice-covered area [%]

rsurf_water, rsurf_veg, rsurf_imp, rsurf_ice
surface runoff on water bodies, in vegetated areas, in impervious areas, on snow and ice [mm]

Module 4:
Snow melt

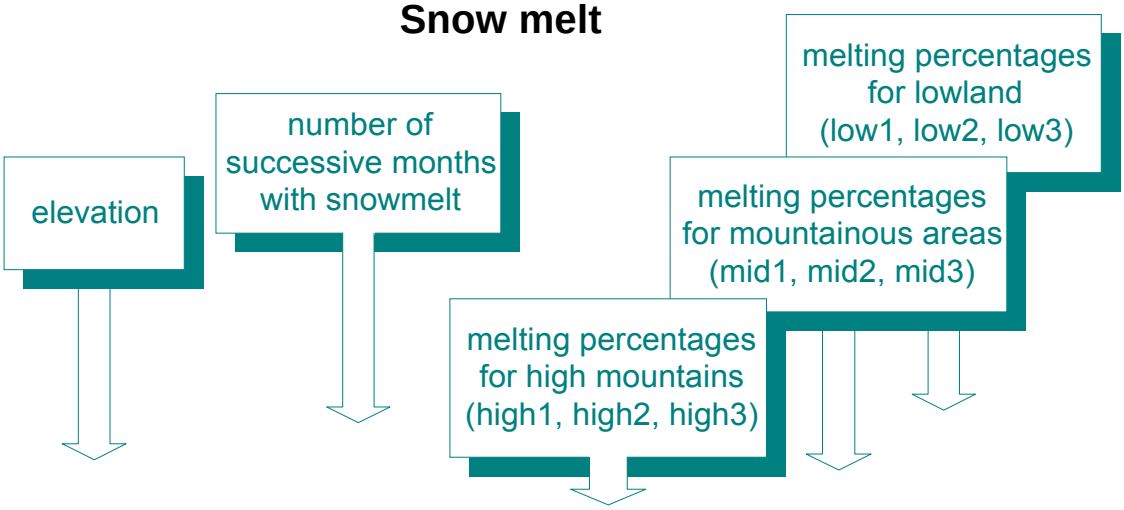

1. Estimation of snow melt runoff

differentiation of 9 cases:

	isnow = 1	**isnow = 2**	**isnow = 3**
elev ≤ 500	smro = sts*low1	smro = sts*low2	smro = sts*low3
500 < elev ≤ 1600	smro = sts*mid1	smro = sts*mid2	smro = sts*mid3
elev > 1600	smro = sts*high1	smro = sts*high2	smro = sts*high3

elev	mean elevation of the grid cell [m]
sts	snow storage [mm]
isnow	number of successive months with snowmelt
smro	snowmelt runoff [mm]
low1,2,3	percentages of snowmelt for the lowland
mid1,2,3	percentages of snowmelt for mountainous regions
high1,2,3	percentages of snowmelt for high mountains

2. Reduction of snow storage

sts = sts - smro

monthly snow melt in mm

Module 5:
Soil water balance

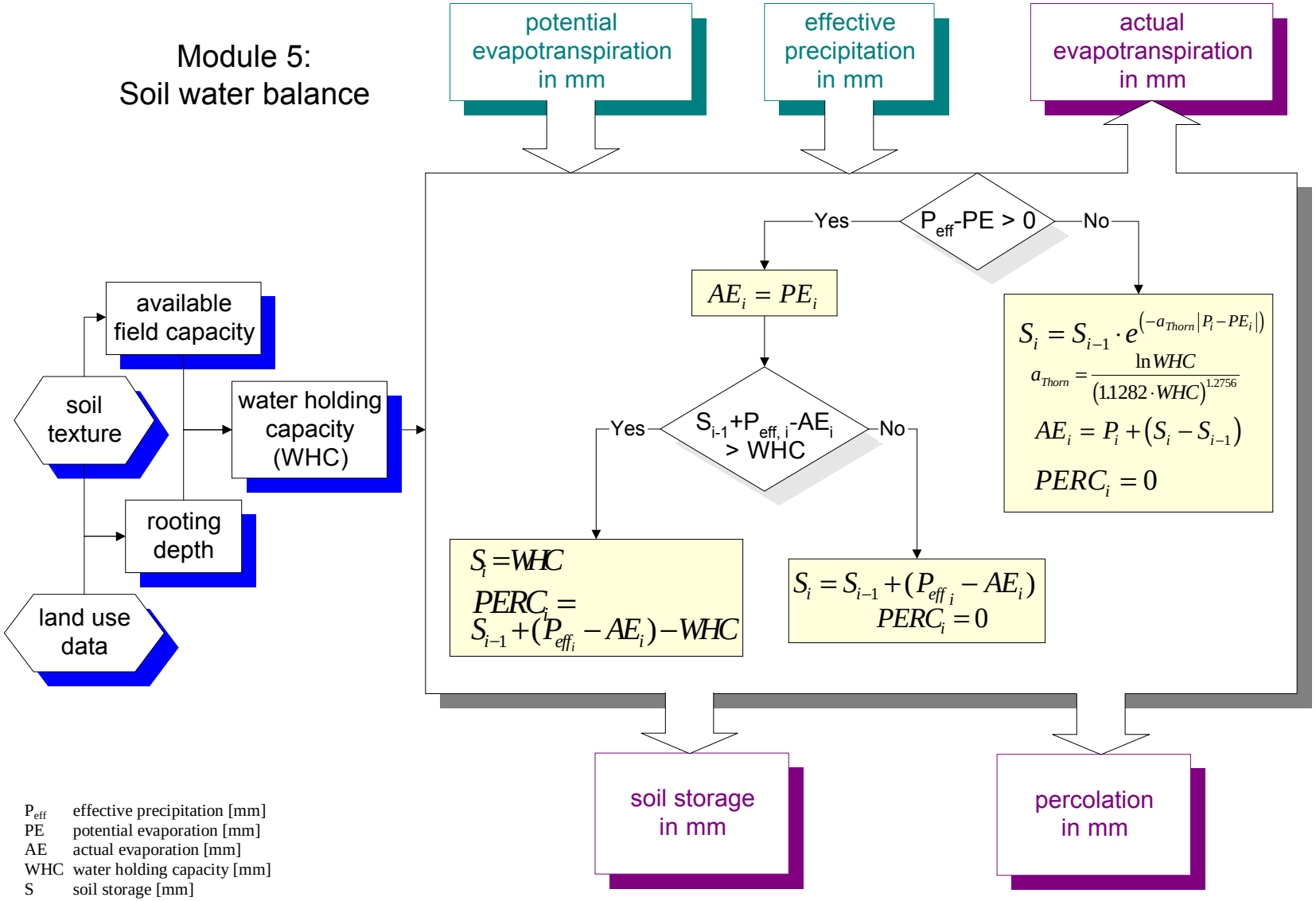

P_{eff}	effective precipitation [mm]
PE	potential evaporation [mm]
AE	actual evaporation [mm]
WHC	water holding capacity [mm]
S	soil storage [mm]

Module 6: Base flow

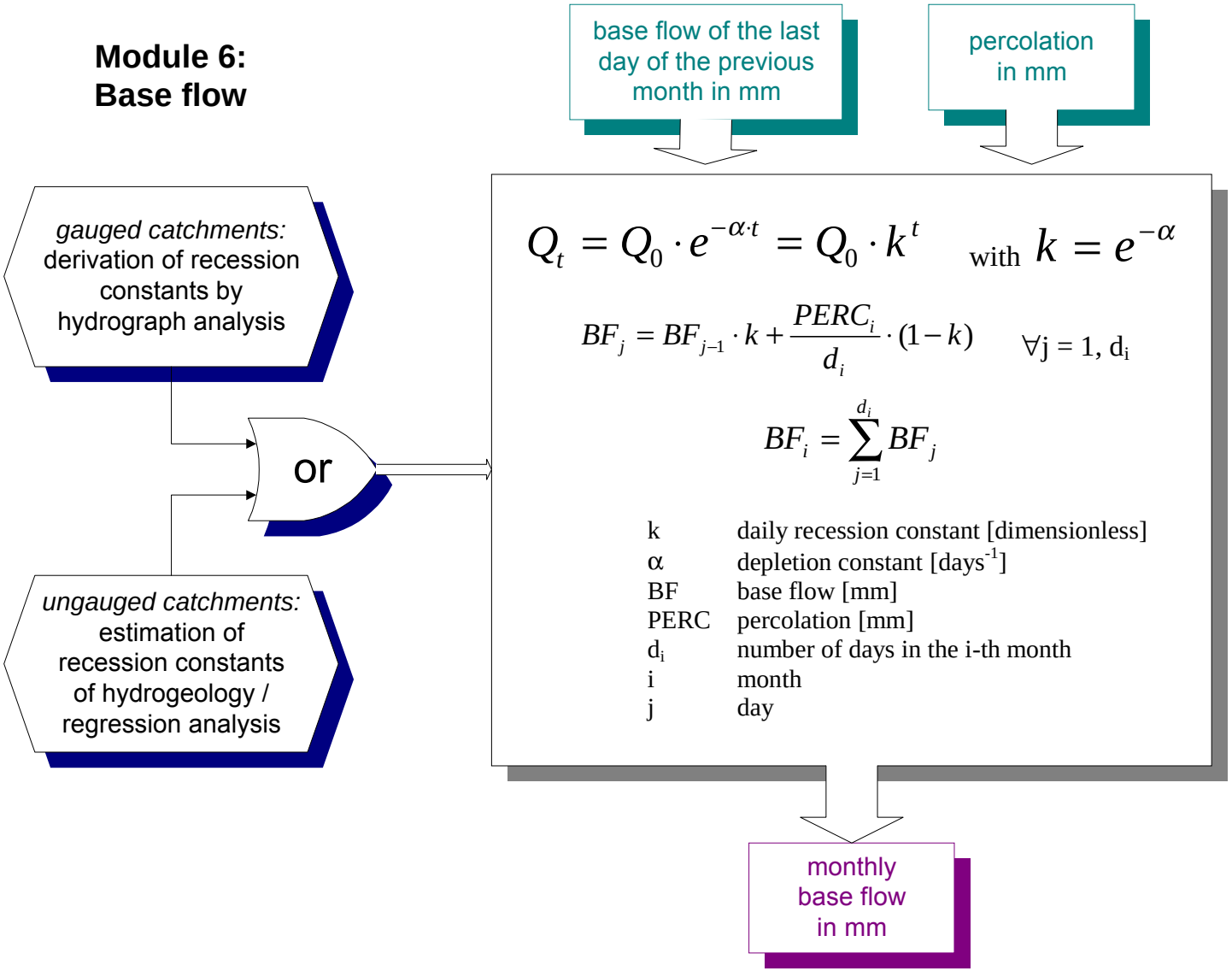

APPENDIX B: Meteorological input data and cover-dependent parameters required for different potential evapotranspiration formulas

	Meteorological input data				*Cover-dependent parameters*
	Temperature	***Radiation***	***Humidity***	***Wind speed***	
Thornthwaite	Mean				
Blanley-Criddle	Mean				
Hamon	Mean				
Hargreave	Mean, Min, Max	Solar			
Jensen-Haise	Mean	Solar			
Makkink	Mean	Solar			
Turc	Mean	Solar			
Turc-Wendling	Mean	Solar			
Penman	Mean	Net	x	x	
Haude	Mean		x		
Priestley-Taylor	Mean	Net			albedo
McNaughton-Black			x		several
Penman-Monteith	Mean	Net	x	x	several
Shuttleworth-Wallace	Mean	Net	x	x	several

after VÖRÖSMARTY ET AL (1998), FEDERER (1996), DVWK (1996), DEYHLE (1995).

APPENDIX C: Data analyses with the Geographic Information System Arc/Info

Derivation of the cell size grids

1. A small C-program was written to calculate sizes of all 0.01° x 0.01° and 0.5° x 0.5° grid cells.
2. Coverages called “longlat_01“ and “longlat_5“ are generated in the Arcedit module of Arc/Info by automatically adding all longitudes and latitudes from a prepared text file. Geographic coordinates are assigned as projection. Polygon coverages are reorganized by the CLEAN and BUILD commands.
3. Cell size attribute information are joined to the polygon coverages by the JOIN command.
4. The two polygon coverages were converted to grids called “area_01“ and “area_5“.

Derivation of the land mask grid

a) Determination of the land area of each grid cell:

The soil texture grid “tex_01“ serves as basis to define a land mask with a 0.01° x 0.01° resolution. The grid “landsoil_01“ is defined by setting all rasters that do not contain the “no data” value to 1.

```
Grid:     if (isnull(tex_01) == 0) landsoil_01 = 1
          :: endif
```

The grid “soilarea_5“ is defined as the sum of all area weighted “landsoil_01“ cells. If the grid “area_01“ contains the areas of each 0.01° x 0.01° grid cell in km², the resulting grid called “soilarea_5“ contains the areas of each 0.5° x 0.5° grid cell in km².

```
Grid:     soilarea_5 = aggregate (landsoil_01 *
          area_01,50,sum,#,#)
```

b) Derivation of the grid “land_mask“:

The grid “land_mask“ is assigned 1 for all 0.5° x 0.5° cells with a land area in km² equal to zero and all model input data unequal to “no data” (which means that they are defined). As model input data the Digital Elevation Model (“dem_5“), a grid containing the water holding capacity (“whcw_5“) and a grid containing climatological data (“prec_jan”) are considered.

```
Grid:     if (soilarea_5 == 0 AND
```

```
isnull(dem_5) == 0 AND
isnull(whcw_5) == 0 AND
isnull(prec_jan) == 0)    land_mask = 1
```

Determination of the land use portions within each grid cell

The portions of urbanized area and of the areas covered by snow and ice can easily be derived in the following steps:

a) Reclassification of the land use grid by setting all values except for the relevant class to "no data". The created grids are called "urban_01" and "snow_ice_01".

b) Computation of the percentages of land use portions using grid algebra:

```
Grid:    urban_5 = aggregate (urban_01 * area_01, 50,
         sum, #,#) / soilarea_5

Grid:    snow_ice_5 = aggregate (snow_ice_01 * area_01,
         50, sum, #,#) / soilarea_5
```

Unfortunately, the land use classification scheme of the US Geological Survey does not distinguish between salt and fresh water. Instead oceans and inland water are summarized as "water bodies" (class 16). To calculate the percentage of inland water areas within each grid cell it is first necessary to find a way to separate salt and fresh water with the help of GIS tools.

- The original land use grid (cell size 0.01°) is reclassified setting all classes except class 16 (water bodies) to "no data". The generated grid is called "landuse_rec1".
- The grid "landuse_rec1" is converted to a polygon coverage. After selecting all polygon features of this coverage the three biggest ones – the Caspian Sea, the Black Sea and the polygon with the Atlantic ocean and the Mediterranean Sea – are unselected. The rest of the selected polygons represent inland waters.
- The polygon coverage is reconverted to a grid called "inland_water" that carries the value 16 for all inland waters and "no data" in the background.
- The original land use grid is reclassified again, this time class 16 (still covering salt and fresh waters) is set to 30 and all other classes are kept. The generated grid is called "landuse_rec2". The new land use grid is produced by merging grid "landuse_rec2" and "inland_water".

This new land use grid can be used to compute the portions of inland water bodies steps a) and b) described above.

Derivation of the European river basins from flow accumulation

a) The gauging stations are imported into Arc/Info as a point coverage, reprojected into the same projection like the flow accumulation grid and then converted to a grid (cell size 1 km²) called “gauging_stat“ having a value unequal to “no data“ for all grid cells with a gauging station within and a “no data“ background.

b) Before this “gauging_stat“ grid can be used to derive watersheds, it has to be checked whether all grid cells containing gauging stations have a high flow accumulation. If they lie beside the stream channel due to inaccurate coordinates or due to imperfections of the flow accumulation grid, they have to be moved manually onto a cell with high flow accumulation.

c) This corrected “gauging_stat“ grid and the flow direction grid (“flow_dir“) are then used to compute the watersheds. All cells of a watershed obtain the value of the cell containing the accompanying gauging station in the “gauging_stat“ grid.

```
Grid:  watersheds = watershed (flow_dir, gauging_stat)
```

e) There are still some imperfections in the flow direction and flow accumulation grids provided by the USGS. Thus, some watersheds were derived incorrectly and had to be corrected by individually adding or subtracting those falsely deduced subbasins.

- The upstream part of the river Rhône down to the gauging station in Chancy is assigned to the river Rhine.
- The river Olt, north of the South Carpathians, drains into the river Mures in the flow direction grid. In reality it flows through the Carpathians in south direction and drains directly into the river Danube.
- The river Adige in Italy in reality drains directly into the Adriatic Sea whereas in the grid it flows into the Po river first.
- The upstream part of the river Maas in the flow direction grid falsely flows into a tributary of the Seine river in France.
- The Russian rivers Western Dvina and Oka falsely border on each other.In fact the basin of the river Dnieper should lie in between these two watersheds.

f) The accurate watershed grid is reprojected and resampled to a cell size of 0.5° x 0.5°.

APPENDIX D: Abbreviations of the effective climate classification after Köppen & Geiger (1932)

1st letter	*Climate*	*meaning*
A	Tropical climates	all months > 18°C
B	Dry climates	precipitation < potential evapotranspiration
C	Warm-temperate climates	coldest month between -3°C and 18°C
D	Snow climates	warmest month > 10°C, coldest month > -3°C
E	Ice climates	warmest month > 10°C

2nd letter	*meaning*
f	all months sufficient precipitation
s	dry period in summer
S	steppe climate

3rd letter	*meaning*
a	warmest month > 22°C
b	warmest month < 22°C, at least 4 months > 10°C
k	dry and cold, annual mean temperature > 18°C